STEADY-STATE TRANSPORT

PROPERTIES OF ANHARMONIC

SYSTEMS

JUZAR THINGNA

NATIONAL UNIVERSITY OF SINGAPORE

2013

STEADY-STATE TRANSPORT

PROPERTIES OF ANHARMONIC

SYSTEMS

JUZAR THINGNA

M. Sc., University of Pune, India

A THESIS SUBMITTED

FOR THE DEGREE OF DOCTOR OF PHILOSOPHY

DEPARTMENT OF PHYSICS

NATIONAL UNIVERSITY OF SINGAPORE

2013

Declaration

I hereby declare that this thesis is my original work and it has been written by me in its entirety. I have duly acknowledged all the sources of information which have been used in this thesis.

This thesis has also not been submitted for any degree in any university previously.

Juzar Thingna

28 April 2013

Acknowledgments

It is a pleasure to thank the few special people who have made this thesis possible with their constant support and guidance.

First of all I would like to thank my dad, who has been my pillar of strength throughout my graduate years. His immense patience and calm pieces of advice have made this thesis possible and no words can truly express how indebted I'm to him.

I am indebted to my supervisor, Prof. Jian-Sheng Wang, for his timely guidance throughout my research. His immense experience and deep knowledge have guided me through several road-blocks during my research. I would like to sincerely thank him for his "Yoda" *like* patience and tolerance with me during our umpteen discussions.

I'm immensely grateful to all my friends Amna, Nadiah, Mariam, Carolina, Nakul, Saran, Nithya, Arch'a'na, Shelly, and especially Bani who have been my greatest support system in Singapore. Without them I would have probably not reached this far.

I'm grateful to several colleagues and collaborators, especially Dahai He, Jose García and Prof. Peter Hänggi for their constant support and deep thought provoking questions.

I would like to express my gratitude towards all the technical and non-technical staff at the Department of Physics and the Center for Computational Science and Engineering, without whom it would have been impossible to concentrate on my research.

Last but not the least I would like to thank and dedicate this thesis to my mom without whom I would not be what I am today.

THIS PAGE IS INTENTIONALLY LEFT BLANK

Contents

Summary

The study of transport, in anharmonic systems, has been one of the most challenging and fascinating field of theoretical physics in recent years. Due to the dissipative nature of the bath and the fact that anharmonic systems seldom have exact solutions, one employs approximations to describe the system in different parameter regimes. In this thesis, we look at different approaches to describe anharmonic systems in a nonequilibrium steady-state condition. We first focus on the reduced density matrix (RDM) of the system and use open-quantum system techniques, employing the Redfield quantum master equation (RQME), to describe an anharmonic system weakly connected to multiple heat baths. Unfortunately the steady-state solution from all second-order master equations, including RQME, is incorrect at the second-order of system-bath coupling. Hence, to overcome this difficulty a novel scheme based on analytic continuation to modify the Redfield solution is proposed. The modified Redfield solution (MRS) is validated using canonical perturbation theory and the solution stemming from the *exact* nonequilibrium Green's function (NEGF) technique.

In the next part, we focus on the field of phononics and develop two *sui generis* formulations to calculate heat current in anharmonic molecular

junctions. The first approach, inspired by the quantum master equation formulation, calculates the steady state and transient heat current in strongly anharmonic systems weakly coupled to heat baths. The theory is then simplified for short-time transients and steady-state, where numerical validation for harmonic systems is provided. Anharmonic molecular junctions like the FPU-β, ϕ^4 and Duffing oscillator models are studied. The FPU-β and ϕ^4 models show peculiar low temperature behavior, which depends on the translational invariance of the anharmonic potential; whereas the Duffing oscillator model shows negative differential thermal conductance, which is essential to build phononic devices. Next, we overcome the weak system-bath coupling approximation using NEGF techniques. The so-called quantum self-consistent mean field (QSCMF) approach treats the anharmonicity perturbatively, but captures strong anharmonic effects in molecular junctions due to the self-consistent procedure. The QSCMF approach is corroborated with the master equation *like* formulation, perturbative NEGF and quantum molecular dynamics.

In the last part of this thesis, we look at the field of spintronics, where the main quantity of interest is the transport of spins. First we study spin transport in an insulator modeled by an anisotropic Heisenberg spin chain connected to thermal heat baths using the MRS. In this system, spin rectification is investigated in detail and its dependence on several system parameters is discussed. In particular it is shown that the rectification ratio can be tuned with the help of the external magnetic field, which could be of potential technological interest to build spin-diodes. From a technological standpoint, understanding semiconductor systems on the nano- or micro-meter scale is essential to build spintronic devices. In order to deal with such

large anharmonic systems a semi-classical approach based on drift-diffusion equation is adopted. The three-dimensional spin drift diffusion (3D-SDD) equations are then applied to study the influence of device geometries on the spin-injection ratio and several tricks to enhance the ratio are proposed.

List of Publications

J. Thingna, J.-S. Wang, and P. Hänggi, "Generalized Gibbs state with modified Redfield solution: Exact agreement up to second order," J. Chem. Phys. **136**, 194110 (2012).

J. Thingna, J. L. García-Palacios, and J.-S. Wang, "Steady-state thermal transport in anharmonic systems: Application to molecular junctions," Phys. Rev. B **85**, 195452 (2012).

D. He, J. Thingna, J.-S. Wang, and B. Li, "Quantum thermal conduction through anharmonic nano-junctions: A self-consistent phonon approach," (in preparation).

L. Zhang, J. Thingna, D. He, J.-S. Wang, and B. Li, "Nonlinearity enhanced interfacial thermal conductance and rectication," (submitting).

J. Thingna, J.-S. Wang, and P. Hänggi, "Spin rectification in thermally driven one-dimensional *XXZ* spin chains," (in preparation).

J. Thingna and J.-S. Wang, "Geometric effects on spin injection: 3D spin drift diffusion model," J. Appl. Phys. **109**, 124303 (2011).

J.-S. Wang, B. K. Agarwalla, H. Li, and J. Thingna, "Nonequilibrium Green's function method for quantum thermal transport,"
e-print arXiv:1303.7317v1 (submitting).

List of Tables

List of Figures

List of Symbols and Abbreviations

List of Symbols

H_{tot} Total Hamiltonian of the system + bath + system-bath coupling.

H_{S} System Hamiltonian.

H_{B} Bath Hamiltonian.

H_{SB} System-bath coupling Hamiltonian.

H_{RN} Renormalization Hamiltonian.

α Bath label for multiple baths.

p Momentum of the particle.

x Conjugate position of the particle.

S System operator coupling to the bath.

B Bath operator coupling to the system.

λ Dimensionless parameter to keep track of the system-bath coupling strength.

ρ_{tot} Density matrix corresponding to the total Hamiltonian.

$U(t_0, t)$ Evolution operator from initial time t_0 to final time t corresponding to the total Hamiltonian.

H_0 System + Bath Hamiltonian.

$U_0(t_0, t)$ Evolution operator from initial time t_0 to final time t corresponding to the system + bath Hamiltonian.

$U_I(t_0, t)$ Evolution operator from initial time t_0 to final time t in the interaction picture.

X^{nm} Hubbart operator in the system Hilbert space.

ρ Reduced density matrix of the system.

$\mathcal{R}$ Relaxation operator.

$C(\tau)$ Bath correlator.

$J(\omega)$ Spectral density.

β Inverse temperature.

Δ_{ij} Energy difference between the system eigenvalues E_i and E_j.

W Transition rates.

$\tilde{W}'$ Real part of the transition rates.

$\tilde{W}''$ Imaginary part of the transition rates.

γ_0 Damping kernel at time $t = 0$.

$\rho^{(0)}$ Zeroth order reduced density matrix of the system.

$\rho^{(2)}$ Second order reduced density matrix of the system.

V' Real part of the derivative of transition rate with respect to energy difference Δ.

V'' Imaginary part of the derivative of transition rate with respect to energy difference Δ.

M Mass of the system particle.

ω_0 Harmonic frequency.

I^L Heat current flowing out of the left lead.

$g^{kl}_{nm}(u; t)$ Freely evolving Green's function from time u to time t.

$\mathcal{I}$ Current operator.

$\chi(\tau)$ Negative derivative of the bath correlator.

σ Thermal conductance.

Ω	Inter-particle harmonic frequency.
λ_0	Strength of the on-site quartic potential.
λ	Strength of the inter-particle quartic potential.
K	Spring-constant matrix.
T_{ijkl}	General four tensor containing strengths of quartic potential.
$G(1, 2, \cdots, n)$	n-point correlation function.
$\mathrm{T_C}$	Contour-order operator on the Keldysh contour.
Σ	Self-energy of the baths.
Σ^{RN}	Renormalization Self-energy due to renormalization Hamiltonian.
$\mathbb{V}^{\mathrm{s}\alpha}$	Matrix containing information about system bath (α) coupling.
G^r	Retarded Green's function.
G^a	Advanced Green's function.
$G^<$	Lesser Green's function.
$G^>$	Greater Green's function.
$\mathcal{T}$	Transmission function.
$n_{\mathrm{L,R}}$	Bose-Einstein distribution for left and right baths.
Γ	Imaginary part of self-energy of the baths.
j	Local spin-current operator for magnetic insulators.
j_{s}	Spin current flowing through the magnetic insulator.
R	Spin rectification ratio.
$\mathbf{j}_{\uparrow,\downarrow}$	Spin-up and spin-down current flowing through the semiconductor.
$\mu_{\uparrow,\downarrow}$	Electrochemical potential for the spin-up and spin-down channels.

$\sigma_{\uparrow,\downarrow}$ Spin dependent electrical conductivity for the up and down channel.

D Spin diffusion constant.

τ Spin relaxation time.

P Spin-injection ratio.

List of Abbreviations

RDM   Reduced density matrix (of the system).

RQME   Redfield quantum master equation.

MRS   Modified Redfield solution.

CPT   Canonical perturbation theory.

NEGF   Nonequilibrium Green's function.

DE   Discrepancy error.

QSCMF   Quantum self-consistent mean field.

NDTC   Negative differential thermal conductance.

QMD   Quantum molecular dynamics.

SDD   Spin drift diffusion.

FM   Ferromagnet.

SC   Semiconductor.

Introduction

> The most exciting phrase to
> hear in science, the one that
> heralds new discoveries, is not
> "Eureka!" ("I found it!") but
> rather "hmm....that's funny...".
>
> —————————————————
>
> Isaac Asimov

The study of transport through nano and molecular junctions has been one of the most intriguing and challenging tasks of condensed matter physics for the past 50-60 years. Typical experimental transport setups involve a system of interest connected to two or more macroscopic baths, which are maintained at different temperatures, chemical potentials, *etc.*, injecting and removing the carriers of transport from the system as illustrated in Fig. 1.1. The system is generally well characterized due to its finite size, whereas the baths are largely unknown. Such archetypal experimental setups have inspired a plethora of transport theories which eliminate the baths and focus on the system and its properties. The cumulation includes: the

Kubo formula [1, 2] which is rigorously valid only in the thermodynamic limit; an offshoot of the scattering theory known as Landauer-Buttiker formalism [3, 4, 5, 6] which is valid as long as the carriers are coherent; the nonequilibrium Green's function method [7, 8] which is best suited for harmonic systems, but can treat anharmonicity in a perturbative manner; the quantum master equation approach [9, 10, 11, 12, 13] which is valid under a weak system-bath coupling approximation and can deal with only small system sizes; the Boltzmann transport equations [14, 15, 16] which are used to study linear response heat transport and typically require the anharmonicity to be treated perturbatively; the hierarchy equation of motion approach [17, 18, 19] which is valid only for Ornstein-Uhlenbeck type of processes and can be solved for extremely small system sizes only; molecular dynamics [20, 21] which is typically employed in the study of thermal transport and is valid only in the high-temperature classical regime and quantum Monte Carlo [22, 23, 24] simulation which require a perturbation either in the anharmonicity or the coupling strength and is best suited only to study transient transport.

Exact treatment of anharmonic systems has been one of the holy grails of such transport theories and some of the most exciting effects like rectification, negative differential resistance, thermoelectric effect, thermomagnetic effect, *etc.* are due to anharmonicity. Inspired by these novel effects we will

focus on theories that can deal with strongly anharmonic systems and explore some of these effects in heat and spin transport. Our primary approach to treat strong anharmonicity rigorously will be the quantum master equation formulation, but we will also look at methods which try to overcome the limitations of the master equation formulation,i.e., weak system-bath coupling and small system sizes.
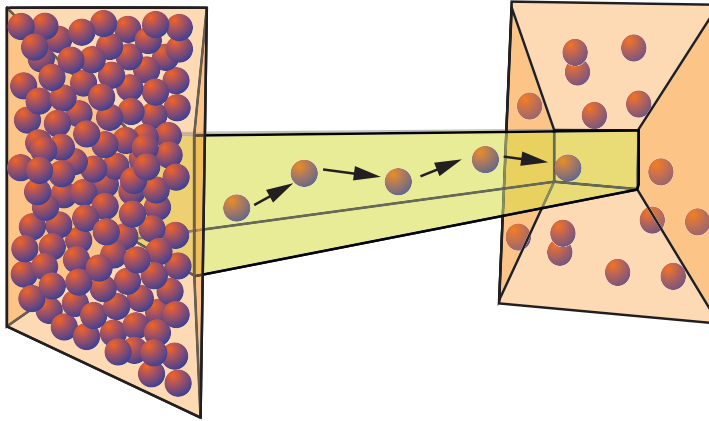
Figure 1.1: An artists perception of a minimal setup required for transport. The baths are depicted by the orange enclosed areas, whereas the system is the lime-green rectangular box in the center. The carriers of transport are depicted by the red spherical objects moving through the system due to high abundance in the left bath as compared to the right.

In this thesis, chapter 2 will be dedicated to the introduction and development of quantum master equation (QME) formalism. Several formally exact master equations either within a time-convolution (time-non-local) [25, 26] or time-convolutionless (time-local) [27, 28, 29, 30, 31, 32] form can be found in the literature, but all these approaches are computationally very demanding and can treat systems possessing an extremely small

Hilbert space dimension only, i.e., 2-4 levels maximum. Our main goal in this chapter will be to accurately calculate the reduced density matrix for relatively large Hilbert space dimensions and treat the underlying anharmonicity exactly. In order to do this we will first introduce some of the techniques of open quantum systems with the introduction of the generic Redfield quantum master equation (RQME). We will then show that the RQME is inaccurate in the steady state and hence propose a modified Redfied solution (MRS) which captures the steady state reduced density matrix correct up to second order in the system-bath coupling. Besides being accurate the MRS will allow us to handle large system Hilbert spaces up to 2^{10} levels, which is a huge improvement over the 2-4 levels used in the literature. Thus using the MRS we will be able to accurately evaluate any local quantity of interest, including currents, for relatively large Hilbert space dimensions in the nonequilibrium steady state condition.

In chapter 3 away from the predominant field of electronic transport we will cover the field of heat transport commonly known as phononics. The earliest works in this field date back to Debye and Peierls [33, 34] who studied heat transfer within solids. Inspired by their work most of the research in this field is concentrated on the classical heat transport either in the form of theoretical considerations [20, 35, 36, 37, 38, 39, 40, 41] or using simulation techniques like molecular dynamics [21]. Even though

these techniques give us good insight at the classical properties they can not be applied at low temperatures, where quantum effects become essential and hence techniques like the nonequilibrium Green's function (NEGF) [42, 43, 44, 45, 46, 47], quantum molecular dynamics [48], and master equation formulation [9, 10, 11, 12, 13] have been developed to tackle the low-temperature regime accurately.

Our main focus in this chapter will be on two most popular techniques to deal with quantum anharmonic heat transport namely the master equation formulation and the nonequilibrium Green's function (NEGF) method. Since all systems do not permit a unique local heat current operator definition we develop a master equation *like* formulation inspired by the fundamental definition of heat current, i.e., change in energy of the heat bath. The formulation suffers from the weak system-bath coupling limitation and hence to explore the strong-coupling regime we develop a self-consistent formulation using NEGF techniques. The so-obtained quantum self-consistent mean field (QSCMF) approach will not only allow us to explore the strong system-bath coupling regime but also the strong anharmonic regime.

Next we look at spin transport in chapter 4, which has been one of the most promising field of the past two decades. The explosive interest in the field started with a spin-interference device proposed by Datta and Das [49] in 1990 and has led to a vibrant and exciting new field of spintronics[1]

---

[1]The term was coined by S. A. Wolf in 1996, as a name for a DARPA initiative for

[50, 51]. In its infant days, it was the pioneering work of Mott [52, 53] who realized that at low temperatures the electrons of majority and minority spins do not mix in the scattering process, which led to the two-current model of spin transport. The model, commonly referred to as the spin drift diffusion (SDD) model, has been extended by several authors [54, 55, 56] and it provides an explanation for various magnetoresistive phenomenon. Despite its high success the model assumes that the spins diffuse in one spatial dimension only, which is not true for actual experimental geometries. This has led to the two-dimensional [57] and quasi three-dimensional [58] theories, which effectively solve multiple one-dimensional spin drift diffusion (1D-SDD) equations. Despite the enormous popularity of the SDD model, it is a semi-classical approach valid only for metals and semiconductors, and cannot be applied to magnetic insulators where quantum effects are essential for spin-transport. Hence in recent years various approaches like the Mazur inequality [59, 60], Bethe Ansatz [61], quantum Monte Carlo [22, 62], Luttinger liquid theory [63, 64] and master equation [65, 66, 67, 68] have been employed to study magnetic insulators under different regimes of validity.

In the first part of chapter 4 we will explore the true power of the MRS, proposed in chapter 2, by studying spin transport in magnetic insulators modeled as spin-1/2 anisotropic Heisenberg spin chains. One of the biggest

_____

novel magnetic materials and devices.

disadvantage of formulations based on the master equation approach is the inability to deal with experimentally relevant system sizes. Hence in the next part we will look at the problem of spin-injection from a ferromagnet to a semiconductor, termed as the conductivity mismatch problem [69, 70], from the semi-classical SDD point of view. Our goal will be to generalize the problem for three-dimensional experimental devices and study the effects of device geometry on the spin injection ratio, which is one of the most important prerequisites to build spintronic devices.

Thus in this chapter we have presented a brief synopsis of the various theoretical and numerical techniques available in the literature to address heat and spin transport. This chapter has also shed some light on the problems that will be addressed in the chapters to follow.

THIS PAGE IS INTENTIONALLY LEFT BLANK

Chapter 2

Reduced density matrix formulation

> Science is the belief in the
> ignorance of experts.
>
> —————————————————
>
> Richard Phillips Feynman

In this chapter, reduced density matrix (RDM) formulation within the framework of open quantum systems is introduced. The Redfield quantum master equation (RQME) is derived using a simplistic perturbative approach and several approximations typically used in the literature are discussed. A particular focus is on the steady-state accuracy and a unique analytic continuation approach is proposed to improve the accuracy of the Redfield solution up to second order in the system-bath coupling. Detailed verification of the analytic continuation approach is provided for the equilibrium case, whereas for the non-trivial non-equilibrium problem the method is numerically verified.

2.1 Redfield master equation

The theory of open quantum systems is one of the most promising fields to deal with anharmonic systems interacting with an environment. The main goal here is to calculate the reduced system dynamics in terms of the RDM, which typically is approached using a wide variety of approximate master equations [71, 72, 73, 74, 75].

2.1.1 Derivation from a microscopic model

In this section we will derive one of the most general perturbative master equation, known as the Redfield quantum master equation (RQME). The derivation outlined here employs only the *weak* system-bath coupling approximation and no other ad-hoc approximations will be made. Interested readers can refer to several textbooks [75, 76, 77] for alternative derivations. We start by defining a general Hamiltonian system given by,

$$H_{tot} \;\; = \;\; H_{\mathrm{S}} + \sum_{\alpha} \left(H_{\mathrm{B}}^{\alpha} + \lambda H_{\mathrm{SB}}^{\alpha} + \lambda^2 H_{\mathrm{RN}}^{\alpha} \right) , \qquad (2.1)$$

where H_{S} denotes a general anharmonic system Hamiltonian. Here

$$H_{\mathrm{B}}^{\alpha} \;\; = \;\; \sum_{n=1}^{\infty} \left(\frac{p_n^{\alpha^2}}{2m_n^{\alpha}} + \frac{m_n^{\alpha} \omega_n^{\alpha^2}}{2} x_n^{\alpha^2} \right) , \qquad (2.2)$$

describes the αth thermal environment as an infinite collection of harmonic

oscillators, each having a mass m_n^α and a frequency ω_n^α.

$$H_{\text{RN}}^\alpha \;=\; S^{\alpha^2}\left(\frac{1}{2}\sum_{n=1}^{\infty}\frac{c_n^{\alpha^2}}{m_n^\alpha\omega_n^{\alpha^2}}\right),\qquad (2.3)$$

is the potential renormalization in which the variable S^α denotes any system

operator connected with the αth bath and

$$\begin{aligned}H_{\text{SB}}^\alpha \;&=\; S^\alpha\otimes B^\alpha, &(2.4)\\[2mm] &=\; S^\alpha\otimes\left(-\sum_{n=1}^{\infty}c_n^\alpha x_n^\alpha\right),\end{aligned}$$

is the system-bath coupling Hamiltonian, wherein the c_n^α represent the

system-bath coupling constant of the n-th oscillator with the system op-

erator S^α. Typically, the potential renormalization term H_{RN} is included in

the system Hamiltonian, but this treatment leads to inconsistencies in the

perturbation expansion ($\because H_{\text{RN}}$ has a pre-factor of λ^2) and hence through-

out this thesis this term will be treated separately and consistently. The

collective bath operator is $B^\alpha = -\sum_{n=1}^{\infty}c_n^\alpha x_n^\alpha$. The above Hamiltonian has

been studied extensively to model quantum dissipation and goes under the

label of Zwanzig-Caldeira-Leggett model [78, 79, 80].

Throughout this thesis we will set $\hbar = 1$ and $k_{\text{B}} = 1$ and treat the bath

as a set of harmonic oscillators as described by Eq. (2.2), but the ideas

outlined here can be quite easily generalized to spin or fermionic baths.

The *total* density matrix at any time 't' is given by,

$$\rho_{tot}(t) = U(t, t_0)\rho_{tot}(t_0)U(t, t_0)^{\dagger}, \qquad (2.5)$$

where $U(t, t_0) = \exp\left[-i\left(H_S + \sum_{\alpha}\left(H_B^{\alpha} + \lambda H_{SB}^{\alpha} + \lambda^2 H_{RN}^{\alpha}\right)\right)\left(t - t_0\right)\right]$ is the time evolution operator. Expanding the evolution operator up to 2-nd order in the parameter λ using the Kubo identity[1] [81] and setting the initial time $t_0 = 0$ we obtain,

$$U(t, 0) = U_0(t, 0)U_I(t, 0),$$

$$U_0(t, 0) = e^{-i H_o t},$$

$$U_I(t, 0) = \mathbb{I} - \sum_{\alpha}\left(i\int_0^t ds\left(\lambda\tilde{H}_{SB}^{\alpha}(s) + \lambda^2\tilde{H}_{RN}^{\alpha}(s)\right)\right.$$
$$\left. + \lambda^2\int_0^t ds\tilde{H}_{SB}^{\alpha}(s)\int_0^s du\tilde{H}_{SB}^{\alpha}(u)\right), \qquad (2.6)$$

where $H_o = H_S + \sum_{\alpha} H_B^{\alpha}$, $U_I(t, 0)$ is the evolution operator in the interaction picture and all operators with $\sim$'s are the Heisenberg evolution (also known as free evolution) under H_o, that is, $\tilde{O}(x) = e^{i H_o x} O e^{-i H_o x}$.

---

[1]The exact Kubo identity is given by,

$$e^{\beta(A+B)} = e^{\beta A}\left[\mathbb{I} + \int_0^{\beta} d\beta' e^{-\beta' A} B e^{\beta'(A+B)}\right].$$

Differentiating Eq. (2.5) with respect to time t we obtain,

$$
\begin{aligned}
\frac{\mathrm{d}\rho_{tot}(t)}{\mathrm{d}t} &= -i\,[H_\circ, \rho_{tot}(t)] - \sum_\alpha \Bigg(i\,\left[\left(\lambda H_{SB}^\alpha + \lambda^2 H_{RN}^\alpha\right), \tilde{\rho}(t)\right] \\
&\quad + \lambda^2 \int_0^t \mathrm{d}q \Big\{ [\tilde{H}_{SB}^\alpha(q-t), \tilde{\rho}(t)]H_{SB}^\alpha + H_{SB}^\alpha[\tilde{\rho}(t), \tilde{H}_{SB}^\alpha(q-t)] \Big\} \Bigg),
\end{aligned}
\tag{2.7}
$$

where contrary to the operators $\tilde{\rho}(x) = \mathrm{e}^{-i\,H_\circ x}\,\rho\,\mathrm{e}^{i\,H_\circ x}$. Above and henceforth all operators without the time argument are assumed to be in the Schrödinger representation. While deriving Eq. (2.7) we have assumed that the different baths are uncorrelated and hence we have only one summation index α over the baths. Now using decoupled initial conditions[2] $\rho_{tot}(0) = \rho_S(0)\Pi_\alpha^\otimes \rho_B^\alpha(0)$, tracing over the bath degrees of freedom and using[3] $\langle B \rangle = 0$ we get,

$$
\frac{\mathrm{d}\rho(t)}{\mathrm{d}t} = -i\,[(H_S + \lambda^2 \sum_\alpha H_{RN}^\alpha), \rho(t)] + \lambda^2 \mathcal{R},
\tag{2.8}
$$

where $\rho(t)$ is the RDM of the system and the *relaxation* operator $\mathcal{R}$, which ensures that the system is damped by the bath, is given by,

$$
\begin{aligned}
\mathcal{R} &= -\sum_\alpha \int_0^t \mathrm{d}q \Big\{ [S^\alpha, \tilde{S}^\alpha(q-t)\rho(t)]\mathrm{C}^\alpha(t-q) \\
&\quad - [S^\alpha, \rho(t)\tilde{S}^\alpha(q-t)]\mathrm{C}^\alpha(q-t) \Big\}.
\end{aligned}
\tag{2.9}
$$

---

[2] $\Pi_\alpha^\otimes$ denotes tensor product over α matrices.

[3] If $\langle B \rangle \neq 0$ then add and subtract $\langle B \rangle$. The positive part is added to the system Hamiltonian and since it is a constant it only shifts the energy levels by a constant. This is commonly referred to as the centering of the bath.

Above $C^\alpha(t-q) = \langle B^\alpha \tilde{B}^\alpha(q-t) \rangle$ is the bath correlator. Since Eq. (2.8) is accurate up to 2-nd order in the coupling strength we have taken the liberty to replace $\tilde{\rho}_s(t)$ with $\rho(t)$ appropriately.

As shown in Append. (A) in case of the harmonic oscillator bath the bath correlator and the damping kernel at time $t = 0$ are given by,

$$C(\tau) = \int_0^\infty \frac{d\omega}{\pi} J(\omega) \left(\coth\left(\frac{\beta\omega}{2}\right) \cos(\omega\tau) - i\sin(\omega\tau) \right), \quad (2.10)$$

$$\gamma_0 = 2 \int_0^\infty \frac{d\omega}{\pi} \frac{J(\omega)}{\omega}, \quad (2.11)$$

where $J(\omega) = \pi \sum_{n=1}^\infty c_n / (2 m_n \omega_n) \, \delta(\omega - \omega_n)$ is the spectral density used to model the properties of the bath and β is the inverse temperature of the corresponding bath[4].

Using the damping kernel at zero time we can now recast the potential renormalization term in the Zwanzig-Caldeira-Leggett model as,

$$H_{RN} = S^2 \frac{\gamma_0}{2}. \quad (2.12)$$

The redundant super-script α has been dropped above and should be implicitly assumed henceforth for notational simplicity.

Now if we know the eigenvalues E_n and the eigenvectors $|n\rangle$ of the system Hamiltonian, i.e., $H_s|n\rangle = E_n|n\rangle$, we can re-write the freely evolving system

---

[4]Various methods to phenomenologically model the bath are given in Append. (A)

operator in the energy eigen-basis as

$$\langle n|\tilde{S}(\tau)|m\rangle \;=\; \mathrm{e}^{i\,\Delta_{nm}\tau}\,S\,,\tag{2.13}$$

where $\Delta_{nm} = E_n - E_m$. Appropriately inserting the Hubbard operators $X^{nm} = |n\rangle\langle m|$ in Eq. (2.8) and setting the dimensionless parameter $\lambda = 1$, we obtain the 2-nd order RQME in its time local representation as [73, 75, 76, 77]

$$\frac{\mathrm{d}\rho_{nm}}{\mathrm{d}t} \;=\; -i\,\Delta_{nm}\rho_{nm} + \sum_{ij}\mathcal{R}^{ij}_{nm}\rho_{ij}\,,\tag{2.14}$$

where the relaxation four tensor $\mathcal{R}^{ij}_{nm}$ is given by

$$\mathcal{R}^{ij}_{nm} \;=\; \sum_{\alpha}\left[S^{\alpha}_{ni}S^{\alpha}_{jm}\left(W^{\alpha}_{ni}+W^{\alpha*}_{mj}\right) - \delta_{j,m}\sum_{l}S^{\alpha}_{nl}S^{\alpha}_{li}W^{\alpha}_{li}\right.$$
$$\left. -\delta_{n,i}\sum_{l}S^{\alpha}_{jl}S^{\alpha}_{lm}W^{\alpha*}_{lj}\right].\tag{2.15}$$

Above the *transition* rates W^{α}_{ij} take the form

$$W_{ij} \;=\; W'_{ij} + i\,W''_{ij}\,,$$
$$W'_{ij} \;=\; \mathrm{Re}\left[\int_{0}^{t}\mathrm{d}\tau\,\mathrm{e}^{-i\,\Delta_{ij}\tau}\,\mathrm{C}(\tau)\right],$$
$$W''_{ij} \;=\; \mathrm{Im}\left[\int_{0}^{t}\mathrm{d}\tau\,\mathrm{e}^{-i\,\Delta_{ij}\tau}\,\mathrm{C}(\tau)\right] + \frac{\gamma_0}{2}\,.\tag{2.16}$$

Later, in order to make certain equations compact we define

$$
\begin{aligned}
\tilde{W}_{ij} &= \tilde{W}'_{ij} + i\,\tilde{W}''_{ij}, \\
\tilde{W}'_{ij} &= W'_{ij} = \mathrm{Re}\left[\int_0^t \mathrm{d}\tau\, \mathrm{e}^{-i\,\Delta_{ij}\tau}\, \mathrm{C}(\tau)\right], \\
\tilde{W}''_{ij} &= W''_{ij} - \frac{\gamma_0}{2} = \mathrm{Im}\left[\int_0^t \mathrm{d}\tau\, \mathrm{e}^{-i\,\Delta_{ij}\tau}\, \mathrm{C}(\tau)\right].
\end{aligned} \qquad (2.17)
$$

Both the definitions above W_{ij} and $\tilde{W}_{ij}$ will be interchangeably called as transition rates since they only differ by a constant in the imaginary part as shown in Eq. (2.17).

In Eq. (2.14) the effect of the various baths comes as an additive effect to the Redfield super-operator $\mathcal{R}$ and hence for most of this thesis the α summation will be dropped for notational simplicity. The reader from now on should always imagine an extra α summation inside the $\mathcal{R}$ super-operator if not explicitly specified. Also, in Eq. (2.14) and henceforth the explicit time dependence of ρ will also be suppressed.

While deriving the RQME we have made only the weak-coupling approximation, which implies that the strength of the collective coupling $\sum_n c_n$ should be weak. The above time-local form captures all the non-Markovian effects due to the explicit time dependence in the transition rates and greatly simplifies the steady state numerical calculations as compared to its equivalent time non-local [25, 26] counterpart.

2.1.2 Further assumptions and limitations

Solving the Redfield master equation is a numerically challenging task and hence several approximations are imposed on Eq. (2.14). One of the most commonly used assumptions in the secular approximation or the rotating-wave approximation (RWA) in which the terms rotating much faster than the characteristic frequencies of the problem are replaced by their average. Following ref. [82], in the rotating frame the reduced density matrix transforms into $\tilde{\rho}_{nm} = \rho_{nm} \exp[-i \Delta_{nm} t]$ and hence Eq. (2.14) reads,

$$\frac{\mathrm{d}\tilde{\rho}_{nm}}{\mathrm{d}t} = \sum_{ij} \mathcal{R}_{nm}^{ij} \tilde{\rho}_{ij} \, \mathrm{e}^{-i(\Delta_{ij} - \Delta_{nm})t} \ . \tag{2.18}$$

Now by assuming that the system energy spectrum has no degeneracy and averaging all terms of the form $\exp[-i(\Delta_{nm} - \Delta_{ij})t]$, where $\Delta_{nm} - \Delta_{ij} \neq 0$, to zero we obtain the RWA master equation as,

$$\frac{\mathrm{d}\rho_{nn}}{\mathrm{d}t} = \sum_{i} \mathcal{R}_{nn}^{ii} \rho_{ii} \, ,$$
$$\frac{\mathrm{d}\rho_{nm}}{\mathrm{d}t} = -i \Delta_{nm} \rho_{nm} + \mathcal{R}_{nm}^{nm} \rho_{nm} \, , \tag{2.19}$$

where the master equation is now split into diagonal and off-diagonal elements in the original unrotated basis. In RWA $\mathcal{R}_{nm}^{nm}$ is forced to contain only real parts which gives Eq. (2.19) exactly the same form as the Lindblad

master equation [76]. Importantly the dynamics of the diagonal elements using the RWA is same as the Pauli master equation [71].

Another common approximation used in the literature is known as neglecting the Lamb-shifts [75, 76]. In this approximation the imaginary part of the transition rates W_{ij} is set to zero, arguing that these lead to only a constant shift in the system energy spectrum. Surprisingly, after neglecting the Lamb-shifts in the steady state the equation takes the same form as the steady-state Pauli master equation.

Both the RWA and neglecting the Lamb-shifts are difficult to justify and unfortunately we cannot trace these approximations back to any microscopic model. Also the time transients given by all these models are quite different, but "fortunately" all these approximations lead to the same equilibrium state given by the canonical distribution. This observation itself gives us some hint that the approximated master equations are only valid in the limit $\lambda \to 0$ at long times, which we will discuss further in the next section.

2.2 Accuracy of perturbative master equations in the steady-state

The RQME obtained in Sec. 2.1.1 is a first order differential equation for the RDM and one naively expects that the solution of RQME is correct up to 2-nd order in the system-bath coupling strength. Some authors [83, 84]

have previously pointed out that this naive intuition might be misleading in the long time limit and here we try to corroborate this finding with a different method.

We start out with the generic perturbation series expansion[5] to all orders in the system-bath coupling of the time-local, formally exact master equation; i.e.,

$$\frac{\partial \rho}{\partial t} = \left(\bar{\Delta} + \sum_{n=2,4,6,\cdots}^{\infty} \lambda^n \mathrm{R}^{(n)}(t) \right) \rho \,, \tag{2.20}$$

and the reduced density matrix,

$$\rho = \sum_{n=0,2,4,\cdots}^{\infty} \lambda^n \rho^{(n)} \,. \tag{2.21}$$

Above $\bar{\Delta}$ is a four tensor depending on the system Hamiltonian. The operator $\mathrm{R}^{(n)}(t)$ denotes a super-operator of rank 4 which depends both on the system operator and the bath correlators[6]. We now rearrange ρ into a column vector and split it into its diagonal part (ρ_d) and off-diagonal part (ρ_od). Then, using the RQME (Eq. (2.14)) the 0-th order tensor in

---

[5]The series for ρ and $\frac{\partial \rho}{\partial t}$ holds if and only if $\langle B \rangle = 0$ for all baths, if not then the series will contain odd terms as well.

[6]Recall we set the initial time $t_0 = 0$ and hence the operator $\mathrm{R}^{(n)}(t)$ does not depend on t_0

Eq. (2.20) can be rewritten as a matrix assuming the form,

$$\bar{\Delta} \;\equiv\; \begin{pmatrix} 0 & 0 \\ 0 & \bar{\Delta}_{22} \end{pmatrix}, \qquad (2.22)$$

where $\bar{\Delta}_{22}$ is a diagonal matrix with Δ_{ij} $(i \neq j)$ forming the diagonal. The

four tensors $R^{(n)}(t)$ are also split accordingly; i.e.,

$$R^{(n)}(t) \;\equiv\; \begin{pmatrix} R_{11}^{(n)}(t) & R_{12}^{(n)}(t) \\ R_{21}^{(n)}(t) & R_{22}^{(n)}(t) \end{pmatrix}, \qquad (2.23)$$

with no restrictions made for the form of the sub-matrices. For the specific

case of $n = 2$, $R^{(2)}(t)$ is the same as the Redfield tensor given in Eq. (2.15).

In order to obtain the steady state we set $\partial\rho/\partial t = 0$ and take the limit

$t \to \infty$. Because the stationary problem is not dependent on time we will

drop the parentheses from the tensor, i.e., $R^{(n)}(\infty) \equiv R^{(n)}$. Therefore, using

Eqs. (2.20) and (2.21) we obtain:

$$\left(\bar{\Delta} + \sum_{n=2,4,6,\cdots}^{\infty} \lambda^n R^{(n)} \right) \sum_{m=0,2,4,\cdots}^{\infty} \lambda^m \rho^{(m)} = 0 \,. \qquad (2.24)$$

In order to obtain ρ correct up to 2-nd order we equate the coefficients

of the different powers of λ equal to zero so that we obtain independent

equations to calculate $\rho^{(0)}$ and $\rho^{(2)}$. This implies,

1. Setting the co-efficient of λ^0 equal to zero yields,

$$\rho_{\mathrm{od}}^{(0)} \;=\; 0 \,. \tag{2.25}$$

2. Setting the co-efficient of λ^2 equal to zero implies,

$$R_{11}^{(2)} \rho_{\mathrm{d}}^{(0)} \;=\; 0 \,, \tag{2.26}$$

$$\bar{\Delta}_{22} \rho_{\mathrm{od}}^{(2)} \;=\; -R_{21}^{(2)} \rho_{\mathrm{d}}^{(0)} \,. \tag{2.27}$$

3. Setting the co-efficient of λ^4 equal to zero provides the condition,

$$R_{11}^{(2)} \rho_{\mathrm{d}}^{(2)} \;=\; -R_{12}^{(2)} \rho_{\mathrm{od}}^{(2)} - R_{11}^{(4)} \rho_{\mathrm{d}}^{(0)} \,. \tag{2.28}$$

Equation (2.27) shows that in order to obtain the 2-nd order off-diagonal elements we need only the 0-th order and 2-nd order relaxation tensor which can be obtained from the RQME using Eq. (2.15). In contrast, in order to obtain the 2-nd order diagonal elements from Eq. (2.28) one requires knowledge of the 4-th order relaxation tensor $R_{11}^{(4)}$, which is difficult to obtain [85, 86, 87], and hence it is important to look at alternate techniques to obtain these 2-nd order diagonal elements correctly.

2.3 Second order steady-state density matrix

As seen in the previous section the RQME fails to give the correct solution in the steady state and is strictly valid in the limit $\lambda \to 0$. Also since the evaluation of the 4-th order relaxation tensor is highly cumbersome, in this section we will look at alternate techniques of obtaining the RDM correct up to 2-nd order of system-bath coupling.

2.3.1 Dyson expansion for open quantum systems

Our first alternative approach is based on the Dyson expansion. In this approach we do not obtain a differential equation in $\rho(t)$ as we did for the RQME, but rather obtain a linear equation for $\rho(t)$ starting from Eq. (2.5). Since we have already expanded the evolution operator $U(t,0)$ in Eq. (2.6) we use it in Eq. (2.5) to obtain,

$$
\begin{aligned}
\rho_{tot} &= \tilde{\rho}_{tot}(t) - i\,\lambda \int_0^t \mathrm{d}u\,\Big[\tilde{H}_{SB}(u-t),\tilde{\rho}_{tot}(t)\Big] \\
&\quad + \lambda^2 \int_0^t \mathrm{d}u \int_0^u \mathrm{d}q\,\Big\{\tilde{H}_{SB}(u-t)\Big[\tilde{\rho}_{tot}(t),\tilde{H}_{SB}(q-t)\Big] \\
&\quad + \Big[\tilde{H}_{SB}(q-t),\tilde{\rho}_{tot}(t)\Big]\tilde{H}_{SB}(u-t)\Big\}\,.
\end{aligned}
\tag{2.29}
$$

The right hand side of the above equation contains only the freely evolving density matrix $\tilde{\rho}_{tot}(t)$. Since we will choose decoupled thermal equilibrium initial conditions and $[H_\mathrm{o}, \rho_{tot}(0)] = 0$, the freely evolving density matrix

$\tilde{\rho}_{tot}(t) = \rho_{tot}(0) = \rho_{\rm S}(0) \otimes \rho_{\rm B}(0)$. Here itself we get a hint that there is something possibly wrong with the Dyson expansion because even in the long time the reduced density matrix will depend on the initial condition of the system. Ignoring this anomaly we try to evaluate the 2-nd order terms obtained from this expansion. After tracing the bath degrees of freedom and setting $\lambda = 1$ we get,

$$
\begin{aligned}
\rho^{(2)}(t) &= \int_0^t {\rm d}u \int_0^t {\rm d}q \tilde{S}(u-t)\tilde{\rho}(t)\tilde{S}(q-t){\rm C}(u-q) \\
&\quad - \int_0^t {\rm d}u \int_0^u {\rm d}q \tilde{S}(u-t)\tilde{S}(q-t)\tilde{\rho}(t){\rm C}(q-u) \\
&\quad - \int_0^t {\rm d}u \int_0^u {\rm d}q \tilde{\rho}(t)\tilde{S}(q-t)\tilde{S}(u-t){\rm C}(u-q) , \qquad (2.30)
\end{aligned}
$$

where $\rho^{(2)}(t)$ is the 2-nd order reduced density matrix. Now inserting the Hubbard operators X^{nm} appropriately and calculating only the 2-nd order off-diagonal elements we obtain,

$$
\rho^{(2)}_{nm} = i \sum_i \frac{S_{ni}S_{im}}{\Delta_{nm}} \left[W^*_{in}\tilde{\rho}_{nn} + W_{im}\tilde{\rho}_{mm} - \left(W_{ni} + W^*_{mi} \right)\tilde{\rho}_{ii} \right], (2.31)
$$

where the transition rates have been defined in Eq. (2.16). In case of the diagonal elements we get,

$$
\rho^{(2)}_{nn} = \sum_i S_{ni}S_{in} \left[\int_0^t {\rm d}u \int_0^t {\rm d}q \, {\rm e}^{-i\,\Delta_{ni}(u-q)} \, {\rm C}(u-q)\tilde{\rho}_{ii} \right.
$$

$$-\int_0^t du \int_u^t dq \left\{ e^{-i\,\Delta_{ni}(u-q)}\,C(q-u) + c.c \right\} \tilde{\rho}_{nn} \Bigg] \,, \quad (2.32)$$

where c.c indicates complex conjugate. In order to simplify the diagonal terms we change the integration variables $u - q = \tau$ and $u + q = \tau'$. The change of variables allows us to integrate the τ' integral analytically to obtain,

$$\rho_{nn}^{(2)} \;=\; \sum_i S_{ni} S_{in} \left[\bar{V}_{ni} \rho_{ii}^{(0)} - \bar{V}_{in} \rho_{nn}^{(0)} \right] \,,$$

where

$$\bar{V}_{ni} \;=\; \int_0^t d\tau (t-\tau)\, e^{-i\,\Delta_{ni}\tau}\, C(\tau) + \int_0^t d\tau (t-\tau)\, e^{i\,\Delta_{ni}\tau}\, C^*(\tau) \,. (2.33)$$

Clearly the operator $\bar{V}$ has a divergent ($\propto t$) and a non-divergent part in the steady state. Thus with the Dyson expansion we end up with two major problems:

1. The density matrix in the long time limit depends on the initial condition.

2. At second order itself the diagonal terms of the RDM diverge.

Despite these difficulties, the RQME gives us one heuristic method to resolve these issues. Let us look at the 2-nd order off-diagonal elements

obtained from the RQME via Eqs. (2.27) and (2.15),

$$\rho_{nm}^{(2)} \;=\; i \sum_i \frac{S_{ni}S_{im}}{\Delta_{nm}} \left[W_{in}^* \rho_{nn}^{(0)} + W_{im} \rho_{mm}^{(0)} - \left(W_{ni} + W_{mi}^* \right) \rho_{ii}^{(0)} \right].(2.34)$$

Comparing the above equation with Eq. (2.31) we are prompted to believe $\tilde{\rho} \equiv \rho^{(0)}$, where $\rho^{(0)}$ is obtained via the RQME using Eqs. (2.25), (2.26) and (2.15) as

$$\sum_i \left(S_{ni}S_{in}\tilde{W}_{ni}' - \delta_{n,i} \sum_l S_{nl}S_{li}\tilde{W}_{li}' \right) \rho_{ii}^{(0)} \;=\; 0\,,$$

$$\rho_{ij}^{(0)} \;=\; 0\,, \quad (i \neq j)\,, \quad (2.35)$$

along with an additional constrain $\mathrm{Tr}(\rho^{(0)}) = 1$. If we believe this equivalence is true then it immediately solves our first problem because now the density matrix at long times will not depend on the initial conditions. It also ensures that the equilibrium RDM at zero system-bath coupling is the canonical distribution. Miraculously the co-efficient of the divergent term in 2-nd order RDM is equal to $\sum_i \left(S_{ni}S_{in}\tilde{W}_{ni}' - \delta_{n,i} \sum_l S_{nl}S_{li}\tilde{W}_{li}' \right) \rho_{ii}^{(0)}$, which according to Eq. (2.35) is zero in the steady state. Hence the steady-state RDM does not diverge. Thus by this ad-hoc procedure we can compute the RDM up-to 2-nd order as,

$$\sum_i \left(S_{ni}S_{in}\tilde{W}_{ni}' - \delta_{n,i} \sum_l S_{nl}S_{li}\tilde{W}_{li}' \right) \rho_{ii}^{(0)} = 0\,,$$

$$\rho_{nm}^{(0)} = 0 \,,$$

$$\rho_{nm}^{(2)} = i \sum_i \frac{S_{ni} S_{im}}{\Delta_{nm}} \left[W_{in}^* \rho_{nn}^{(0)} + W_{im} \rho_{mm}^{(0)} - \left(W_{ni} + W_{mi}^* \right) \rho_{ii}^{(0)} \right],$$

$$\rho_{nn}^{(2)} = 2 \sum_i S_{ni} S_{in} \left[V_{ni}'' \rho_{ii}^{(0)} - V_{in}'' \rho_{nn}^{(0)} \right] , \qquad (2.36)$$

where

$$V_{ni}'' = \frac{1}{2} \left(\int_0^t d\tau \tau \, e^{-i \Delta_{ni} \tau} \, C(\tau) + \int_0^t d\tau \tau \, e^{i \Delta_{ni} \tau} \, C^*(\tau) \right) ,$$

$$\therefore V_{ni}'' = \frac{\partial \tilde{W}_{ni}''}{\partial \Delta_{ni}} \,. \qquad (2.37)$$

Naively, even though the above procedure seems logical, we will see later in Sec.2.4.1 that it does not match the results from canonical perturbation theory. This indicates that the ad-hoc equivalence $\tilde{\rho} \equiv \rho^{(0)}$ does not seem to give the right physics. Despite this fact one important lesson we learn is that in case of open quantum systems it is extremely important to include effects of the baths even for the 0-th order RDM.

2.3.2   Analytic continuation approach: Modified Red-field Solution

As seen above, due to the various problems with the Dyson expansion the steady-state RDM is incorrect and hence we will now look at an alternative procedure to obtain the stationary RDM correct up to 2-nd order in the

system-bath coupling. As seen in Sec.2.2 the RQME gives the 0-th order
and the 2-nd order off-diagonal elements of the RDM correctly. Therefore,
we use Eqs. (2.25) and (2.26) along with the Redfield tensor $\mathcal{R} = \mathrm{R}^{(2)}$ to
arrive at the 0-th order RDM,

$$\sum_i \left(S_{ni} S_{in} \tilde{W}'_{ni} - \delta_{n,i} \sum_l S_{nl} S_{li} \tilde{W}'_{li} \right) \rho_{ii}^{(0)} = 0,$$

$$\rho_{ij}^{(0)} = 0, \quad (i \neq j). \quad (2.38)$$

The 2-nd order off-diagonal elements, i.e., $n \neq m$ follow from Eq. (2.27)
as,

$$\rho_{nm}^{(2)} = i \sum_i \frac{S_{ni} S_{im}}{\Delta_{nm}} \left[W_{in}^* \rho_{nn}^{(0)} + W_{im} \rho_{mm}^{(0)} - \left(W_{ni} + W_{mi}^* \right) \rho_{ii}^{(0)} \right]. (2.39)$$

If we naively construct the diagonal elements by merely substituting
$n = m$ in Eq. (2.39), then the equation exhibits an indeterminate $0/0$
singularity. This indicates that even though we cannot substitute $n = m$
directly, the limit $m \to n$ might exist. If such a limit indeed exists and is
unique, then by use of the uniqueness theorem [88] the 2-nd order diagonal
elements can be obtained by this limiting procedure. In order to perform
this limit $m \to n$ we consider each element of the 2-nd order RDM to
be a function of the bare system energies E_i $(i = 1, \cdots, N)$. In the energy
parameter space we vary only one of the energies E_m and let it continuously

approach the energy E_n, via a small complex parameter z; i.e., we set $E_m \to E_n - z$.

In doing so, we start by splitting the transition rates W_{ij} into its real and its imaginary parts, using Eq. (2.17) to obtain:

$$
\begin{aligned}
\rho_{nm}^{(2)} &= \frac{1}{i\,\Delta_{nm}} \sum_i S_{ni} S_{im} \Bigg\{ \left[\left(\tilde{W}_{ni}' + \tilde{W}_{mi}' \right) \rho_{ii}^{(0)} - \tilde{W}_{in}' \rho_{nn}^{(0)} - \tilde{W}_{im}' \rho_{mm}^{(0)} \right] \\
&\quad + i \left[\left(\tilde{W}_{ni}'' - \tilde{W}_{mi}'' \right) \rho_{ii}^{(0)} + \left(\tilde{W}_{in}'' + \frac{\gamma_0}{2} \right) \rho_{nn}^{(0)} \right. \\
&\quad - \left. \left(\tilde{W}_{im}'' + \frac{\gamma_0}{2} \right) \rho_{mm}^{(0)} \right] \Bigg\}.
\end{aligned}
\tag{2.40}
$$

We next let $E_m \to E_n - z$ and perform the limit $z \to 0$. Therefore, Eq. (2.40) becomes,

$$
\begin{aligned}
\rho_{nn}^{(2)} &= \lim_{z \to 0} \Bigg\{ \frac{1}{i\,z} \sum_i S_{ni} S_{in} \left[\left(\tilde{W}_{ni}'(0) + \tilde{W}_{ni}'(-z) \right) \rho_{ii}^{(0)} \right. \\
&\quad - \left. \left(\tilde{W}_{in}'(0) + \tilde{W}_{in}'(z) \right) \rho_{nn}^{(0)} \right] \\
&\quad + \frac{1}{z} \sum_i S_{ni} S_{in} \left[\left(\tilde{W}_{ni}''(0) - \tilde{W}_{ni}''(-z) \right) \rho_{ii}^{(0)} \right. \\
&\quad - \left(\tilde{W}_{in}''(0) - \tilde{W}_{in}''(-z) \right) \rho_{nn}^{(0)} \\
&\quad + \left. \left(\tilde{W}_{in}''(-z) + \frac{\gamma_0}{2} \right) z \frac{\partial \rho_{nn}^{(0)}}{\partial E_n} \right] \Bigg\},
\end{aligned}
\tag{2.41}
$$

where,

$$
\begin{aligned}
\tilde{W}_{ij}(z) &= \int_0^\infty \mathrm{d}\tau\, \mathrm{e}^{-i\,(\Delta_{ij}+z)\tau}\, \mathrm{C}(\tau)\,, \\
\tilde{W}_{ij}^*(z) &= \int_0^\infty \mathrm{d}\tau\, \mathrm{e}^{i\,(\Delta_{ij}+z^*)\tau}\, \mathrm{C}^*(\tau)\,.
\end{aligned}
\tag{2.42}
$$

Because $\rho_{mm}^{(0)}$ (being the un-normalized 0-th order RDM) depends on the energy E_m we made use of the Taylor expansion of $\rho_{mm}^{(0)}$ around the energy E_n to retain up to the first order:

$$
\lim_{E_m \to E_n} \rho_{mm}^{(0)} \simeq \rho_{nn}^{(0)} + z\frac{\partial \rho_{nn}^{(0)}}{\partial E_n}\,.
\tag{2.43}
$$

Noting that $\lim_{z \to 0} \tilde{W}_{in}''(-z) = \tilde{W}_{in}''(0) = \tilde{W}_{in}''$ Eq. (2.41) can be recast as,

$$
\rho_{nn}^{(2)} = \sum_i S_{ni}S_{in}\left[V_{ni}''\rho_{ii}^{(0)} - V_{in}''\rho_{nn}^{(0)}\right] + W_{in}''\frac{\partial \rho_{nn}^{(0)}}{\partial E_n} + \bar{\rho}_{nn}^{(2)}\,,
\tag{2.44}
$$

where we have absorbed γ_0 in W according to Eq. (2.17) and ,

$$
\begin{aligned}
\bar{\rho}_{nn}^{(2)} = \lim_{z \to 0}\frac{1}{i\,z}\Bigg\{ &\sum_i S_{ni}S_{in}\left[\left(\tilde{W}_{ni}'(0) + \tilde{W}_{ni}'(-z)\right)\rho_{ii}^{(0)}\right. \\
&\left. - \left(\tilde{W}_{in}'(0) + \tilde{W}_{in}'(z)\right)\rho_{nn}^{(0)}\right]\Bigg\}\,,
\end{aligned}
\tag{2.45}
$$

and V_{ij}'' has been defined in Eq. (2.37). In the limit $z \to 0$ it follows from Eq. (2.42) that $\lim_{z \to 0} \tilde{W}_{ni}'(-z) = \lim_{z \to 0} \tilde{W}_{ni}'(z) = \tilde{W}_{ni}'(0) = \tilde{W}_{ni}'$.

Therefore, in this limit the term in the curly bracket in Eq. (2.45) assumes precisely the same form as the L.H.S. of Eq. (2.38), hence it is equal to zero. Consequently, Eq. (2.44) becomes,

$$\rho_{nn}^{(2)} = \sum_i S_{ni} S_{in} \left[V''_{ni} \rho_{ii}^{(0)} - V''_{in} \rho_{nn}^{(0)} + W''_{in} \frac{\partial \rho_{nn}^{(0)}}{\partial E_n} \right] . \qquad (2.46)$$

Eq. (2.46) is independent of the way in which the energy E_m approaches E_n and hence this limit procedure is unique. The uniqueness of the limit is crucial to ensure that the resulting thermal steady state of the system is also unique.

The diagonal elements of the density matrix obey the normalization condition $\text{Tr}(\rho) = 1$. Since we performed an analytic continuation to obtain the 2-nd order diagonal elements there is no guarantee the normalization condition is preserved. Therefore we can write the normalization condition explicitly as,

$$\begin{aligned} \rho_{nn} &= \frac{\rho_{nn}^{(0)} + \rho_{nn}^{(2)}}{\sum_i (\rho_{ii}^{(0)} + \rho_{ii}^{(2)})} \\ &\simeq \rho_{nn}^{(0)} + \rho_{nn}^{(2)} - \rho_{nn}^{(0)} \sum_i \rho_{ii}^{(2)}, \end{aligned} \qquad (2.47)$$

where we have ignored the 4-th and higher order terms and used the condition $\sum_i \rho_{ii}^{(0)} = 1$, which is required to determine $\rho^{(0)}$ uniquely. Therefore,

upon normalizing Eq. (2.46) with help of Eq. (2.47) we obtain,

$$
\begin{aligned}
\rho_{nn}^{(2)} &= \sum_i S_{ni} S_{in} \left[V_{ni}'' \rho_{ii}^{(0)} - V_{in}'' \rho_{nn}^{(0)} + W_{in}'' \frac{\partial \rho_{nn}^{(0)}}{\partial E_n} \right] \\
&\quad - \rho_{nn}^{(0)} \sum_{i,j} S_{ji} S_{ij} W_{ij}'' \frac{\partial \rho_{jj}^{(0)}}{\partial E_j} \, .
\end{aligned}
\tag{2.48}
$$

In order to use Eq. (2.48) to calculate the 2-nd order diagonal elements we need to know the derivative of the 0-th order RDM $\partial \rho_{nn}^{(0)} / \partial E_n$. This derivative derives from Eq. (2.38), which is satisfied by $\rho^{(0)}$ and subsequently differentiate with respect to the energy E_n to find

$$
\frac{\partial \rho_{nn}^{(0)}}{\partial E_n} = \frac{\sum_{i \neq n} S_{ni} S_{in} \left(V_{ni}' \rho_{ii}^{(0)} + V_{in}' \rho_{nn}^{(0)} \right)}{\sum_{i \neq n} S_{ni} S_{in} \tilde{W}_{in}'} \, ,
\tag{2.49}
$$

where $V_{ij}' = \partial \tilde{W}_{ij}' / \partial \Delta_{ij}$.

The procedure to obtain the modified Redfield solution (MRS) outlined above (Eqs. (2.38), (2.39) and (2.48)) is quite well suited for numerical studies: Numerical simulations with the RQME are very cumbersome because the Redfield super-operator $\mathcal{R}$ scales as the fourth power [77] of the system Hilbert space dimension N. Therefore, in the steady state the computational complexity of the problem typically scales proportional to N^6, assuming that the analytic forms of the transition rates W_{ij} are known. On the other hand, in our MRS all components of the RDM can be obtained by reference to the transition rates W_{ij} only, which scale as N^2. Thus,

in the modified solution the computational complexity becomes drastically reduced to be of order N^3. This fact is equivalent to solving the quantum master equation with use of the continued fraction scheme [89]; it thus enables us to study systems with much larger Hilbert space dimension.

2.4 Verifying the Modified Redfield Solution

In this section we validate the conjecture, that the MRS is the correct distribution up to 2-nd order in the system-bath coupling[7]. In the equilibrium case we provide an analytical proof by comparing the MRS with the generalized Gibbs distribution via canonical perturbation theory (CPT), whereas in the non-equilibrium case since the form of the steady-state density matrix is unknown we provide numerical evidence to validate our solution.

2.4.1 Comparison with canonical perturbation theory

In equilibrium, the RDM of a system connected finitely with a heat bath is given by the generalized Gibbs distribution [90] $\rho^{\mathrm{eq}} \propto \mathrm{Tr_B}(\mathrm{e}^{-\beta H_{\mathrm{tot}}})$. Cognizance of this fact allows us to formulate a perturbative expansion for the generalized Gibbs distribution termed as canonical perturbation theory, as shown in Append. B.

According to CPT (Eqs. (B.11), (B.12), and (B.13)) the reduced density

---

[7]Comparing Eqs. (2.48) and (2.36) we immediately see that the MRS and Dyson expansion do not match. In this section we will prove that the MRS matches CPT implying that the Dyson expansion does not.

matrix up to 2-nd order in the system-bath coupling reads

$$\rho_{nm}^{\mathrm{CPT}} = \rho_{nm}^{(0),\mathrm{CPT}} + \rho_{nm}^{(2),\mathrm{CPT}},$$

$$\rho_{nm}^{(0),\mathrm{CPT}} = \frac{\mathrm{e}^{-\beta E_n}}{Z_{\mathrm{S}}}\delta_{n,m}, \tag{2.50}$$

$$\rho_{nm}^{(2),\mathrm{CPT}} = \frac{D_{nm}}{Z_{\mathrm{S}}} - \frac{\mathrm{e}^{-\beta E_n}\sum_i D_{ii}}{(Z_{\mathrm{S}})^2}\delta_{n,m}, \tag{2.51}$$

wherein $Z_{\mathrm{S}} = \sum_l \exp[-\beta E_l]$ and the D matrix elements are given by,

$$D_{nm} = \frac{1}{\Delta_{mn}}\sum_l \left(\tilde{D}_{nl}S_{lm} - \tilde{D}_{ml}S_{ln}\right) \quad (n \neq m),$$

$$\tilde{D}_{nl} = S_{nl}\,\mathrm{e}^{-\beta E_n}\left(\int_0^\beta \mathrm{d}x\mathrm{C}(-i\,x)\,\mathrm{e}^{-x\Delta_{ln}} - \frac{\gamma_0}{2}\right). \tag{2.52}$$

$$D_{nn} = \sum_l \bar{D}_{nl}S_{ln},$$

$$\bar{D}_{nl} = S_{nl}\,\mathrm{e}^{-\beta E_n}\left[\beta\left(\int_0^\beta \mathrm{d}x\mathrm{C}(-i\,x)\,\mathrm{e}^{-x\Delta_{ln}} - \frac{\gamma_0}{2}\right)\right.$$
$$\left. - \int_0^\beta \mathrm{d}x\mathrm{C}(-i\,x)x\,\mathrm{e}^{-x\Delta_{ln}}\right]. \tag{2.53}$$

2.4.1.1 Comparing the 0-th order result

Let us first compare the 0-th order reduced density matrix. For the harmonic baths described by Eq. (2.2) it can be shown that the bath correlator $\mathrm{C}(\tau)$ obeys the Kubo-Martin-Schwinger (KMS) condition [1, 81, 91] $\mathrm{C}(-\tau) = \mathrm{C}(\tau - i\,\beta)$. This implies that the real part of the transition rates

$\tilde{W}'_{ij}$ obey the detailed balance condition [92] given by,

$$\tilde{W}'_{ij} = e^{-\beta\Delta_{ij}} \tilde{W}'_{ji}. \tag{2.54}$$

Thus an analytic form of the 0-th order MRS can be obtained upon using Eq. (2.38) as,

$$\rho^{(0)}_{nm} = \frac{e^{-\beta E_n}}{Z_S}\delta_{n,m}, \tag{2.55}$$

where $Z_{\mathrm{s}} = \sum_l e^{-\beta E_l}$. A direct comparison between Eq. (2.55) and Eq. (2.50) yields the expected result that at the 0-th order CPT agrees with our 0-th order MRS.

2.4.1.2 Comparing the 2-nd order result

More intriguing is the comparison of the MRS with the 2-nd order CPT-result. The 2-nd order reduced density matrix obtained from CPT can be manipulated further so that it indeed matches precisely our MRS. In order to demonstrate this we first simplify the integral occurring in $\tilde{D}$ (Eq. (2.52)) by using the definition of the bath correlator $C(\tau)$ (Eq. (2.10)) to obtain

$$\int_0^\beta dx C(-i\,x)\,e^{-x\Delta_{ij}} = -\int_0^\infty \frac{d\omega}{\pi} J(\omega)\left(\frac{n_\omega}{\omega - \Delta_{ij}} - \frac{(n_\omega + 1)}{\omega + \Delta_{ij}}\right) \tag{2.56}$$
$$-\frac{e^{-\beta\Delta_{ij}}}{\pi}\int_0^\infty d\omega J(\omega)\left(\frac{n_\omega}{\omega + \Delta_{ij}} - \frac{(n_\omega + 1)}{\omega - \Delta_{ij}}\right),$$

where we have interchanged the ω- (stemming from $C(\tau)$) and x- integration

and performed the x-integral analytically. We next express the right hand side in terms of the transition rates $\tilde{W}_{ij}$, which enter in our MRS. Using the Sokhotskyi-Plemelj formula[8] [93] the imaginary part of the transition rates is given by,

$$\tilde{W}''_{ij} = P \int_0^\infty \frac{d\omega}{\pi} J(\omega) \left(\frac{n_\omega}{\omega - \Delta_{ij}} - \frac{(n_\omega + 1)}{\omega + \Delta_{ij}} \right). \tag{2.57}$$

Therefore, using the above equation, Eq. (2.56) can be expressed as,

$$-\int_0^\beta dx\, e^{-x\Delta_{ij}}\, C(-i\,x) = \tilde{W}''_{ij} + e^{-\beta\Delta_{ij}}\, \tilde{W}''_{ji}. \tag{2.58}$$

2-nd order off-diagonal comparison

Upon use of Eq. (2.58) the 2-nd order off-diagonal elements from CPT (Eq. (2.51)) can be expressed in terms of W''_{ij} as

$$
\begin{aligned}
\rho^{(2),\mathrm{CPT}}_{nm} &= \frac{1}{\Delta_{nm}} \sum_i S_{ni} S_{im} \left[\frac{e^{-\beta E_i}}{Z_S} \left(W''_{ni} - W''_{mi} \right) \right. \\
&\quad \left. + \frac{e^{-\beta E_n}}{Z_S} W''_{in} - \frac{e^{-\beta E_m}}{Z_S} W''_{im} \right],
\end{aligned}
\tag{2.59}
$$

where we have absorbed the γ_0 into $\tilde{W}''_{ij}$, according to Eq. (2.17). Formally

---

[8]The Sokhotskyi-Plemelj formula is given by,

$$\int_0^\infty e^{\pm i\,\Omega\tau}\, d\tau = \pi\delta(\Omega) \pm i\, P\left(\frac{1}{\Omega} \right).$$

Here, P denotes the principal value.

adding the real part of the transition rates W'_{ij} into Eq. (2.59), but noting that this so added contributions vanish identically by virtue of detailed balance (Eq. (2.54)), we find the result for $n \neq m$ as,

$$
\rho_{nm}^{(2),\text{CPT}} = i \sum_i \frac{S_{ni} S_{im}}{\Delta_{nm}} \left[W_{in}^* \frac{e^{-\beta E_n}}{Z_S} + W_{im} \frac{e^{-\beta E_m}}{Z_S} \right.
$$
$$
\left. - (W_{ni} + W_{mi}^*) \frac{e^{-\beta E_i}}{Z_S} \right] . \tag{2.60}
$$

Upon comparing Eq. (2.39) with Eq. (2.60) we find that the CPT and our modified Redfield solution are identical.

2-nd order diagonal comparison

Most importantly, we next test the agreement between the 2-nd order diagonal elements from CPT with our MRS. Noting that the integral occurring in Eq. (2.53) is the derivative of Eq. (2.58) w.r.t Δ_{ij} we obtain,

$$
\rho_{nn}^{(2),\text{CPT}} = \sum_i S_{ni} S_{in} \left(\frac{e^{-\beta E_i}}{Z_S} V''_{ni} - \frac{e^{-\beta E_n}}{Z_S} V''_{in} \right)
$$
$$
- \beta \frac{e^{-\beta E_n}}{Z_S} \left[\sum_i S_{ni} S_{in} W''_{in} - \sum_{i,l} S_{li} S_{il} \frac{e^{-\beta E_l}}{Z_S} W''_{il} \right] , \tag{2.61}
$$

where V''_{ij} has been defined in Eq. (2.37). Because $\partial \rho_{ii}^{(0)} / \partial E_i = -\beta \rho_{ii}^{(0)}$, Eq. (2.48) exactly matches Eq. (2.61). Thus, CPT up to 2-nd order and our MRS are indeed in perfect agreement. This shows that in the weak, but finite coupling limit the long-time thermal reduced density matrix stemming

from a non-Markovian theory is of the generalized Gibbs form, a point which has been a topic of fierce debate in the literature [81, 94, 95, 96].

2.4.2 Numerical verification

As seen in the previous section the MRS is accurate up to second order in system-bath coupling for a system in equilibrium. In this section our goal will be two-fold:

1. To numerically verify the MRS for a system connected with two baths.

2. To compare the MRS with some of the other commonly used master equations.

In the nonequilibrium case with two temperatures T_L and T_R one of the main challenges has been to obtain a general form of the reduced density matrix. Till date very little progress has been made in this field and *exact* results are only available for a system of harmonic oscillators [97].

In order to numerically compare our results with the exact results of Dhar *et al.* [97] obtained via nonequilibrium Greens function (NEGF) techniques [44] we choose the system Hamiltonian to be a single harmonic oscillator given by,

$$H_s \;\;=\;\; \frac{p^2}{2M} + \frac{1}{2}M\omega_0^2 x^2\,, \tag{2.62}$$

where $x, p, M,$ and ω_0 are the position, momentum, mass and angular fre-

quency of the oscillator, respectively. The above Hamiltonian also turns

out to be an explicit and simple example where the rotating wave approxi-

mation described in sec. 2.1.2 cannot be correctly applied thus ensuring the

usefulness of the MRS.

The system is connected linearly to two baths, via the position coor-

dinate, having temperatures T_L and T_R. This implies that in Eq. (2.4)

$S^{L,R} = x$. Both the baths are chosen to be of the Lorentz-Drude type with

$$J(\omega) = \frac{M\gamma\omega}{1 + (\omega/\omega_D)^2}, \tag{2.63}$$

where ω_D is the cut-off frequency and γ is the phenomenological Stoke-

sian damping coefficient (Append. A.3.3) and the imaginary parts of the

transition rates $\tilde{W}''_{ij}$ are calculated using the Richardson extrapolation (Ap-

pend. A.4). The reduced density matrix is then calculated order by order

and we use the QR algorithm [98] to obtain the zeroth order RDM with the

additional constraint $\text{Tr}(\rho^{(0)}) = 1$. Once the zeroth order RDM is known

the second order is easily calculated and the overall computational com-

plexity of the algorithm is only N^3, due to the QR algorithm, where N is

the system Hilbert space dimension.

Next we define a discrepancy error DE^X by,

$$DE^X = \frac{\rho^{NEGF} - \rho^X}{\gamma/\omega_0}, \tag{2.64}$$

where ρ^{NEGF} is the exact reduced density matrix via NEGF, ρ^{X} is the reduced

density matrix obtained from other perturbative method; being either the

modified Redfield solution (X = MRS) or the Redfield quantum master

equation (X = RQME) and γ/ω_0 is a dimensionless parameter specifying

the system-bath coupling strength.

At the lowest order, i.e. 0-th order, it can be quite easily shown that

the MRS, RQME and NEGF match. This should be expected since as we

saw in Sec. 2.2 the error in the RDM is at the 2-nd order in system-bath

coupling and not the 0-th order. Also since γ/ω_0 is $O(\lambda^2)$ it is obvious

that if ρ^{X} (X = MRS or RQME) matches ρ^{NEGF} up to 2-nd order then the

discrepancy error DE^{X} should be zero in the limit $\gamma/\omega_0 \to 0$.

In Fig.2.1 we plot the discrepancy error for only the ground state of

the RDM. Since we have kept the temperature low the ground state is a

good representation of the RDM. As shown in the top panel as $\gamma/\omega_0 \to 0$

the discrepancy error vanishes clearly indicating that the MRS matches the

NEGF result up to 2-nd order in system-bath coupling. Whereas in case

of the RQME the discrepancy error (Fig. 2.1: bottom panel) is a constant

as $\gamma/\omega_0 \to 0$. Thus, it seems that for the nonequilibrium problem as well,

the MRS gives an accurate solution up to 2-nd order in the system-bath

coupling whereas the RQME fails completely in this limit. Temperature

difference (Temperature) does not seem to play a role here and for all tem-
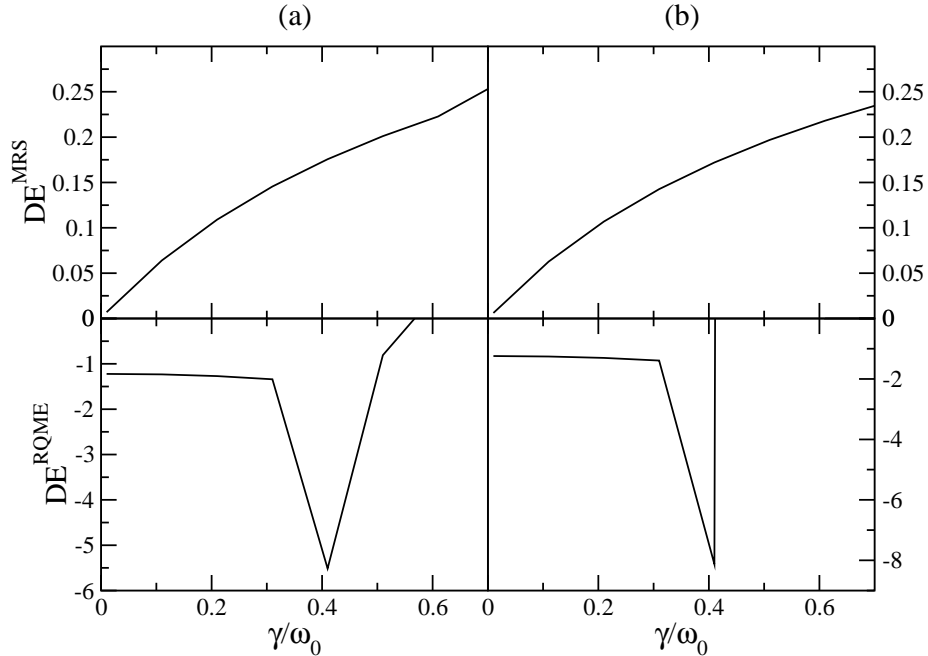
Figure 2.1: Plot of discrepancy error for the ground state population as a function of dimensionless system-bath coupling strength (γ/ω_0) for a harmonic oscillator connected to two heat baths. Top panel shows the discrepancy error for the MRS and the bottom panel is for the RQME. Figure (a) is for temperatures $T_L = 156K$ and $T_R = 140K$, whereas figure (b) is for $T_L = 156K$ and $T_R = 78K$. Other parameters used for the calculation are: $M = 1u$, $\omega_0 = 1.3 \times 10^{14}$ Hz, and $\omega_D = 10\omega_0$.

perature differences (temperatures) the features are nearly the same[9]. This is illustrated by Fig. 2.1(b) which has a greater temperature difference but the essential features are the similar to Fig. 2.1(a).

Next we compare the populations of the lowest few levels of the MRS with those obtained from Redfield quantum master equation and Lindblad master equation as shown in Fig. 2.2. The model is again a single particle harmonic oscillator linearly coupled to Lorentz-Drude heat baths. For this

[9]In case of higher temperature even the higher energy levels are populated and hence one needs to look at discrepancy error as a matrix for different values of γ/ω_0
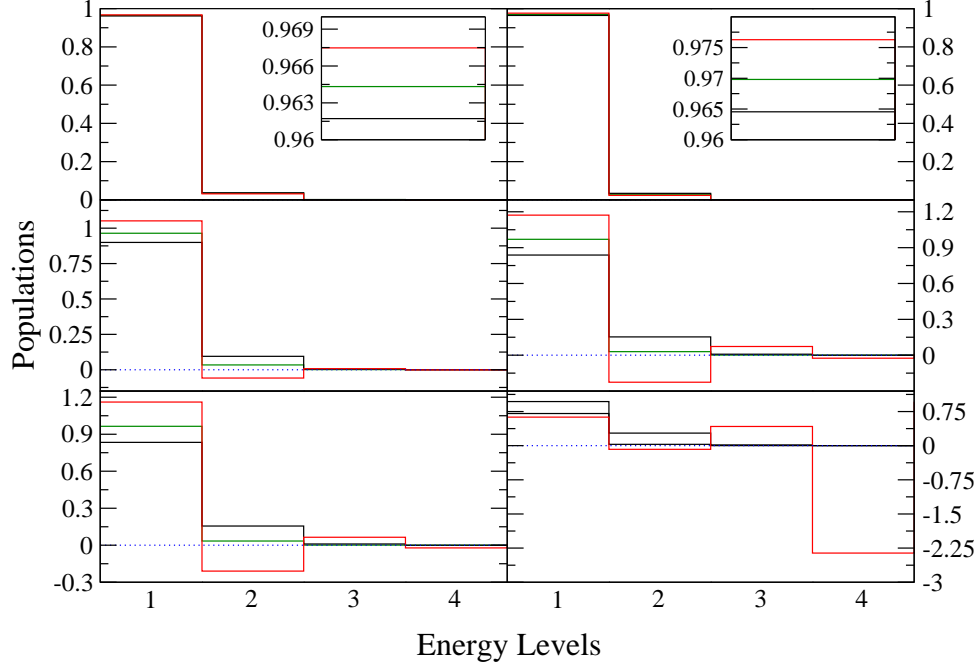
Figure 2.2: Histogram of Populations obtained via modified Redfield formalism (Black), Redfield master equation (Red), and Lindblad master equation (Green) for a single harmonic oscillator system connected to one bath (Left) and two baths (Right). Top row corresponds to coupling strength $\gamma/\omega_0 = 0.01$. The insets show the populations only for the first energy level. Middle row corresponds to coupling strength $\gamma/\omega_0 = 0.25$ and bottom row corresponds to coupling strength $\gamma/\omega_0 = 0.5$. The parameters used for this simulation are: $M = 1\mathrm{u}$, $\omega_0 = 1.3\mathrm{x}10^{14}$ Hz, and $\omega_\mathrm{D} = 10\omega_0$. In case of one bath problem T $= 187$K, whereas in case of two baths $\mathrm{T_L} = 187$K and $\mathrm{T_R} = 168$K.

model we have already proved that the MRS is correct for both equilibrium and nonequilibrium situations and hence it serves as a good testing ground for other master equations. We first look at the results from the Lindblad master equation (green lines in Fig. 2.2), which has been extensively used in the literature [76, 77]. The Lindblad master equation is mainly preferred due to the ease in computation and its preservation of positivity. Despite

these advantages, the Lindblad solution is exactly the same for different values of coupling strength as shown in Fig. 2.2. This clearly indicates that the Lindblad solution can not capture the effects of finite system-bath coupling, this numerical observation is a corroboration to the analytical proof given in ref. [99] for the equilibrium problem. On the other hand the RQME depicts severe deviations from the MRS even for small, but finite coupling strengths. At slightly larger coupling strengths the RQME gives negative probabilities as shown in the middle panel of Fig. 2.2. This unphysical property of the RQME to give negative populations has been severely critiqued before [100, 101, 102]. Since the MRS does not produce negative populations for these coupling strengths we can now assess that the reason for this breakdown is rooted in the incorrect 2-nd order diagonal elements. It is important to point out that the MRS does not guarantee positivity and for slightly larger coupling strengths ($\gamma/\omega_0 \geq 0.6$) the MRS gives negative populations indicating a breakdown of the 2-nd order approximation. Nevertheless the MRS provides a decisive and salient improvement over the RQME in that the coupling strengths that can be probed accurately becomes sizable.

2.5 Summary

In summary, the Redfield master equation was derived from a micro-

scopic model where only the weak system-bath coupling approximation was made. Some of the commonly used assumptions like the rotating wave approximation and neglecting the Lamb-shifts were discussed along with their consequences on the solution of the master equation. For a general second order master equation it was shown that in order to obtain second order accuracy in the long time limit we require the fourth order relaxation tensor which is quite cumbersome to obtain. Specifically, only the second order diagonal elements required the knowledge of the fourth order relaxation tensor.

In order to obtain the second order diagonal elements correctly we attempted the use of Dyson expansion and found obscure divergences and dependence on initial conditions at all times. Being unphysical we then resorted to our novel technique termed as the the modified Redfield solution in which we used analytic continuation techniques to obtain the 2-nd order diagonal elements from the correct 2-nd order off-diagonal ones. We then showed that the MRS matches exactly the generalized Gibbs distribution up to second order in system-bath coupling for the equilibrium one bath problem. In the end, we also numerically checked our MRS with the exact NEGF results for a harmonic system connected to two baths. Subtle calculations confirmed that the MRS gives the correct second order elements, whereas the RQME doesn't match the exact solution up to second order.

Lastly, we compared the commonly used master equations, i.e., Lindblad and Redfield formulations, with our MRS and pointed out the limitations of these methods. This undoubtedly confirmed that the MRS is a novel technique which allows one to *correctly* probe finite system-bath coupling strengths in anharmonic systems in the long time limit.

Chapter 3

Thermal transport

> If I have seen further than others, it is by standing upon the shoulders of giants.
>
> — Isaac Newton

In this chapter, formulations to study thermal transport in anharmonic molecular junctions will be introduced. In the first part, a formulation similar to the quantum master equation approach will be presented. The master equation *like* formulation will treat the anharmonicity *exactly* whereas the system-bath coupling will be treated perturbatively. Special emphasis will be laid on the steady state transport properties of several anharmonic examples like the FPU-β, ϕ^4 and Duffing oscillator models. In the next part, we will introduce a heuristic method based on nonequilibrium Green's function (NEGF) approach termed as quantum self-consistent mean field (QSCMF) method, which in principle can treat any strength of system-bath coupling. Several comparisons to other known approaches will be presented which

will clarify the validity regime of QSCMF.

3.1 Master equation like formulation

Recently, anharmonic systems have gained a lot of attention in the field of thermal transport due to their various technological applications [103, 104, 105, 106, 107, 108]. This has led to a renewed interest in the quantum master equation formulation and several attempts have been made to calculate transport properties in anharmonic systems using this novel approach [9, 10, 11, 12, 13]. In this section our main goal is to develop a rigorous theory similar to the Redfield quantum master equation (RQME) to calculate heat current in systems with strong anharmonicity.

3.1.1 Second order perturbation theory

In this section we will calculate heat current up to second order in the system-bath coupling. Although we will mainly focus on bosonic Hamiltonian the approach outlined here could be easily extended to fermionic ones and more interestingly a combination of both. We will start with the basic definition of heat current,

$$I^{\mathrm{L}}(t) = - \left\langle \frac{\mathrm{d}H_{\mathrm{B}}^{\mathrm{L}}(t)}{\mathrm{d}t} \right\rangle , \tag{3.1}$$

which is inspired by the change in energy of the (infinite) bath. In general one needs to distinguish between heat current ($I^L_{heat}(t)$) and energy current ($I^L_{energy}(t)$) as[1],

$$I^L_{heat}(t) = I^L_{energy}(t) - \mu I^L_{particle}(t),\qquad(3.2)$$

where μ is the chemical potential and $I^L_{particle}(t)$ is the particle current. Fortunately, in case of harmonic oscillator baths since there are no conserved particles that are transported the particle current is zero causing the heat current to be the same as energy current.

The averaged operator above is to be interpreted in the Heisenberg way, $i\,dA/dt = [A, H_{tot}]$. Throughout this section we will restrict ourselves to two baths, which is the minimum number to study transport properties. The baths will be labeled with super-scripts 'L' and 'R' indicating left and right heat baths and hence throughout this derivation the summation label α will take only two values. The time evolution will be handled perturbatively, much as one derives the RQME as outlined in Sec. 2.1.1. Using the Heisenberg equation of motion in Eq. (3.1) we obtain,

$$I^L(t) = -\lambda\langle A^L(t)\rangle,\qquad(3.3)$$

[1]In order to understand the relation between heat and energy current one can look at the analogous reversible thermodynamic relation $dQ = dE - \sum_i \mu_i dN_i$

where

$$
\begin{aligned}
A^{\mathrm{L}}(t) &= \left(F^{\mathrm{L}} \otimes E^{\mathrm{L}}\right)(t), \\
F^{\mathrm{L}} &= S^{\mathrm{L}}, \\
E^{\mathrm{L}} &= i\left[B^{\mathrm{L}}, H_{\mathrm{B}}^{\mathrm{L}}\right].
\end{aligned}
\tag{3.4}
$$

We recall that S^{L} is the system operator connected to the bath operator B^{L} of the left bath. The time evolution of the operator $A^{\mathrm{L}}(t)$ is defined in terms of the evolution operator,

$$
A^{\mathrm{L}}(t) = \mathrm{U}(t, t_0)^{\dagger} A^{\mathrm{L}}(t_0) \mathrm{U}(t, t_0).
\tag{3.5}
$$

Now we expand the evolution operator $\mathrm{U}(t, t_0)$ as we did in Sec. 2.1.1 up to first order in λ as,

$$
\begin{aligned}
\mathrm{U}(t, t_0) &= \mathrm{U}_0(t, t_0)\mathrm{U}_{\mathrm{I}}(t, t_0), \\
\mathrm{U}_0(t, t_0) &= \mathrm{e}^{-i\,H_0(t-t_0)}, \\
\mathrm{U}_{\mathrm{I}}(t, t_0) &= \mathbb{I} - i\,\lambda \sum_{\alpha} \int_0^{t-t_0} \mathrm{d}s\, \tilde{H}_{\mathrm{SB}}^{\alpha}(s).
\end{aligned}
\tag{3.6}
$$

Here $\tilde{H}_{\mathrm{SB}}^{\alpha}(s)$ is the free evolution operator according to $\mathrm{U}_0(t, t_0)$. Above since we have only expanded up to first order in λ the second order term H_{RN}^{α} plays no role. Using the above expression of the evolution operator in

Eq. (3.5) we get,

$$A^{\mathrm{L}}(t) \;=\; \tilde{A}^{\mathrm{L}}(t) - i\,\lambda \int_0^t \mathrm{d}u \left[\tilde{A}^{\mathrm{L}}(t), \tilde{H}^{\mathrm{L}}_{\mathrm{SB}}(u) \right], \qquad (3.7)$$

where $\tilde{A}^{\mathrm{L}}(s)$ is again a free evolution. In order to obtain Eq. (3.7), similar to Sec. 2.1.1 we have set the initial time $t_0 = 0$ and exploited the fact that the two heat baths are not directly coupled. In case of the current formulation we expand only to first order because $\mathrm{I}^{\mathrm{L}}(t)$ in Eq. (3.3) is already first order in λ.

From now on to simplify notation we will drop the bath label α. It is worth noting that even though Eq. (3.7) has only the left bath label, the right bath comes in due to the free evolution of the operators ($\because H_{\mathrm{o}} = H_{\mathrm{S}} + \sum_\alpha H_{\mathrm{B}}^\alpha$). Now since in Eq. (3.7) we require only the free evolution $\tilde{A}(t) = \tilde{F}(t) \otimes \tilde{E}(t)$ we express the operators $\tilde{F}(t)$ and $\tilde{E}(t)$ in terms of the free evolving Hubbard operator at time t as,

$$\tilde{F}(t) \;=\; \sum_{n,m} F_{nm} \tilde{X}^{nm}(t), \qquad (3.8)$$

with $\tilde{X}^{nm}(t) = \mathrm{U}_{\mathrm{o}}(t,0)^\dagger |m\rangle\langle n| \mathrm{U}_{\mathrm{o}}(t,0)$, where $|n\rangle, |m\rangle$ are eigenvectors of the system Hamiltonian in the energy eigenbasis as defined in Sec. 2.1.1.

Similarly,

$$\tilde{S}(u) \;\; = \;\; \sum_{kl}\sum_{nm} S_{kl} g_{nm}^{kl}(u;t)\tilde{X}^{nm}(t)\,, \tag{3.9}$$

where

$$g_{nm}^{kl}(u;t) \;\; = \;\; \mathrm{Tr}\left[(\tilde{X}^{mn})^{\dagger}\mathrm{U}_{0}^{\dagger}(u,t)\tilde{X}^{kl}\mathrm{U}_{0}(u,t)\right]\,, \tag{3.10}$$

is a freely evolving Green's function of the system.

Now the operator $A(t)$ can be expressed in terms of $\tilde{X}(t)$ using Eqs. (3.8) and (3.9) in Eq. (3.7) as,

$$\begin{aligned}
\lambda A(t) \;\; = \;\; & \lambda \sum_{n,m}\tilde{X}^{nm}(t)\otimes F_{nm}\tilde{E}(t) \\
& -i\,\lambda^{2}\int_{0}^{t}\mathrm{d}u\left(\sum_{\substack{i,j\\n,k,l}}\tilde{X}^{nj}(t)\otimes F_{ni}S_{kl}g_{ij}^{kl}\tilde{E}(t)\tilde{B}(u)\right. \\
& \left. -\sum_{\substack{i,j\\m,k,l}}\tilde{X}^{im}(t)\otimes F_{jm}S_{kl}g_{ij}^{kl}\tilde{B}(u)\tilde{E}(t)\right). \tag{3.11}
\end{aligned}$$

Similar to our RQME derivation outlined in Sec. 2.1.1 we use factorized initial condition $(\rho_{\mathrm{tot}}(0) = \rho_{\mathrm{B}}^{\mathrm{L}}(0)\otimes\rho_{\mathrm{S}}(0)\otimes\rho_{\mathrm{B}}^{\mathrm{R}}(0))$ and then trace over the

bath degrees of freedom to obtain,

$$
\begin{aligned}
\langle A(t) \rangle &= \sum_{n,m} \langle \tilde{X}^{nm}(t) \rangle F_{nm} \langle E(t) \rangle \\
&\quad -i \sum_{n,m} \langle \tilde{X}^{nm}(t) \rangle \sum_{j} \left(F_{nj} S_{jm}^{>}(t) - S_{nj}^{<}(t) F_{jm} \right) , \quad (3.12)
\end{aligned}
$$

where,

$$
\begin{aligned}
S_{ij}^{>}(t) &= S_{ij} \int_{0}^{t} \mathrm{d}u \, \mathrm{e}^{-i \, \Delta_{ij} u} \, \chi(u) , \quad (3.13) \\
S^{<}(t) &= \left(S^{>}(t) \right)^{\dagger} , \\
\chi(u) &= \mathrm{Tr}_{\mathrm{B}} \left(\tilde{E}(t) \tilde{B}(t - u) \rho_{\mathrm{B}} \right) , \quad (3.14)
\end{aligned}
$$

and we have used $g_{nm}^{kl}(u; t) = \mathrm{e}^{i \, (u-t) \Delta_{kl}} \, \delta_{k,n} \delta_{l,m}$ for time-independent H_{s}. We have also set the dimensionless parameter $\lambda = 1$ above. Finally, noting that $\langle B \rangle = 0$ gives $\langle E(t) \rangle = 0$, the heat current in Eq. (3.3) can be expressed as,

$$
\begin{aligned}
\mathrm{I}(t) &= \mathrm{Tr} \left(\rho^{(0)}(t) \mathcal{I}(t) \right) , \\
\mathcal{I}(t) &= i \, \left(S S^{>}(t) - S^{<}(t) S \right) , \quad (3.15)
\end{aligned}
$$

where $S^{<}$ and $S^{>}$ are defined in Eq. (3.13). Above $\rho^{(0)}(t)$ is the lowest order contribution to the RDM obtained by solving the RQME (Eq. (2.14)) with system-bath coupling strength $\lambda \to 0$. In the steady state, as shown in

Chap. 2, an explicit form of equations (Eq. (2.38)) to solve for $\rho^{(0)}(\infty)$ can be obtained. It is important to stress at this stage that since the current operator $\mathcal{I}(t)$ is already up to second order in system-bath coupling we have taken the liberty to replace $\tilde{X}^{nm}(t)$ by $\rho^{(0)}(t)$. This approximation takes into account the fact that we require the accuracy of the current only up to second order in system-bath coupling and is quite similar to the closure condition in the derivation of the RQME (Sec. 2.1.1) where we replaced $\tilde{\rho}_{\mathrm{s}}(t)$ with $\rho(t)$.

Thus, Eq. (3.15) is a master equation *like* formulation which provides a concrete way to calculate the heat current not only in the steady state but at any time t. The explicit time dependence in the operators $S^{<}(t)$ and $S^{>}(t)$ is sometimes referred to as being non-Markovian. In our 2-nd order formulation we come across new bath-correlators $\chi(\tau)$, which have been defined in Eq. (3.14). In terms of the spectral density defined in Append. A, Eq. (A.4), the new bath correlator is given by,

$$\chi(\tau) = \int_0^\infty \frac{\mathrm{d}\omega}{\pi} \omega \mathrm{J}(\omega) \left(\coth\left(\frac{\beta\omega}{2}\right) \sin(\omega\tau) + i\cos(\omega\tau) \right) . \quad (3.16)$$

Comparing the new bath correlator $\chi(\tau)$ with the bath correlator occurring in the RQME $C(\tau)$ (Eq. (2.10)) we find that,

$$\chi(\tau) = -\frac{C(\tau)}{\mathrm{d}\tau} , \quad (3.17)$$

and hence the operator $S^>(t)$ can be computed as,

$$S^>_{ij}(t) \;=\; S_{ij}\left(\mathrm{C}(0) - e^{-i\Delta_{ij}t}\mathrm{C}(t) - i\Delta_{ij}\tilde{W}_{ij}\right).\tag{3.18}$$

Note that, similar to our derivation of the RQME nothing particular to the harmonic baths has been invoked. Any other bath, e.g. spin baths [109], can be used as long as we can compute its bath correlators $\mathrm{C}(\tau)$ and $\chi(\tau)$. Thus only the relaxation rates $\tilde{W}$ (Eq. (2.17)) and the operators $S^<(t)$, $S^>(t)$ are affected.

Earlier works employing the master equation to calculate heat current have made additional approximations like symmetrization of the heat current [10, 110], use of the Pauli master equation to calculate the reduced density matrix [10, 11, 12] or the use of Green-Kubo formula [9, 13], which is strictly valid for thermodynamic systems [111]. Although all these approximations provide a simpler route to calculate current, they can not be justified from physical or mathematical grounds and as we have seen above none of these approximations are needed in our derivation. A subtle implication of using only the weak system-bath coupling approximation is the possibility of extending our theory to higher orders, which in case of any other method can not be envisaged.

3.1.1.1 Transient heat current at short times

One of the most intriguing aspects of heat current occurs in the short time limit. Cuansing *et al.* [112] found that at short times the heat current for harmonic systems always flows into the baths. This counter intuitive phenomenon is mainly because at the initial time $t_0 = 0$ when we connect the two baths to the system we pump in extra energy which inevitably flows into the baths.

The interesting question obviously is that whether such a phenomena is true for anharmonic systems as well? and if so how does our perturbative theory compare to the exact results obtained via NEGF [113]. In order to answer these questions we first look at the short-time limit of Eq. (3.15). Performing a Taylor expansion of the bath correlator $C(\tau)$ at short times we obtain,

$$C(\tau) = C(0) + \tau C_1 + O(\tau^2),\tag{3.19}$$

where C_1 is some unknown function evaluated at $\tau = 0$. The relaxation rate $\tilde{W}_{ij}$ from Eq. (2.17) is therefore given by,

$$\begin{aligned}\tilde{W}_{ij} &= \int_0^\tau d\tau'\, e^{-i\,\Delta_{ij}\tau'}\, C(\tau'),\\&\approx \int_0^\tau d\tau'\, C(0) + \tau'\,(C_1 - i\,\Delta C(0)),\end{aligned}$$

$$\approx \quad C(0)\tau \,, \tag{3.20}$$

up to leading order in τ. Thus using Eq. (3.18) the operator $S^>$ becomes,

$$S^>_{ij}(\tau) \quad \approx \quad -S_{ij}C_1\tau \,. \tag{3.21}$$

Noting that the imaginary part of $\mathrm{Im}[C(0)] = 0$ (Eq. (2.10)), the heat-current in the short-time limit can be simplified as

$$I(t) \quad \approx \quad 2C''(\tau)\mathrm{Tr}\left(\rho^{(0)}(0)SS\right) \,, \tag{3.22}$$

where $\rho^{(0)}(0)$ is the initial condition of $\rho^{(0)}$ and $C''(\tau)$ is the imaginary part of the bath correlator function $C(\tau)$ at short-times, which by definition is always negative indicating the current always flows into the baths.

It is also interesting to see that at short times the current is mainly influenced by the bath and the form of the coupling, whereas the system plays a minimal role in this regime. For the specific case of the system comprising of a single harmonic oscillator the above perturbative result is exact and true for any system-bath coupling strength [113].

3.1.1.2 Steady-state heat current

Next we will simplify Eq. (3.15) so that it is only applicable to the steady state. In order to do this we will first set $t = \infty$. Since the bath

correlator decays with time $C(\infty)$ will be zero for the steady state problem. Also by definition $\text{Im}[C(0)] = 0$ and thus only the transition rates $\tilde{W}_{ij}$ will contribute to the the current operator

$$\mathcal{I}_{ij} = \sum_l S_{il} S_{lj} \left(\Delta_{lj} \tilde{W}_{lj} + \Delta_{li} \tilde{W}_{li}^* \right) . \tag{3.23}$$

In the steady state, according to Eq. (2.38) $\rho^{(0)}(\infty)$ is diagonal which immediately gives us the heat current as,

$$\text{I} = 2 \sum_{l,i} \Delta_{li} \rho_{ii}^{(0)} |S_{il}|^2 \tilde{W}_{li}' , \tag{3.24}$$

where $\tilde{W}_{ij}'$ is defined in Eq. (2.17) and we have dropped the time label $(= \infty)$ for notational simplicity. The simplified steady state heat current is the same as the one proposed by Wu *et al.* [12] based on phenomenological modeling and physical intuitions, which in case of a single harmonic oscillator can be mapped to a Landauer formula [11].

3.1.2 Few simple applications

In this section we apply the master equation *like* formulation outlined above to evaluate the steady state heat current for a variety of bosonic anharmonic systems. One of the main difficulties in the numerical implementation for bosonic systems is the number of basis vectors required to correctly represent the system at fixed temperatures. In order to correctly

capture all finite temperature effects we choose a system Hilbert space large enough so that even at the highest temperature the probability of finding the particles in the highest energy levels is approximately zero. We do this by iteratively increasing the size of the system Hilbert space until at least five energy levels have a population less than 10^{-15}. Thus, in case of bosonic systems we are limited to molecular junctions consisting of one or two particles only. With such one or two particle molecular junctions we can treat system Hilbert space of ~ 1600 levels, which are enough to reach around five times the Debye temperature.

Next we shift our attention to thermal transport, where one of the important transport coefficient is the thermal conductivity. But for molecular junctions, since the cross-sectional area of the system interacting with the bath is not well defined, we can not define the thermal conductivity of the system. Hence in such cases we define thermal conductance as,

$$\sigma = \lim_{T_{\mathrm{L}} \to T, T_{\mathrm{R}} \to T} \frac{\mathrm{I}^{\mathrm{L}}}{T_{\mathrm{L}} - T_{\mathrm{R}}} \,. \tag{3.25}$$

In order to numerically evaluate the thermal conductance we choose a small temperature difference between the two baths such that the limit in Eq. (3.25) becomes valid. For all the systems considered in this section we find that a temperature difference of 10% is optimal and even if we decrease the temperature difference further the conductance of the system
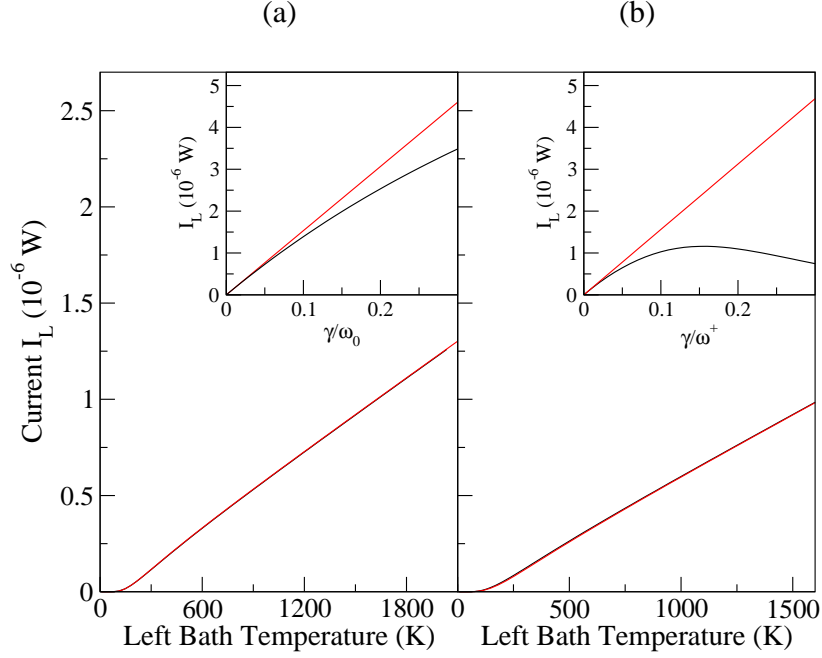
Figure 3.1: Graph of current (I^L) vs temperature of the left lead (T_L) using Landauer formula (black) and the master equation *like* formulation (red) for the Lorentz-Drude model. The insets show current as a function of the strength of the dimensionless system-bath coupling strength squared. (a) shows the current comparison for a harmonic one particle system and (b) shows the comparison for a harmonic two particle case. The parameters used for the one particle system are; $M = 1u$ and $\omega_0^2 = 60.321$ meV/Å^2. The parameters used for the two particle case are; $M = 1u$, $\omega_0^2 = 30.1605$, and $\Omega^2 = 30.1605$ meV/Å^2. The common bath parameters are; $\gamma = 6.0321$ $\sqrt{\text{meV}}$/Å, $\omega_D = 10$ eV, and $T_R = 0.9T_L$. For both the insets the same system parameters and bath parameters are used except $T_L = 350$ K and γ is varied. For the two particle inset $\omega^+ = \sqrt{\omega_0^2 + \Omega^2}$.

does not change.

3.1.2.1 Harmonic oscillator system

We will first validate our approach by comparing with the exact NEGF formulation [44] for harmonic systems. Due to the computational limitations we will consider only one and two particle systems given by the

Hamiltonian,

$$H_{\mathrm{s}} \; = \; \sum_{i=1,2} \left\{ \frac{p_i^2}{2M} + \frac{M\omega_0^2}{2} x_i^2 \right\} + \frac{M\Omega^2}{2} (x_1 - x_2)^2 \,, \qquad (3.26)$$

where ω_0 and Ω are the on-site and inter-particle harmonic frequencies respectively. For the one particle case the sum is over a single particle and $\Omega = 0$. The above system is then connected to the Lorentz-Drude heat baths via the position operator, i.e., $S^{\mathrm{L}} = S^{\mathrm{R}} = x_1$ for the one particle case and $S^{\mathrm{L}} = x_1, S^{\mathrm{R}} = x_2$ for two particles.

As shown in Fig. 3.1 we compare the master equation *like* formulation (red curve) with the standard Landauer formula for heat current (black curve). The Landauer formula, which can be derived using NEGF techniques [44] or the Langevin equation approach [114] is rigorous and exact for harmonic systems . For the one and two particle case we find no noticeable difference between the Landauer and master equation *like* formulation for the entire temperature range as shown in Figs. 3.1a and 3.1b respectively. The insets show heat current as a function of the dimensionless system-bath coupling strength. We see that for both one and two particle cases curves exactly overlap in the weak system-bath coupling regime, i.e., up to $\gamma \sim 0.01\sqrt{\omega_0^2 + \Omega^2}$ and in the strong coupling regime $\gamma \sim 0.2\sqrt{\omega_0^2 + \Omega^2}$ a considerable difference is observed as expected.

3.1.2.2 FPU-β and ϕ^4 model

One of the greatest advantages of the master equation *like* formulation is the power to deal with strongly anharmonic systems. We will now look at two commonly studied anharmonic models; FPU-β and ϕ^4 model, whose Hamiltonians are given by

$$
\begin{aligned}
H_{\mathrm{S}} &= \sum_{i=1,2} \left\{ \frac{p_i^2}{2M} + \frac{M\omega_0^2}{2} x_i^2 \right\} + \frac{\Omega^2}{2} (x_1 - x_2)^2 \\
&\quad + \sum_{i=1,2} \lambda_0 x_i^4 + \lambda (x_1 - x_2)^4 \,,
\end{aligned}
\tag{3.27}
$$

where λ_0 and λ are the on-site and inter-particle quartic potentials. When $\lambda_0 = 0$ the model is referred to as the FPU-β model, whereas $\lambda = 0$ corresponds to the ϕ^4 model. Similar to the harmonic oscillator case the system is again connected to Lorentz-Drude heat baths with $S^{\mathrm{L}} = S^{\mathrm{R}} = x_1$ for one particle and $S^{\mathrm{L}} = x_1, S^{\mathrm{R}} = x_2$ for two particles. In Fig. 3.2 we plot the conductance, defined in Eq. (3.25), as a function of average temperature $T = (T_{\mathrm{L}} + T_{\mathrm{R}})/2$ for one particle ϕ^4 model (Fig. 3.2a) and for two particle FPU-β model (Fig. 3.2b). For the one particle ϕ^4 model (Fig. 3.2a), we see that even with the slightest amount of anharmonicity the system behaves quite differently as compared to the harmonic case. The anharmonicity not only changes the behavior at the high temperature (classical regime), but also changes the behavior of low-temperature thermal conductance (quan-
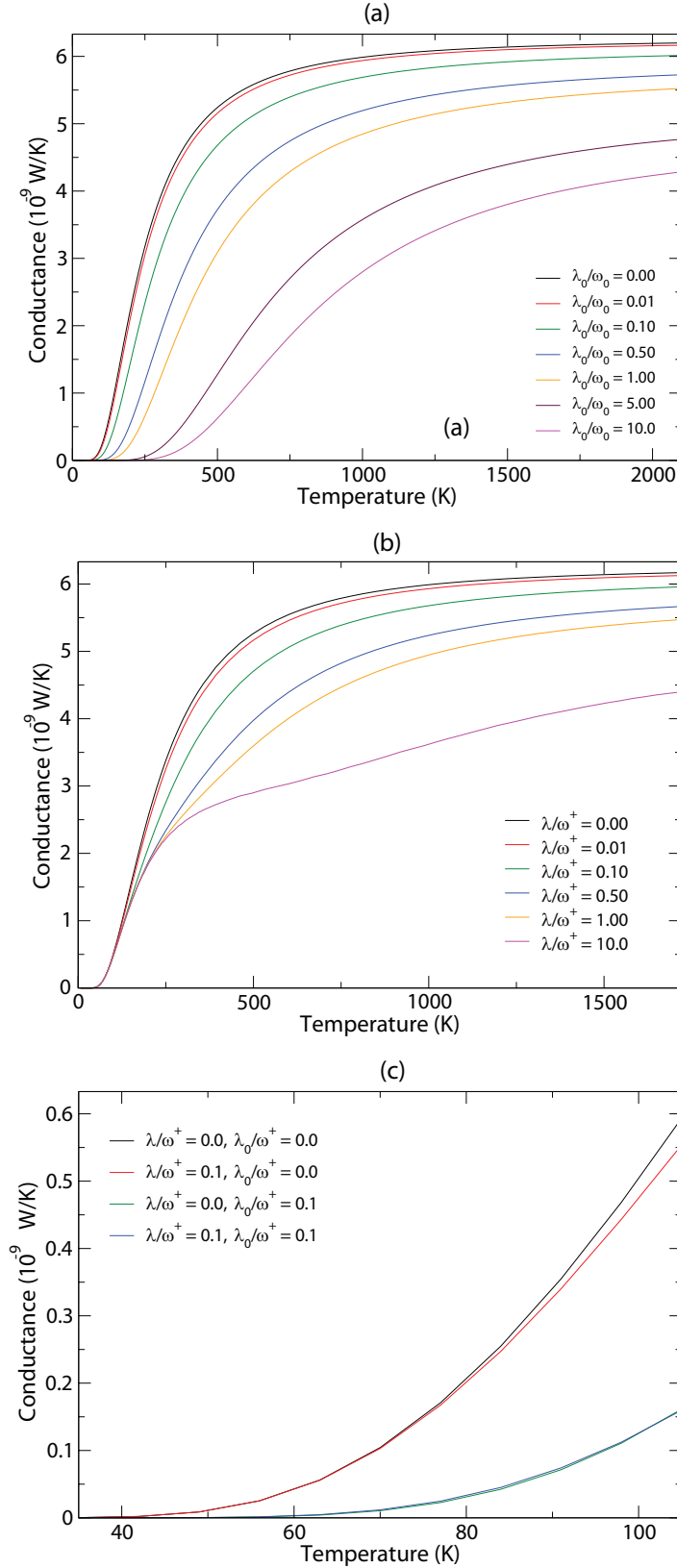
Figure 3.2: Graph of conductance (σ) vs temperature $[T = (T_L + T_R)/2]$ for the one and two particles FPU-β and ϕ^4 models using the Lorentz-Drude heat baths. Fig. (a) shows conductance for a one particle ϕ^4 model, (b) for a two particle FPU-β model and (c) shows the low-temperature behavior for a two particle FPU-β + ϕ^4 model. The parameters used for the one particle system are; $M = 1$u and $\omega_0^2 = 60.321$ meV/$\mathring{A}^2$, whereas for the two particle case are; $M = 1$u, $\omega_0^2 = 30.1605$, $\Omega^2 = 30.1605$ meV/$\mathring{A}^2$, and $\omega^+ = \sqrt{\omega_0^2 + \Omega^2}$. The common bath parameters are; $\gamma = 6.0321$ $\sqrt{\text{meV}}/\mathring{A}$, $\omega_D = 10$ eV, and $T_R = 0.9 T_L$. λ_0/ω_0, λ/ω^+ and λ_0/ω^+ has the unit of $\mathring{A}^{-2}$.

tum regime).

Next, we will look at the two particle FPU-β model, i.e., with $\lambda_0 = 0$ as shown in Fig. 3.2b. Surprisingly, the low temperature behavior of the FPU-β model is not affected by the strength of the anharmonicity. This is in stark contrast to the result obtained for the one particle case and possibly could be due to the translational invariance of the anharmonic potential. In order to validate this claim we vary both λ_0 and λ as shown in Fig. 3.2c. Clearly, if $\lambda_0 \neq 0$ the translational invariance of the anharmonic potential is broken and the thermal conductance strongly depends on the anharmonic strength at low temperatures, whereas for $\lambda_0 = 0$ the low temperature thermal conductance is ballistic, i.e., the strength of λ plays no role.

3.1.2.3 Duffing oscillator system

Lastly, we look at the Duffing oscillator model, which represents a particle trapped in a double-well potential. The system Hamiltonian for the Duffing oscillator model is given by,

$$H_{\mathrm{s}} \;=\; \sum_{i=1,2} \left\{ \frac{p_i^2}{2M} - \frac{M\omega_0^2}{2}x_i^2 + \lambda_0 x_i^4 \right\} + \frac{\Omega^2}{2}(x_1 - x_2)^2\,, \qquad (3.28)$$

where importantly the harmonic on-site potential has a negative sign giving the potential a double-well nature. Recently, using molecular dynamics simulations Ai *et al.* [115] have pointed out this model exhibits negative

differential thermal conductance (NDTC) in the classical regime making it an interesting candidate for the study of quantum thermal transport.

We apply the master equation *like* formulation to evaluate the thermal conductance for the one particle Duffing oscillator model as shown in Fig. 3.3a. First let us look at the two extreme cases when $\lambda_0/\omega_0 = 0.01$ and $\lambda_0/\omega_0 = 10$. The barrier height of the double-well potential is inversely proportional to λ_0 and thus when $\lambda_0/\omega_0 = 0.01$ the particle remains confined to either one side of the barrier (indicated by the nearly degenerate eigenvalues in Table 3.1), whereas in case of $\lambda_0/\omega_0 = 10.0$ the barrier is so low that the molecule simply experiences an overall quartic potential. Both these cases may be considered as the molecule experiencing only an effective quartic on-site potential. In these cases no NDTC behavior is observed in the quantum regime.

For intermediate values of the quartic term $[\lambda_0/\omega_0 = 0.05; 0.10]$ we observe negative differential thermal conductance (NDTC) behavior in the quantum regime (see Fig. 3.3a inset). In order to explain this quantum behavior we analyze the lowest three eigenvalues and their populations given by $\rho^{(0)}$ as tabulated in Table 3.1. Since the maxima of the double-well potential barrier is at 0.0 eV, we can clearly see from Table 3.1 that for $\lambda_0/\omega_0 = 0.05; 0.10$ the lowest three levels, which have a finite occupation, are just below the maxima of the barrier. Thus, due to quantum nature the
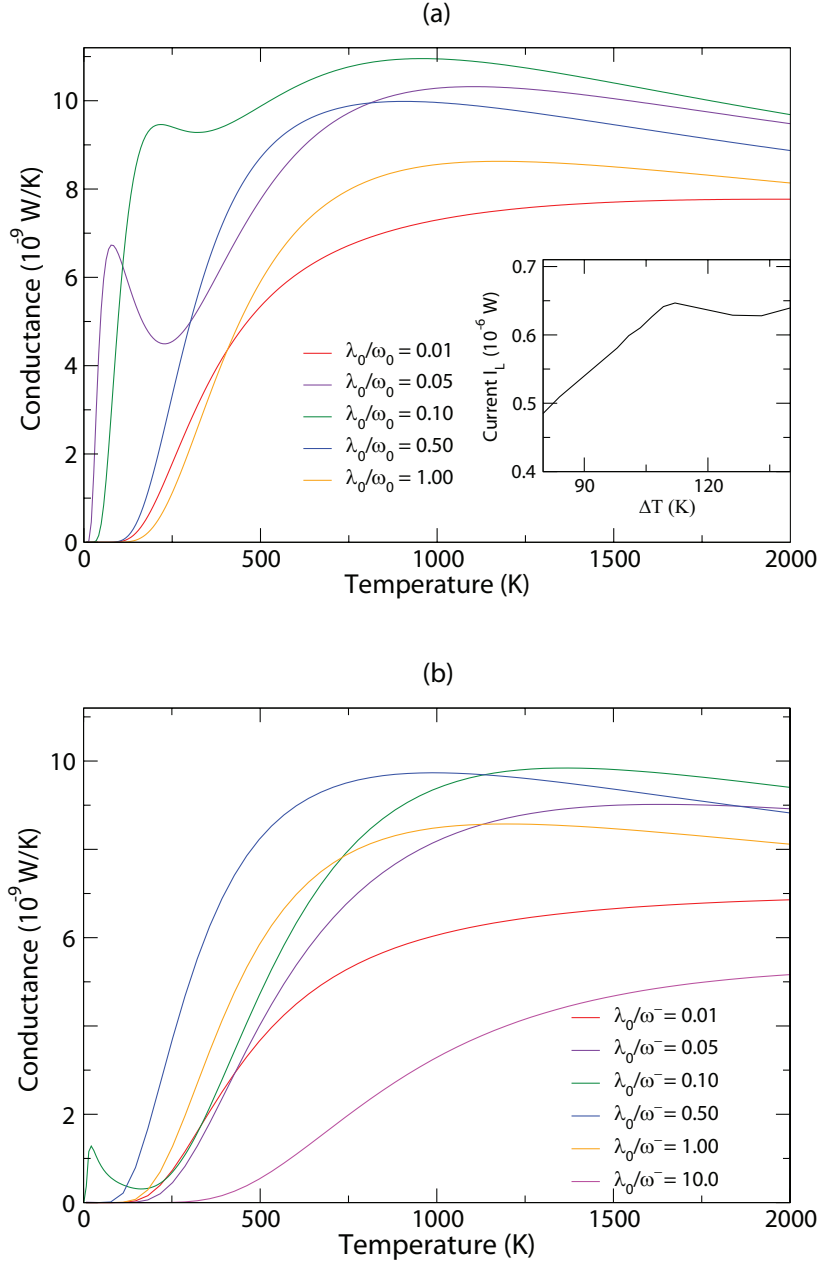
Figure 3.3: Graph of conductance (σ) vs temperature $[T = (T_{\mathrm{L}} + T_{\mathrm{R}})/2]$ for the one (Fig. (a)) and two (Fig. (b)) particles Duffing oscillator model using the Lorentz-Drude heat baths. Fig. (a) inset shows current vs temperature difference at $T_{\mathrm{L}} = 140$K and $\lambda_0/\omega_0 = 0.05$ Å^{-2}. For the one particle system $\omega_0^2 = 60.321$ meV/Å^2, whereas for the two particle case $\omega_0^2 = 90.4815$, $\Omega^2 = 30.1605$ meV/Å^2, and $\omega^- = \sqrt{\omega_0^2 - \Omega^2}$. The common parameters are; $M = 1$u, $\gamma = 6.0321$ $\sqrt{\mathrm{meV}}$/Å, $\omega_{\mathrm{D}} = 10$ eV, and $T_{\mathrm{R}} = 0.9 T_{\mathrm{L}}$.

64

molecule can tunnel through the barrier and is not confined well within the double-well as in the case of $\lambda_0/\omega_0 = 0.01$, which gives rise to the NDTC behavior.

Next, let us try to explain the behavior of thermal conductance as a function of temperature for a specific case of $\lambda_0/\omega_0 = 0.05$. The lowest two energy levels for the parameters used in Fig. 3.3a are quite close, ~ 12.5meV (130 K). This is the exact temperature range at which the thermal conductance increases sharply indicating that the bath modes corresponding to that energy difference start conducting heat. In between 100 to 300 K, since the third energy level is quite far apart the system behaves like a two-level system, commonly referred to as the spin-boson model [10]. In this temperature range since only two levels transfer heat the current saturates causing the thermal conductance to decrease with increasing temperature. It is only above 210 K that the third energy level starts gaining some finite population as shown in Table 3.1 and thus beyond this temperature, i.e., ~ 300K, the thermal conductance again starts to increase.

In case of the two particle Duffing oscillator model we observe similar behavior to the one particle case as shown in Fig. 3.3b. An analysis similar to the one particle case, explaining the behavior of thermal conductance, can be made with the eigenvalues and the populations shown in Table 3.1. For $\lambda_0/\sqrt{\omega_0^2 - \Omega^2} = 0.01, 0.05$ the barrier is very high and hence

λ'	Eigenvalues		Populations in%	
	One particle	Two particle	One particle	Two particle
Å^{-2}	$(10^{-3}$ eV)		(T = 210 K)	(T = 105 K)
	-449.54	-1815.01	49.78	49.99
0.01	-449.53	-1815.01	49.77	49.00
	-356.11	-1702.86	0.22	0.00
	-130.41	-424.28	67.33	50.25
0.05	-117.94	-424.19	32.60	49.74
	-6.26	-287.59	0.05	0.00
	-74.89	-214.66	86.13	59.21
0.10	-43.44	-211.45	13.84	40.77
	75.73	-85.70	0.01	0.01
	10.60	18.01	99.53	99.96
0.50	103.44	88.18	0.46	0.03
	242.11	135.98	0.00	0.00
	39.79	78.57	99.92	99.99
1.00	163.29	186.79	0.07	0.00
	320.20	217.78	0.00	0.00
	133.16	266.28	99.99	99.99
10.0	390.44	518.69	0.00	0.00
	688.89	528.42	0.00	0.00

Table 3.1: Table of first three eigenvalues and corresponding populations for the one particle ($\lambda' = \lambda_0/\omega_0$) and two particle ($\lambda' = \lambda_0/\sqrt{\omega_0^2 - \Omega^2}$) molecule confined in a double-well potential.

the molecule remains confined to either one side of the well indicated by the nearly degenerate eigenvalues and corresponding 50-50% probabilities [see Table 3.1]. For $\lambda_0/\sqrt{\omega_0^2 - \Omega^2} = 0.1$ we can observe NDTC [not shown] in the quantum regime because only for this value the barrier is neither too high nor too low and hence the molecule can tunnel through the barrier, since the populated states are just below 0.0 eV (barrier maxima) as seen from Table 3.1.

The two particle system brings another interesting aspect, i.e., the role

of inter-particle anharmonic interactions. If the system Hamiltonian contains an extra term of the form $\lambda(x_1 - x_2)^4$, where λ is the inter-particle anharmonic spring constant, then $\lambda \neq 0$ plays a small role in determining whether the system shows NDTC or not. As we have seen before the inter-particle anharmonic spring constant does not affect the low-temperature thermal conductance and since NDTC in the Duffing oscillator models is observed in the low-temperature quantum regime we do not expect NDTC to be affected by λ. At high temperatures the effect of λ is to shift the thermal conductance to a lower value as compared to the harmonic spring. This behavior is also expected since anharmonic interaction between the atoms leads to more scattering causing the thermal conductance to decrease as compared to a harmonic interaction. Thus, in both one and two particle systems NDTC behavior can be observed by only tuning the height of the barrier, i.e., λ_0 and other inter-particle effects seem to play a small role.

3.2 Quantum self-consistent mean field approximation

One of the cornerstones to study thermal transport exactly in harmonic systems has been the nonequilibrium Green's function (NEGF) method [44]. Primarily, the NEGF approach has been used to calculate steady-state thermal transport in harmonic systems using the Landauer formula, which has been inspired by the study in mesoscopic electrical transport [3, 4].

Only recently has this approach been applied to study concrete anharmonic examples [45, 46, 47], where the anharmonicity is treated perturbatively and the system-bath coupling exactly. This is the exact opposite limit compared to our master equation *like* formulation, where the anharmonicity is treated exactly and the system-bath coupling perturbatively. Captivated by this fact, in this section our main goal is to develop a formulation based on the NEGF method to deal with anharmonic systems with strong system-bath interaction. We will mainly focus on this so-called quantum self-consistent mean field approximation (QSCMF) and validate this approach by comparing with the other existing methods.

3.2.1 Theory

In this section we will formulate the QSCMF approach for systems containing quartic anharmonicity. One of our main inspirations behind this formulation has come from the earlier works in classical [116, 117, 118] self-consistent phonon theory and the quantum corrections [119] thereof. The QSCMF approach formulated here is not as general as the master equation *like* formulation outlined in Sec. 3.1, i.e., it can not deal with any general system Hamiltonian, but its main advantage is the possibility of exploring the strong system-bath coupling regime. Thus, we begin with a specific

form of the system Hamiltonian given by

$$H_{\mathrm{s}} = \frac{1}{2M}\mathbb{P}^{\mathrm{T}}\mathbb{P} + \frac{1}{2}\mathbb{X}^{\mathrm{T}}K\mathbb{X} + M^2 \sum_{ijkl} T_{ijkl}x_i x_j x_k x_l \,, \qquad (3.29)$$

where $\mathbb{P}$ and $\mathbb{X}$ are column vectors consisting of all system momentum (p_i) and positions (x_i) respectively. K is commonly referred to as the spring constant matrix and T_{ijkl} is an arbitrary four-tensor containing information about the strength of the quartic anharmonicity. In order to simplify notation we shift to the mass-normalized position co-ordinates, i.e., we use the transformation $u_i = \sqrt{M}x_i$ and obtain

$$H_{\mathrm{s}} = \frac{1}{2}\dot{\mathbb{U}}^{\mathrm{T}}\dot{\mathbb{U}} + \frac{1}{2}\mathbb{U}^{\mathrm{T}}K\mathbb{U} + \sum_{ijkl} T_{ijkl}u_i u_j u_k u_l \,, \qquad (3.30)$$

where $\mathbb{U}$ and $\dot{\mathbb{U}}$ are column vectors representing the mass-normalized positions and conjugate momenta respectively.

We will first formulate the quantum self-consistent mean field approach and in order to do this we will first define a n-point correlation function given by,

$$G(1, 2, \cdots, n) = -i \left\langle \mathrm{T_c}u(1)u(2)\cdots u(n) \right\rangle, \qquad (3.31)$$

where $\mathrm{T_c}$ is the contour-order operator on the Keldysh contour [120] and

$u(i) = u_{j_i}(\tau_i)$; where j_i is the space index and τ_i is a variable on the Keldysh contour from $-\infty$ to $+\infty$ and back from $+\infty$ to $-\infty$. Using standard procedure of differentiation [44, 121] on the contour and fixing the system-bath coupling operator $S^{\text{L,R}}$ as the position operator the equation of motion for the $2-$point correlation[2] function is,

$$\left(I\frac{\partial^2}{\partial \tau_1^2} + K + \Sigma^{\text{RN}} + \Sigma \right) G(1,2)$$

$$= 4i \sum_{j_3,j_4,j_5} T_{j_1 j_3 j_4 j_5} \langle \text{T}_c u_{j_3}(\tau_1) u_{j_4}(\tau_1) u_{j_5}(\tau_1) u_{j_2}(\tau_2) \rangle - I\,\delta(1,2)\,, \text{(3.32)}$$

where I is an identity matrix, $\delta(1,2) = \delta(\tau_1,\tau_2)\delta_{j_1,j_2}$ is a delta function, Σ^{RN} will be termed as the renormalized self-energy due to the potential renormalization term H_{RN} from Eq. (2.1), Σ is the self-energy of the baths in contour time and the term $\Sigma G(\tau_1,\tau_2)\left[= \int_{\text{C}} d\tau' \Sigma(\tau_1,\tau') G(\tau',\tau_2)\right]$ is a convolution over the Keldysh contour. The self-energy of the baths contains all the information about the baths and the system-bath coupling and in case of the Rubin baths, discussed in Append. A.3.1, the self-energy of the baths[3] can be obtained by solving,

$$\frac{\partial^2 g^\alpha(\tau_1,\tau_2)}{\partial \tau_1^2} + K^\alpha g^\alpha(\tau_1,\tau_2) = -I\,\delta(\tau_1,\tau_2)\,,$$

---

[2]The 2-point correlation function is the usually referred to as the contour ordered Green's function.

[3]In case of the phenomenological bath models, like the exponential cut-off model and the Lorentz-Drude model (described in Apend. A.3.2 and A.3.3 respectively), since there is no Hamiltonian governing the baths one can only make indirect connections between the self-energy and the spectral density of these models as shown in Ref. [122].

$$\Sigma(\tau_1, \tau_2) \;=\; \sum_\alpha \mathbb{V}^{\text{s}\alpha} g^\alpha(\tau_1, \tau_2) \mathbb{V}^{\alpha\text{s}}. \qquad (3.33)$$

The renormalized self-energy is given by,

$$\Sigma^{\text{RN}} \;=\; \sum_\alpha \mathbb{V}^{\text{s}\alpha} \frac{\gamma_0^\alpha}{2} \mathbb{V}^{\alpha\text{s}}, \qquad (3.34)$$

where K^α, g^α are the spring constant matrix and the Green's function of the αth lead. $\mathbb{V}^{\text{s}\alpha} = (\mathbb{V}^{\alpha\text{s}})^{\text{T}}$ is a matrix containing one's only for the elements which connect the αth lead to the system, whereas all other elements are zero. Since $g^{\text{L,R}}$ are infinite dimension matrices the dimensions of $\mathbb{V}^{\text{s}\alpha}$ are $N \times \infty$, where N is the number of atoms in the system.

Equation (3.32) relates the $2-$point correlation function $G(1,2)$ to the $4-$point correlation function $i \langle \text{T}_c u_{j_3}(\tau_1) u_{j_4}(\tau_1) u_{j_5}(\tau_1) u_{j_2}(\tau_2) \rangle$ and is the first equation of a BogoliubovBornGreenKirkwoodYvon (BBGKY) hierarchy [8]. Unfortunately, the BBGKY hierarchy does not close onto itself and hence we truncate it by assuming,

$$-i\,G(1,2,3,4) \sim G(1,2)G(3,4) + G(1,3)G(2,4) + G(1,4)G(2,3)\,. \; (3.35)$$

The above decomposition is like a mean-field approximation and is exact if there is no anharmonicity, i.e., Wick's theorem [123] holds. However we still make this bold *ad-hoc* assumption in order to simplify our calculations.

Using the above approximation and the fact that T_{ijkl} is symmetric under the permutation of indices the equation of motion (with space and contour time labels explicit) transforms into,

$$
\begin{aligned}
\frac{\partial^2 G_{j_1 j_2}(\tau_1, \tau_2)}{\partial \tau_1^2} &+ \sum_{j_3} \left\{ K_{j_1 j_3} G_{j_3 j_2}(\tau_1, \tau_2) + \Sigma^{\mathrm{RN}}_{j_1 j_3} G_{j_3 j_2}(\tau_1, \tau_2) \right. \\
&+ \left. \int_C \mathrm{d}\tau' \Sigma_{j_1 j_3}(\tau_1, \tau') G_{j_3 j_2}(\tau', \tau_2) \right\} \\
&= 12i \sum_{j_3, j_4, j_5} T_{j_1 j_3 j_4 j_5} G_{j_4 j_5}(0) G_{j_3 j_2}(\tau_1, \tau_2) - \delta_{j_1, j_2} \delta(\tau_1, \tau_2),
\end{aligned} \tag{3.36}
$$

where we have used the fact that in the steady state due to time translation invariance $G_{j_4 j_5}(\tau_1, \tau_1) = G_{j_4 j_5}(0)$. Rearranging the above equation using,

$$
\tilde{K}_{j_1 j_3} = K_{j_1 j_3} + K^{\mathrm{RN}}_{j_1 j_3} + 12i \sum_{j_4, j_5} T_{j_1 j_3 j_4 j_5} G_{j_4 j_5}(0), \tag{3.37}
$$

we obtain

$$
\left(I \frac{\partial^2}{\partial \tau_1^2} + \tilde{K} + \Sigma \right) G(1,2) = -I\,\delta(1,2). \tag{3.38}
$$

Now if we define $\left(I\, \partial^2 / \partial \tau_1^2 + \tilde{K} \right) g = -I\,\delta(1,2)$, we can easily see that G follows the standard Dyson equation [124] given by,

$$
G = g + g\Sigma G. \tag{3.39}
$$

Thus, we have the standard solution [8] to the retarded Green's function in the frequency domain as,

$$G^r[\omega] = \frac{1}{\omega^2 - \tilde{K} - \Sigma^r(\omega)}, \tag{3.40}$$

where $\Sigma^r(\omega)$ is the retarded self-energy of the baths. Now using Langreth's theorem [125] the lesser Green's function can be obtained using $G^< = G^r \Sigma^< G^a$, where $G^a = (G^r)^\dagger$. Noting that $G(0) = G^<(0)$ we can iteratively obtain G^r, since for each evaluation of $\tilde{K}$ we need $G^<$. According to Eq. (3.38) the anharmonic problem has been essentially converted to a harmonic one and we can easily obtain the heat current for a system connected to two baths using the Landauer formula [44] as,

$$I^L = \int_0^\infty \frac{d\omega}{2\pi} \omega \mathcal{T}(\omega)(n_L - n_R), \tag{3.41}$$

where $n_{L,R} = (\exp[\omega/T_{L,R}] - 1)^{-1}$ is the Bose-Einstein distribution for phonons, and $\mathcal{T}[\omega]$ is known as the transmission coefficient [126] given by,

$$\mathcal{T}[\omega] = \mathrm{Tr}(G^r \Gamma_L G^a \Gamma_R), \tag{3.42}$$

where $\Gamma_{L,R} = -2\mathrm{Im}[\Sigma^r_{L,R}(\omega)]$ and we have split the self-energy of the bath as $\Sigma^r(\omega) = \Sigma^r_L(\omega) + \Sigma^r_R(\omega)$.

Let us end this section by a short comment on the QSMF approach. In the above outlined approach the mean-field like approximation Eq. (3.35) neglected all the higher order correlations and converted them to 2-point correlation functions. Although this crude approximation helps us to make the system ballistic it implies that the mean-free path of the phonons in our approach is infinite. Hence intuitively our approach should only be valid for extremely small system sizes where the mean-free path of the phonon is much larger than the system size.

3.2.2 Corroborating the QSCMF approach

The QSCMF approach outlined above made use of an uncontrolled mean-field *like* approximation and in this section we will try to compare our approach to various other techniques to validate our theory and elucidate its limitations. We will first compare the QSCMF approach to the master equation *like* approach outlined in Sec. 3.1. In order to make this comparison, as shown in ref. [122], we connect the self-energy of the bath to the spectral density via,

$$\bar{\Sigma}^r_{\mathrm{L,R}}(\omega) = \frac{1}{\pi}\mathrm{P}\int_{-\infty}^{\infty} \frac{\mathrm{J}^{\mathrm{L,R}}(\omega')}{\omega - \omega'}\mathrm{d}\omega' - i\,\mathrm{J}^{\mathrm{L,R}}(\omega)\,. \qquad (3.43)$$

The above relation can be easily justified by obtaining the Green's functions via the Langevin equation approach [114] and using the basic definition of
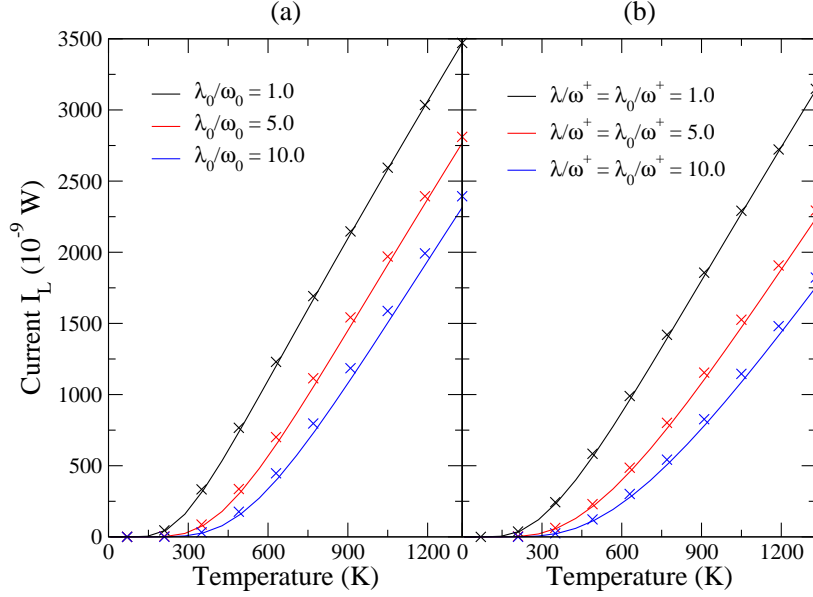
Figure 3.4: Graph of current (I^{L}) vs temperature $[T = (T_{\mathrm{L}} + T_{\mathrm{R}})/2]$ for the one and two particles FPU-β and ϕ^4 models using the Lorentz-Drude heat baths. Fig. (a) shows heat current for a one particle ϕ^4 model and (b) shows the heat current for a two particle FPU-$\beta + \phi^4$ model. The parameters used for the one particle system are; $M = 1\mathrm{u}$ and $\omega_0^2 = 60.321$ meV/$\mathring{\mathrm{A}}^2$. The parameters used for the two particle case are; $M = 1\mathrm{u}$, $\omega_0^2 = 30.1605$, $\Omega^2 = 30.1605$ meV/$\mathring{\mathrm{A}}^2$, and $\omega^+ = \sqrt{\omega_0^2 + \Omega^2}$. The common bath parameters are; $\gamma = 6.0321 \sqrt{\mathrm{meV}}/\mathring{\mathrm{A}}$, $\omega_{\mathrm{D}} = 10$ eV, $T_{\mathrm{L}} = 1.25T$ and $T_{\mathrm{R}} = 0.75T$. The unit for λ_0/ω_0, λ/ω^+ and λ_0/ω^+ is $\mathring{\mathrm{A}}^{-2}$.

spectral density given after Eq. (2.11). For computational convenience and consistency throughout this section we will choose the spectral density of the Lorentz-Drude form given by Eq. (A.15) and the system Hamiltonian will take the same form as Eq. (3.27).

Fig. 3.4 shows the comparison between QSCMF (solid lines) and master equation *like* approach (crosses) in the weak system-bath coupling regime. Since the master equation *like* approach becomes computationally very de-

manding for number of atoms ≥ 3, we restrict our comparison to one and two particle systems as shown in Figs. 3.4a and 3.4b respectively. Since the master equation *like* formulation makes no assumptions for the strength of the anharmonicity it should be considered as a numerically exact result, bearing in mind that the system-bath coupling is weak. Surprisingly, the QSCMF approach matches the master equation *like* formulation for very strong values of anharmonicity. In order to understand this astonishingly good match for strong anharmonicity we try to analyze the QSCMF approach from a Feynman diagrammatic [127, 128] point of view, where the perturbation is carried out in the strength of the anharmonicity. In our QSCMF approach we have modified the spring constant matrix K to $\tilde{K}$ by adding the anharmonic term to it as shown in Eq. (3.37). Equivalently we could have added the anharmonic term to the self-energy. This extra addition to the self-energy due to the anharmonicity is termed as the non-linear self-energy [44, 47] and in our case the frequency independent non-linear self energy gives rise only to the lowest order Feynman diagram. This implies that the anharmonicity should be very weak, but fortunately we perform a self-consistent cycle. The self-consistency sums up all the higher order Feynman diagrams which can be reduced to the lowest order one and hence partially takes into account all orders of anharmonic perturbation.

The above heuristic argument perhaps sheds some light onto why the
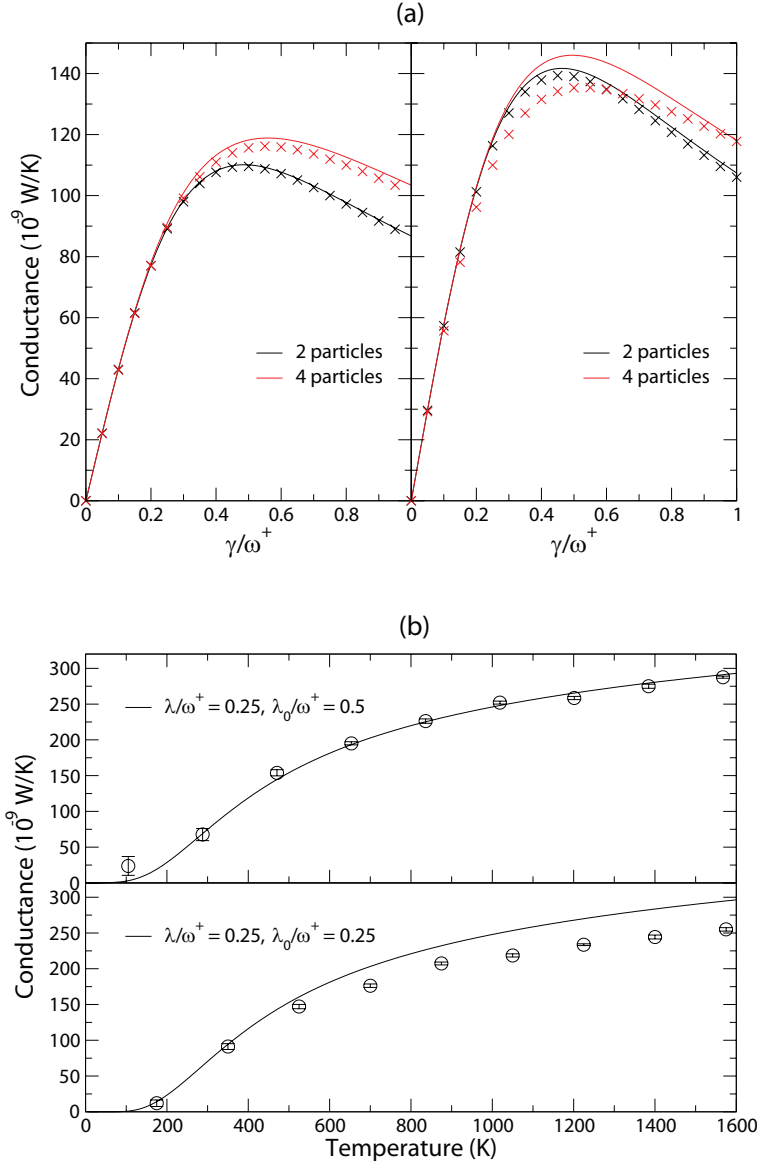
Figure 3.5: (a) shows a graph of conductance (σ) vs dimensionless system-bath coupling strength squared γ/ω^+ for the ϕ^4 model using the Lorentz-Drude (LD) heat baths at $T = 300$K (left panel) and $T = 1000$K (right panel). The ϕ^4 model has parameters $\lambda_0/\omega^+ = 0.01$ and $\lambda/\omega^+ = 0.0$ ($\mathring{A}^{-2}$). Fig. (b) shows the graph of σ vs temperature [$T = (T_L + T_R)/2$] for the two particle (top panel) and 8 particle (bottom panel) FPU-$\beta + \phi^4$ model using the LD heat baths. Solid lines correspond to the QSCMF approach, whereas the crosses are for perturbative NEGF in (a) and circles for QMD method in (b). The common parameters are: $M = 1$u, $\omega_0^2 = 30.1605$, $\Omega^2 = 30.1605$ meV/$\mathring{A}^2$, $\omega^+ = \sqrt{\omega_0^2 + \Omega^2}$, $\gamma = 6.0321$ $\sqrt{\text{meV}}/\mathring{A}$, and $\omega_D = 10$ eV.

QSCMF approach is valid for strong anharmonicity. In order to validate our approach for strong system-bath coupling we compare the QSCMF with perturbative NEGF [47] and quantum molecular dynamics (QMD) [48] as shown in Figs. 3.5a and 3.5b respectively. The perturbative NEGF approach of Wang *et al.* [47, 129] takes into account the lowest order Feynman diagram + the next order diagram. Unfortunately this perturbative approach can not be formulated in a self-consistent form and hence is strictly valid for weak anharmonicity[4]. Since the perturbative NEGF approach takes into account the second order Feynman diagrams it might shed some light on when the higher order diagrams (which are neglected in QSCMF) become important. As it can be clearly seen in Fig. 3.5a for two particle case perturbative NEGF and QSCMF match very well even in the strong system-bath coupling regime. In case of 4 particles the match is not so good, especially at high temperature, indicating a significant contribution from the higher order diagrams even for weak anharmonicity. This is understandable because the higher order diagrams are the origin for the phonon mean-free path and since the system size is increasing the mean-free path should play some role in the process of thermal transport. Similar result is found in Fig. 3.5b where we compare with QMD. The quantum molecular dynamics approach should be valid most accurately in the high temperature regime

---

[4]It is important to stress here that the perturbative NEGF approach is a controlled approximation and in principle can be extended to higher orders in perturbation.

and as we can clearly see that for the two particle case QSCMF and QMD match perfectly, whereas the comparison gets worse for the 8 particle case. Thus, our exhaustive comparisons for the specific quartic anharmonic potential indicate that for small system sizes the QSCMF approach, due to the self-consistent cycles, is valid for both strong anhamrmonicity and strong coupling.

3.3   Summary

In summary, a master equation *like* formulation for the heat current was derived, which was not only valid in the steady state but also the transients. No *ad-hoc* assumptions were made during the derivation except the weak system-bath coupling approximation, an inherent difficulty in master equation approaches. In case of short-times an analytical result was provided which showed that the heat current always flows into the baths and the major contributing factors are the initial state and the type of the heat baths. In the opposite limit of steady state the formulation was further simplified and was shown to match the earlier works of Wu *et al.* [12], from which a Landauer formula can be obtained. Several interesting anharmonic models were studied and our approach was validated in the harmonic limit by comparing with the NEGF formulation. In case of FPU-β and ϕ^4 model we found that the thermal conductance in these models can be severely affected by the presence of anharmonicity. In specific

we found that if the anharmonic potential is translationally invariant then the low-temperature thermal conductance is same as a harmonic system and anharmonicity plays almost no role at low temperatures. Finally, the Duffing oscillator models for one and two particles were studied and we showed that in the low-temperature regime, i.e., quantum regime, we find negative differential thermal conductance (NDTC), which was explained by analyzing the eigenvalues and populations of the various energy levels in nonequilibrium.

In order to explore the strong system-bath coupling regime we proposed a quantum self-consistent mean field approach (QSCMF) in which we made a bold assumption of applying Wick's theorem to anharmonic systems. The QSCMF approach was mainly based on the Green's function techniques and was limited to quartic anharmonicity and position-position coupling between the system and bath. In order to validate our assumption we compared the QSCMF approach with the master equation *like* formulation, perturbative NEGF and quantum molecular dynamics (QMD) methods. Surprisingly, for one and two particle case the QSCMF approach matched well for even strongly anharmonic systems. This unusual match was accredited to the fact that the self-consistent cycles partially take into account all strengths of anharmonic perturbation and the higher order correlations play a very small role for junction systems, where the system-size is much

smaller than the phonon mean-free path. Comparisons with perturbative

NEGF and QMD also confirmed the above, leading us to a conclusion that

the QSCMF approach is best suited for the study of thermal transport in

molecular junctions.

THIS PAGE IS INTENTIONALLY LEFT BLANK

Chapter 4

Spin transport

> No amount of experimentation can ever prove me right; a single experiment can prove me wrong.
>
> Albert Einstein

In this chapter, the phenomenon of spin transport in magnetic insulators and semiconductors will be studied. In the first part, using the modified Redfield solution (MRS) spin transport in magnetic insulators modeled as spin-1/2 anisotropic Heisenberg chains will be analyzed. The main focus will be on technologically important aspect of spin-rectification which is an essential ingredient to build spin-diodes. In the next part, in order to study spin transport in realistic experimental devices we will adopt a semi-classical approach based on the spin drift-diffusion (SDD) equations. The SDD equations will be used to study the effects of device geometries on the spin injection ratio and 'tricks' to enhance the spin injection ratio will be

discussed.

4.1   Magnetic insulators

Recently, low dimensional magnetic insulators, i.e., systems with fixed spins on a lattice, have been the subject of intense theoretical [22, 62, 65, 66, 67, 68, 50, 130, 131, 132, 133, 134, 135] and experimental investigation [136, 137]. Most of these studies are mainly focused on the linear response regime either to calculate spin-current [61, 138] or to evaluate the Onsager coefficients to obtain the thermomagnetic power [130, 134, 135]. Very little is known about such systems far from equilibrium [64, 132] although many new phenomena may appear in this regime [131]. In this section, our goal is to study spin-rectification, which is a far from equilibrium phenomenon, in such magnetic insulators modeled by spin-1/2 anisotropic Heisenberg chain using the modified Redfield solution.

4.1.1   Model and spin current

In this section, our main goal is to develop a formulation to study spin currents in magnetic insulators. There has been mounting experimental evidence [139, 140, 141, 142] that spin ladder materials like $SrCuO_2$, Sr_2CuO_3, and Cs_2CoCl_4 can be well described by the spin-1/2 anisotropic Heisenberg model (also known as the *XXZ* spin chain model) whose Hamiltonian is

given by

$$H_{\mathrm{s}} \;=\; \sum_{i=1}^{N} \mathcal{J}\left(\sigma_i^x \sigma_{i+1}^x + \sigma_i^y \sigma_{i+1}^y + \Lambda \sigma_i^z \sigma_{i+1}^z\right) - h\sigma_i^z \,, \qquad (4.1)$$

where $\mathcal{J}$ is known as the exchange coupling between the nearest neighbor spins, Λ is the xz magnetic anisotropy, h is the external magnetic field along the z-direction and σ_i^k $(k = x, y, z)$ are the Pauli matrices of the i-th spin. For the above system Hamiltonian, simple limiting cases are when $\Lambda = 0$ (XY model), which corresponds to free spinless lattice fermions via the Jordon-Wigner transformation [143], and $\Lambda \to \infty$, which corresponds to the Ising model.

The above system Hamiltonian, being an integrable quantum model [144], possess a macroscopic number of nontrivial conservation laws (refer [59] and references therein). One of which is the conservation of total spin along the z-direction. The spin conservation law permits us to write a lattice continuity equation and hence define a local spin operator as,

$$\frac{\mathrm{d}\sigma_i^z}{\mathrm{d}t} \;=\; j_{(i-1)\to i} - j_{i\to(i-1)} \,, \qquad (4.2)$$

$$j_{n\to m} \;=\; 2\mathcal{J}\left(\sigma_n^x \sigma_m^y - \sigma_n^y \sigma_m^x\right) \,, \qquad (4.3)$$

where $j_{n\to m}$ is an (n, m)-th element of the local spin operator j, indicating the flow of spin from site n to site m. Typically, in order to evaluate

the spin current one uses the local spin current operator j along with the reduced density matrix ρ, obtained by the master equation approach, to obtain the average spin current $j_\mathrm{s} = \langle j \rangle = \mathrm{Tr}\left(\rho j\right)$. Till date, the reduced density matrix has always been calculated using the Lindblad formulation [72] where an asymmetry is introduced in the Lindblad operators of the two leads which drives a spin current in the system [65, 66, 67, 68]. The driving parameter and the Lindblad operators are phenomenologically justified as representing a spin-chemical potential and magnetic leads, but the actual microscopic form of the Hamiltonian from which these operators arise is intractable. Temperature in the Lindblad formulation is also undefined and since the Lindblad operators for the equilibrium case give a uniform probability distribution it is generally assumed that the Lindblad formulation corresponds to a system connected to baths at infinite temperature.

In order to avoid such phenomenological problems we treat the baths as a set of harmonic oscillators described by Eq. (2.2). Since the baths have no magnetization the concept of spin-chemical potential is inapplicable and hence a spin-chemical potential driving is not possible. Fortunately, the spin Seebeck effect [135] provides us with an alternate driving field, i.e., a thermal gradient, in such non-magnetized harmonic chain baths. Analogous to the Seebeck effect [145] studied in electronic transport, the spin Seebeck effect in our model generates a spin voltage at the system-bath interface in

the presence of a thermal gradient which in turn generates a spin current in the system. Thus, without resorting to the *ad-hoc* Lindblad formulation we can still calculate the spin current in the system with the thermal gradient as the driving field.

Now since the microscopic Hamiltonians of the system and bath are well-defined we focus on the evaluation of the reduced density matrix to calculate the spin current. As seen in case of heat in Sec. 3.1.1, at the lowest order of perturbation the current is second order in the system-bath coupling. This is not only true for heat transport, but is a general statement for any kind of current (*e.g.*, spin, particle, *etc.*). This is mainly due to the fact that transport crucially depends on the coupling with the baths and if the coupling vanishes so does the current. The first order in the coupling can always be made zero by centering of the bath variable described in Sec. 2.1.1 and hence the lowest order current has to be second order in the system-bath coupling. Going back to the specific case of spin transport described above, the local spin-current operator j is independent of coupling strength and hence in order to accurately capture the nonequilibrium effects it is essential to obtain the reduced density matrix correct up to second order in the system-bath coupling. Since all perturbative master equations are inaccurate at the second order in the steady state (Sec. 2.2), we resort to our novel modified Redfield solution described in Sec. 2.3.2

which accurately captures all second order steady state effects. Thus, the local-current operator given by Eq. (4.3) and the Modified Redfield solution outlined in Sec. 2.3.2 give us a clear and accurate prescription to calculate the spin-current[1] in the spin-1/2 anisotropic Heisenberg chain.

4.1.2 Spin rectification

In this section we study the phenomenon of spin rectification which is essential to build spin-diodes in magnetic insulators. Hoogdalem and Loss [64] have studied rectification in the spin-1/2 anisotropic Heisenberg chain using a wide variety of perturbative techniques, with different regions of validity. Their work encompasses: Renormalization group, wherein they consider only the low energy excitation (equivalent to low temperature); Luttinger liquid formulation, wherein they consider $\Lambda \ll 1$ and $h \ll \mathcal{J}$, to essentially treat the system as ballistic and Spin-wave formulation, wherein $\mathcal{J} < 0$, $\Lambda > 1$, and temperature is low. Despite their extensive efforts their techniques fail to capture the anti-ferromagnetic [146] ($\Lambda > 1$ and $\mathcal{J} > 0$) regime for finite sized spin chains. In this regime there has been mounting evidence that the transport is mainly diffusive [65, 66, 67, 147, 148], whereas for $\Lambda < 1$ the system exhibits a ballistic behavior [60, 67, 149]. In this section we will focus on rectification in this unexplored anti-ferromagnetic diffusive transport regime with $\mathcal{J} > 0$ and $\Lambda > 1$, where our approach can

---

[1]It is important to note that since the baths do not have any spins we can not define the spin current as $\frac{d\sigma_L^z}{dt}$ and hence a formulation like Sec. 3.1.1 is impossible.

be easily applied.

We begin by construing rectification as the phenomenon in which if we interchange the temperature of the two baths the backward current would have a different value as compared to the forward current (obtained when the bath temperatures are not interchanged). In order to study this effect we define the forward spin current j_s^+ as the current flowing from left to right, with the left bath at temperature $T_L > T_R$ (temperature of right bath), and the backward current j_s^- as the one flowing from right to left when the temperatures of the left and right bath are interchanged, i.e., $T_R'(= T_L) > T_L'(= T_R)$. Given these definitions we can now quantify the rectification effect using a ratio[2] given by,

$$ R \ = \ \left| \frac{j_s^+ - j_s^-}{j_s^+ + j_s^-} \right| . \tag{4.4} $$

It is important to note that not all systems show rectification and anharmonicity and asymmetry are crucial properties for a system to exhibit a non-zero rectification ratio.

For the specific case of spin transport since we will be working in the diffusive regime ($\mathcal{J} > 0$ and $\Lambda > 1$) the spin current will reduce with system size, but this global effect could overshadow the local effects of magneti-

---

[2]Many times the rectification ratio is also defined as $R = \left| \frac{j_s^+ - j_s^-}{\text{Max.}(j_s^+, j_s^-)} \right|$ due to which $R > 1$, whereas in our definition $R \leq 1$.

zation and thus make the physics at the microscopic level unclear. The rectification ratio R defined above neutralizes the effect of system-size dependence (due to the normalization) of spin current, thus allowing us to understand and probe the local effects better. Also in this regime since $\Lambda \neq 0$ there is inherent anharmonicity in the system. In order to induce asymmetry we couple the system with two Lorentz-Drude baths (described in Append. A.3.3) using different system-bath coupling strengths. The system operator coupling to the bath and the spectral densities of the two baths are given by

$$S^{\mathrm{L}} = \sigma_1^x \quad ; \quad S^{\mathrm{R}} = \sigma_N^x \,, \tag{4.5}$$

$$\mathrm{J}^{\mathrm{L}}(\omega) = \frac{\eta(1+\xi)\omega}{1+(\omega/\omega_{\mathrm{D}})^2} \quad ; \quad \mathrm{J}^{\mathrm{R}}(\omega) = \frac{\eta(1-\xi)\omega}{1+(\omega/\omega_{\mathrm{D}})^2} \,, \tag{4.6}$$

where $-1 < \xi < 1$ is a dimensionless asymmetry parameter and $\sqrt{\eta(1+\xi)}$, $\sqrt{\eta(1-\xi)}$ are the system-bath coupling strength of the left and right bath respectively.

In spin rectification one of the currents (j_{s}^+ or j_{s}^-) is suppressed more than the other, due to anharmonicity and asymmetry in the system. Thus as ΔT increases the partially suppressed current increases much faster than its counterpart causing the rectification ratio R to increase as shown in Fig. 4.1a. Here the solid and dashed lines correspond to even and odd
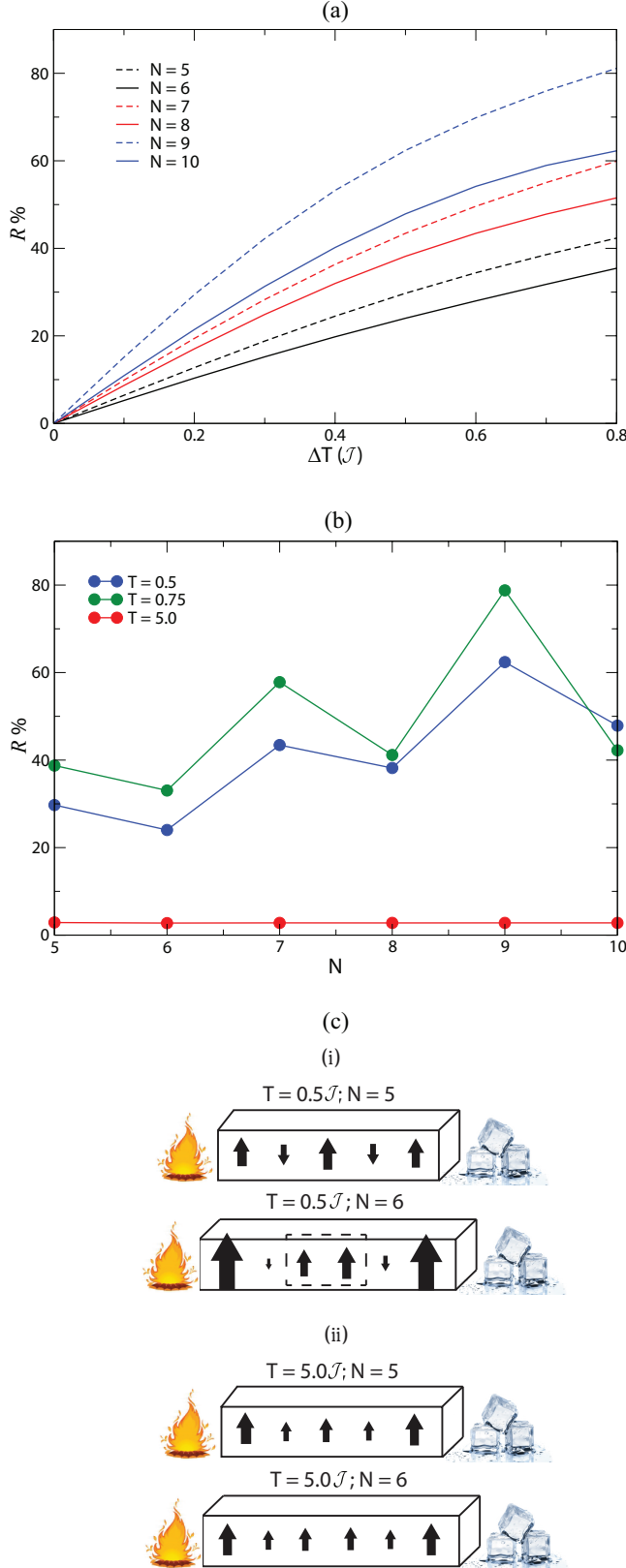
Figure 4.1: (a) shows a graph of rectification ratio R (in percentage %) as a function of the temperature difference $\Delta T = T_{\mathrm{L}} - T_{\mathrm{R}}$ between the two baths for different system sizes N. The average temperature $T = (T_{\mathrm{L}} + T_{\mathrm{R}})/2 = 0.5\mathcal{J}$. In Fig. (b) we plot R vs system size N at different average temperatures T. All curves have the same temperature difference $\Delta T = 0.5\mathcal{J}$. In Fig. (c) we illustrate the $\langle \sigma^z \rangle$ component at each site of a system consisting of 5 (top) and 6 (bottom) spins at two different temperatures: $T = 0.5\mathcal{J}$ in (i) and $T = 5.0\mathcal{J}$ in (ii). The length of each arrow is proportional to the $\langle \sigma^z \rangle$ at that site. In case of Fig. (c) i (bottom) and Fig. (c) ii the largest $\langle \sigma^z \rangle$ is $\approx 5\times$ smaller than the largest $\langle \sigma^z \rangle$ value of Fig. (c) i (top). The common parameters for all these simulations are: $\Lambda = 1.5$, $h = 0.5\mathcal{J}$, $\eta = 0.01\sqrt{\mathcal{J}}$, $\xi = 0.9$, and $\omega_{\mathrm{D}} = 10\mathcal{J}$.

number of spins[3] respectively. Clearly the odd and even numbers cause the rectification ratio R to oscillate which has been depicted in Fig. 4.1b.

The oscillatory behavior of R is prominent at low temperatures, whereas at high temperature the effect becomes negligible. In order to understand the origin of these oscillations we illustrate in Fig. 4.1c the $\langle \sigma_i^z \rangle$ at each site for a system comprising of 5 and 6 spins at two different average temperatures[4] $T = (T_{\rm L} + T_{\rm R})/2 = 0.5\mathcal{J}$ and $= 5.0\mathcal{J}$. Since the two end spins $i = 1, N$ are connected to the baths their $\langle \sigma_{1/N}^z \rangle$ values are greatly influenced by the bath temperature, which causes the z-component of the two end spins to be always in the same direction. This pinning of the end spins permits an anti-ferromagnetic ordering only in the case of odd number of spins as shown in Fig. 4.1c (i) (top). In case of even number of spins (Fig. 4.1c (i) bottom) the system cannot attain its lowest energy anti-ferromagnetic state because one pair of spins forms a ferromagnetic bond (enclosed in dashed lines). This single ferromagnetic bond, which is a result of spin frustration, causes the z-component of spin to be redistributed in other directions causing the $\langle \sigma_i^z \rangle$ to lower at each site. This leads to a reduction in the rectification ratio R for even number of spins as compared to its odd counterparts. The oscillatory behavior is also sensitive to the temperature T and if the temperature

---

[3]Due to the 2^N system Hilbert space our approach is computationally limited to treat at most 10 spins.

[4]Throughout this section all quantities will be measured in units of the exchange coupling $\mathcal{J}$.

becomes very high there is no anti-ferromagnetic order and thus the $\langle \sigma_i^z \rangle$
at each site reduces drastically as shown in Fig. 4.1c (ii). This completely
kills the oscillatory behavior of R and reduces it drastically as depicted by
the red solid line in Fig. 4.1b. Thus we deduce that an oscillatory behavior
in the rectification ratio R as a function of system size is related to the
finite size of spin chain and the absence/presence of spin frustration. To
the best of our knowledge this effect has not been reported in the literature
mainly because nearly all works pertaining to spin transport in insulators
deal with either with very large sizes or mainly calculate at spin current,
where this effect might be absent due to the diffusive behavior.

Next we would like to study the effects of the external magnetic field
h, as shown in Fig. 4.2, on the rectification ratio and see if it can be used
to tune the rectification ratio R. Fig. 4.2a shows the effect on the individ-
ual forward j_s^+ and backward j_s^- currents. At low temperatures (Fig. 4.2a
top) and low magnetic fields the spin current is negative indicating that
the current is carried by the down spins, but as soon as the magnetic field
becomes stronger than the magnetic anisotropy Λ it flips the spin carriers
to up spins indicated by the positive spin current[5]. In case of rectification
R the current carriers must be the same for both forward and backward

[5]The carriers of spin current, i.e., up or down spins are decided by the value of the
spin Seebeck coefficient. In our case since we cannot directly calculate this value, due to
the lack of magnetic baths, we infer from the positive (negative) sign of the current that
the spin Seebeck coefficient must be positive (negative) [130].
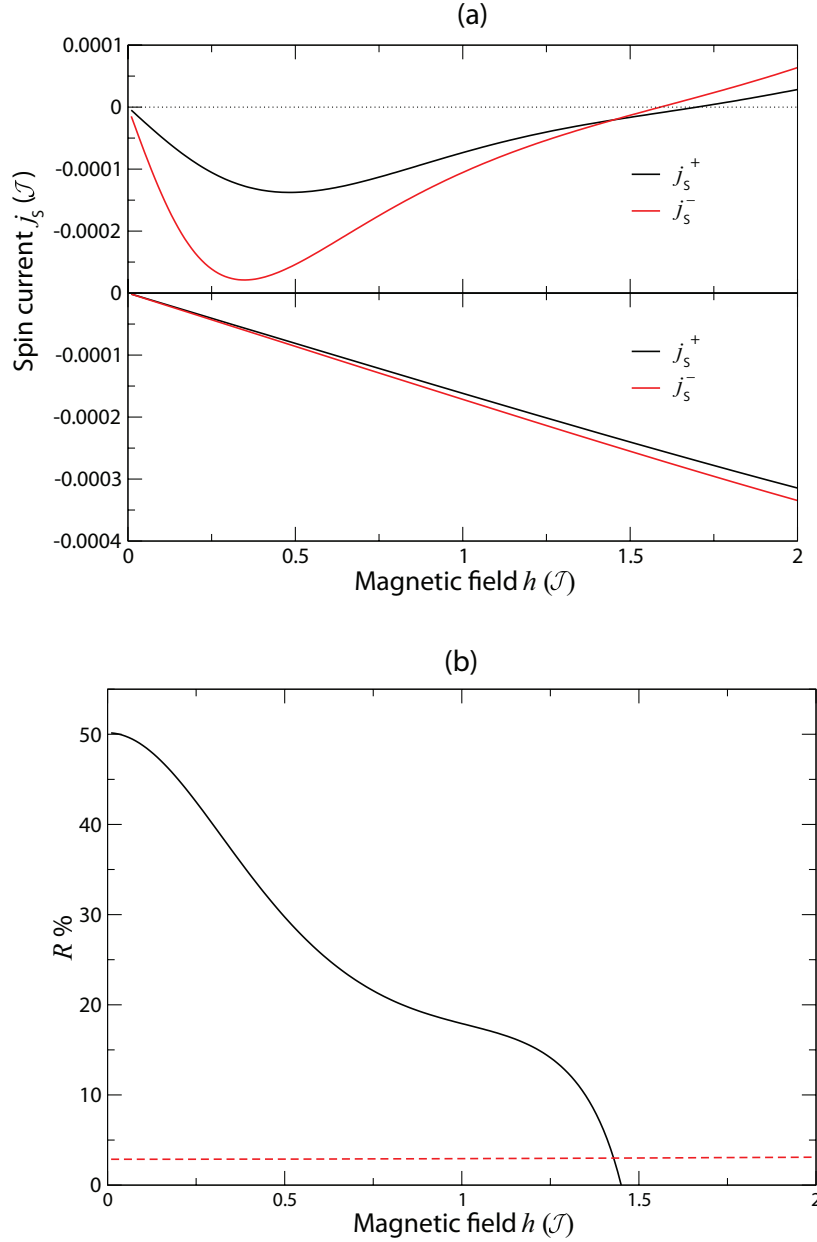
Figure 4.2: (a) shows a graph of forward j_s^+ (black) and backward j_s^- (red) currents as a function of the magnetic field h for average temperature $T = (T_L + T_R)/2 = 0.5\mathcal{J}$ (top) and $T = 5.0\mathcal{J}$ (bottom). In Fig. (b) we plot the rectification ratio R (in percentage %) vs h at average temperature $T = 0.5\mathcal{J}$ (solid black) and $T = 5.0\mathcal{J}$ (dashed red). The common parameters used are: $N = 5$, $\Lambda = 1.5$, $T_L - T_R = 0.5\mathcal{J}$, $\eta = 0.01\sqrt{\mathcal{J}}$, $\xi = 0.9$, and $\omega_D = 10\mathcal{J}$.

currents to have meaningful results, i.e., $R \not> 100\%$. This is not a problem in case of charge and heat transport, where R has been predominantly studied, since there is only one carrier of current, i.e, either electrons or phonons. In case of spin transport due to the up and down nature of spins the transport is characterized by two carriers. Hence it only makes sense to plot rectification R when $h/\mathcal{J} < \Lambda$ as shown in Fig. 4.2b (solid line) to take into account only the current carried by the down spins. Clearly at low temperatures the rectification R can be easily tuned with the external magnetic field $0 < h/\mathcal{J} < \Lambda$ and it shows a variation of $\approx 50\%$ which can be easily detected. Observing Figs. 4.2a (top) and 4.2b (black solid line) we find that even though the rectification R is largest at small magnetic field h the spin current is the smallest in that regime. This might pose a problem in an experimental setup where the strength of the signal plays a crucial role and hence it is judicious to tune the magnetic field at $h/\mathcal{J} \approx \Lambda/4$ (for the parameters in Fig. 4.2a top), where the signal to noise ratio is the highest, to observe spin rectification. Another important parameter is average temperature T and at high temperatures as seen from Fig. 4.2a (bottom) the forward and backward currents are always carried by the down spins. The rectification ratio R (Fig. 4.2b red dashed line) also remains constant and is quite low as compared to the low-temperature regime, making the high-temperature regime undesirable for tuning R. Thus, in small finite sized

magnetic insulators an extremely high value of spin rectification can be obtained in the low-temperature regime and it can be tuned using an external magnetic field whereas the effect diminishes drastically as the temperature increases.

4.2 Semiconductors

Since the advent of spintronics one of the main theoretical challenges has been to describe devices on experimentally relevant spatial scales. As seen in the previous sections a complete quantum mechanical description of such systems would be an unfathomable task at even the nano-meter scale due to the sheer size of the system Hilbert space. Hence, in this section we adopt a semi-classical linear response approach to study spin transport in semiconductors connected to ferromagnetic baths. Following the earlier work of P.C. van Son *et al.* [150] on spin drift and diffusion (SDD) model, in this section we will extend their approach to three spatial dimensions to treat experimentally relevant geometries and study the effect of device geometries on the spin injection ratio of these devices.

4.2.1 Spin drift diffusion equations

As compared to the magnetic insulators described in the previous section, semiconductors have itinerant spins which are carried by the charge carriers in the system. Hence in order to understand efficient spin transport

in semiconductors it is necessary to understand the coupling between charge and spin currents, which was first described by Aronov [151] and later developed by Johnson and Silsbee in terms of thermodynamic processes [152]. P.C. van Son *et al.* [150] later proposed a much simpler semi-classical one-dimensional linear response model based on spin drift and diffusion (1D-SDD) to describe transport across a ferromagnetic (FM) - semiconductor (SC) interface. The 1D-SDD model was successfully applied to current perpendicular to plane geometries of giant magneto-resistance by Valet and Fert and they also established the connection between the diffusive model and the Boltzmann equation [56]. Since then the 1D-SDD has been used to describe spin transport across many local [153, 154] and non-local geometries [155, 156, 157, 158]. Despite its extensive success, a 1D theory is insufficient to describe a three-dimensional experimental geometry [159] and hence in this section we will extend the 1D-SDD model to three spatial dimensions in order to study the geometrical effects on spin transport.

We begin this section by deriving the three-dimensional spin drift diffusion (3D-SDD) equations and in order to do this we assume that far from the interface at temperatures lower than the Curie temperature most scattering events will conserve the spin direction[6] causing the spin up and spin down electrons to flow almost independently of each other [52, 160]. Also,

---

[6]In our semi-classical approach to obtain the SDD equations temperature does not enter explicitly like the previous section, but as stated it is extremely important parameter for the validity of the equations.

if the spin scattering occurs at much longer time-scale than other electron scattering events we can define the electrochemical potentials $\mu_\uparrow$ and $\mu_\downarrow$ for both the spin channels. Thus, in the linear response regime the current carried by the spin-up ($\mathbf{j}_\uparrow$) and spin-down ($\mathbf{j}_\downarrow$) channel[7] is given by Ohm's law:

$$\mathbf{j}_{\uparrow,\downarrow} \;=\; \frac{\sigma_{\uparrow,\downarrow}}{e}\vec{\nabla}\mu_{\uparrow,\downarrow}\,, \tag{4.7}$$

where $\sigma_{\uparrow,\downarrow} = \sigma(1\pm\alpha)/2$ is the spin dependent electrical conductivity[8] and $e\ (>0)$ is the electron charge. Near the interface the spin can diffuse from the up-spin channel to the down-spin channel and in general the diffusion of spin is not restricted to one spatial dimension. Thus the coupling of the two spin channels is governed by the most general diffusion equation in three dimensions given by,

$$\frac{\mu_\uparrow - \mu_\downarrow}{\tau} \;=\; D\nabla^2(\mu_\uparrow - \mu_\downarrow)\,, \tag{4.8}$$

where D is the Diffusion constant, τ is the spin-relaxation time and $\sqrt{D\tau} = \lambda$ is the spin diffusion length. This type of model description is considered semi-classical because the electrons which carry the spins are mainly fol-

---

[7]In our 3D model since vectors will play a crucial role, all vectors from now on will be indicated using a bold font.

[8]Since we are dealing with semiconductors which are mostly isotropic materials σ should be treated here as a number.

lowing classical dynamics, whereas the spins are considered to have two states (up and down) like the quantum case. Also this approach is in stark contrast to our previous sections where we dealt with a microscopic Hamiltonian to describe the system and the baths. In our semi-classical 3D-SDD approach all the intricate details of the material will be ignored and the macroscopic parameters like $\sigma_{\uparrow,\downarrow}$, D and τ will help us engineer the physics of spintronic devices.

Now in order to simplify notation we use the following transformations [153],

$$
\begin{aligned}
\zeta &= \mu_\uparrow - \mu_\downarrow \,, \\
Z &= \frac{\mu_\uparrow + \mu_\downarrow}{2} \,, \\
P &= \frac{(\mathbf{j}_\uparrow - \mathbf{j}_\downarrow) \cdot \hat{n}_1}{(\mathbf{j}_\uparrow + \mathbf{j}_\downarrow) \cdot \hat{n}_1} \,,
\end{aligned}
\tag{4.9}
$$

where P is the amount of polarized spin current and is commonly known as the spin injection ratio and $\hat{n}_1$ is taken as the normal to the surface along the flow direction.

Eqs. (4.7) and (4.8) then transform into:

$$
\nabla^2 \zeta = \frac{\zeta}{\lambda^2} \,,
\tag{4.10}
$$

$$
\vec{\nabla} Z = -\left(\frac{\Delta\sigma}{2\sigma}\right) \vec{\nabla}\zeta + \frac{\mathbf{J}e}{\sigma} \,,
\tag{4.11}
$$

$$P \;=\; \frac{2\sigma_\uparrow \sigma_\downarrow}{\sigma} \frac{(\vec{\nabla}\zeta)\cdot\hat{n}_1}{\mathbf{J}\cdot\hat{n}_1 e} + \frac{\Delta\sigma}{\sigma}\,, \qquad (4.12)$$

where $\Delta\sigma = \sigma_\uparrow - \sigma_\downarrow$ and $\mathbf{J} = \mathbf{j}_\uparrow + \mathbf{j}_\downarrow$ is the total current through the system.

Next we impose the boundary conditions for the transformed equations, keeping in mind that the baths considered here are ferromagnetic and the system a semiconductor leading us to,

$$P_F|_0 \;=\; P_{SC}|_0 = P\,, \qquad (4.13)$$

$$\zeta_{SC}|_0 - \zeta_F|_0 \;=\; 2r_c\left(P - \frac{\Delta\Sigma}{\Sigma}\right)(\mathbf{J}\cdot\hat{n}_1)e\,, \qquad (4.14)$$

$$Z_{SC}|_0 - Z_F|_0 \;=\; r_c\left(1 - \frac{\Delta\Sigma}{\Sigma}P\right)(\mathbf{J}\cdot\hat{n}_1)e\,, \qquad (4.15)$$

$$\zeta|_{\pm\infty} \;=\; 0\,, \qquad (4.16)$$

$$(\mathbf{j}_\uparrow - \mathbf{j}_\downarrow)\cdot\hat{n}_2 \;=\; 0\,, \qquad (4.17)$$

where $\Delta\Sigma = \Sigma_\uparrow - \Sigma_\downarrow = P/\left[r_c\left(1 - P^2\right)\right]$, $\Sigma = \Sigma_\uparrow + \Sigma_\downarrow = \left[r_c\left(1 - P^2\right)\right]^{-1}$, $r_c = \Sigma/(4\Sigma_\uparrow\Sigma_\downarrow)$ is the effective contact resistance (also sometimes called the Kapitza resistance for spin transport) and $\hat{n}_2$ is the normal to the boundary of the domain. The subscript 0 above denotes the interface and Ω is the domain of the device[9]. The boundary condition of Eq. (4.13) ensures that the spin current is conserved at the interface *iff* the interface is a constant potential surface, which is a valid assumption for semiconductors that have

---

[9]Also all equations without the sub-scripts correspond to both the regions.

the in plane conductivity component nearly equal to the out of plane component. Eqns. (4.14) and (4.15) describe the boundary conditions at the FM-SC interface due to mismatch in the conductivity of the two materials [69, 70] where the Kapitza type resistance plays an important role. The crucial boundary condition is Eq. (4.16), which implies that at the edges of the device far away from the interface the spins do not diffuse and essentially the up- and down-spin channels cannot be distinguished. The baths due to their infinite nature satisfy this condition by definition, but the system is always finite and thus Eq. (4.16) cannot be satisfied at all system edges which essentially gives rise to the geometrical effects on spin-injection we will discuss later in Sec. 4.2.2. In addition to Eqs. (4.14), (4.15), (4.16), and (4.13) which are generally used for the 1D-SDD model, we use an additional condition given by Eq. (4.17) for the 3D-SDD model, which ensures that no spin current leaks out of the device.

4.2.2 Geometrical effects on spin injection

In this section we focus on an important aspect of spin transport with itinerant spins known as the spin injection ratio defined in Eq. (4.9), which estimates the amount of spin current injected into the system. A high spin injection ratio indicates a better signal to noise ratio and is considered as a basic prerequisite to build efficient spin-diodes (also known as spin-valves). In order to estimate the spin injection ratio we solve our 3D-SDD equa-

tions, i.e., Eqs. (4.10) and (4.11), using a partial differential equation solver known as Free FEM 3D [161] along with the appropriate boundary conditions (Eqs. (4.13), (4.14), (4.15), (4.16) and (4.17)). Free FEM 3D employs fictitious domain finite element method [162], which allows us to change the device geometry without actually changing the grid thus reducing the computational complexity of the problem drastically. In order to evaluate the spin injection ratio P, which is a variable parameter in the boundary conditions, we solve the equations in the two regions (FM and SC) separately and iteratively vary the boundary conditions till a convergence of 10^{-6} in the spin injection ratio is achieved. To ensure that all the results are well converged with respect to the grid parameters we make sure that for boundaries where Eq. (4.16) needs to be satisfied is $\sim 5 \times$ the spin diffusion length. Also the grid spacing is varied until convergence is achieved. As an additional check we use the converged grid parameters for 1D geometries to ensure that the analytical 1D results [150] are recovered.

In order to study the effect of device geometries on the spin injection ratio, we first look the effect of height (H) of the semiconductor and contact area (CA) for a device geometry shown in Fig. 4.3a inset. The device is made of NiFe ferromagnets and the semiconductor used for this calculation is an n-type GaAs. Kumar *et al.* [154] have shown the effect of nano-pillar ferromagnet on the spin injection ratio by incorporating the effects
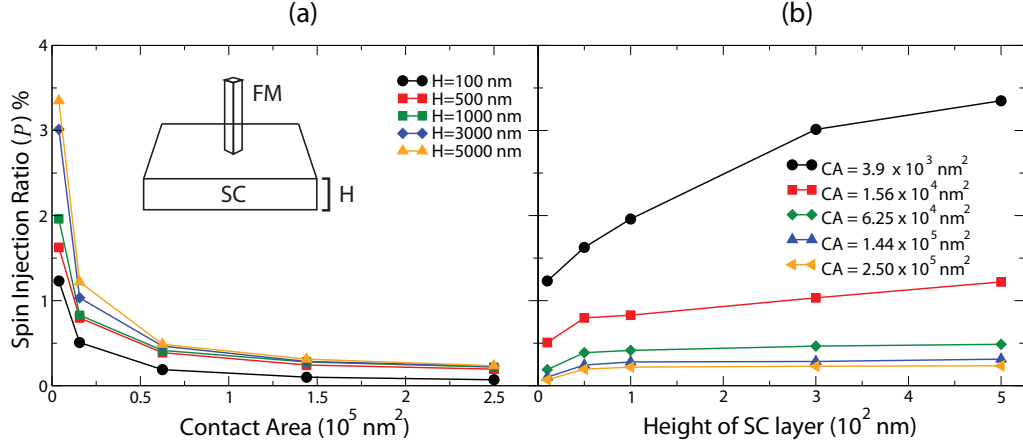
Figure 4.3: Graph of spin injection ratio (P) for a direct contact NiFe-nGaAs device. Fig. (a) shows the spin injection ratio as a function of the contact area for various semiconductor heights. The inset shows a schematic of the device geometry under consideration. Fig. (b) shows P as a function of the semiconductor height for various contact areas. The NiFe ferromagnet parameters used in this calculation are: $\sigma_{\mathrm{NiFe}} = 8.62 \times 10^6 /\Omega\mathrm{m}$, $\lambda_{\mathrm{NiFe}} = 10$ nm, and $\alpha_{\mathrm{NiFe}} = 0.4$. The nGaAs parameters are: $\sigma_{\mathrm{n-GaAs}} = 10^5 /\Omega\mathrm{m}$, $\lambda_{\mathrm{n-GaAs}} = 1$ $\mu\mathrm{m}$, $\alpha_{\mathrm{n-GaAs}} = 0$, and $r_c = 0$ $\Omega\mathrm{m}^2$.

of spreading resistance in the 1D-SDD model, but they could not show the effect of SC height since the model was essentially 1D. It should also be noted that they used a contact area of ~ 12.5 nm^2 which is extremely difficult to reproduce experimentally and hence we study the effect of varying contact area CA on the spin injection ratio P (Fig. 4.3a). It can be seen from the figure that as the contact area increases P decreases rapidly. Due to the rapid decay a contact area of at least $\sim 10^3$ nm^2 would be required in order to achieve a direct contact spin signal into the device. According to our knowledge there has been no experimental evidence of direct contact spin injection into a semiconductor because most experimental geometries
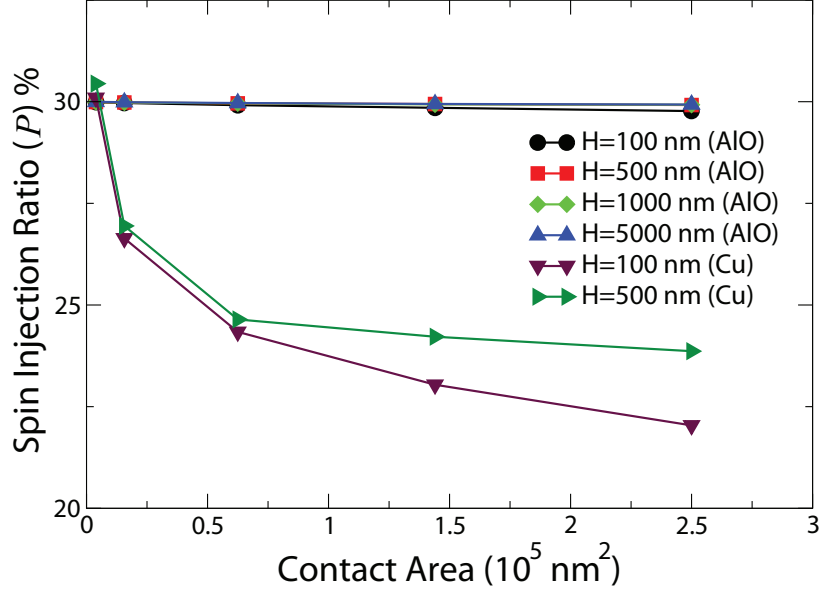
Figure 4.4: Graph of spin injection ratio (P) versus contact area for a NiFe-nGaAs device. Different curves are for different heights of the semiconductor, either for an AlO tunneling barrier or thin Cu film. The NiFe ferromagnet parameters used in this calculation are: $\sigma_{\text{NiFe}} = 8.62 \times 10^6/\Omega\text{m}$, $\lambda_{\text{NiFe}} = 10$ nm, and $\alpha_{\text{NiFe}} = 0.4$. The nGaAs parameters are: $\sigma_{\text{n-GaAs}} = 10^5/\Omega\text{m}$, $\lambda_{\text{n-GaAs}} = 1$ μm, and $\alpha_{\text{n-GaAs}} = 0$. The AlO tunneling barrier has parameters: $r_c = 10^{-7}$ Ωm^2 and $\Delta\Sigma/\Sigma = 0.3$, while the Cu thin film has parameters: $r_c = 0$ Ωm^2, $\sigma_{\text{Cu}} = 59.52 \times 10^6/\Omega\text{m}$, , $\lambda_{\text{Cu}} = 140$ nm,$\alpha_{\text{Cu}} = 0$, $r_c = 0$ Ωm^2 and thickness of Cu $= 50$ nm.

have a contact area of $\sim 10^5$ nm^2. We also study the effect of sample height

on the spin injection ratio (Fig. 4.3b). For a given contact area the spin

injection ratio increases nearly linearly for small sample thickness, but as

the sample thickness approaches the order of λ_{SC} the rate of change of the

spin injection ratio reduces drastically. Thus, in order to achieve better

spin injection in direct contact devices a smaller contact area and a sample

height $\gg \lambda_{SC}$ are required.

Since extremely small contact areas are not feasible experimentally we

104

investigate the role of tunneling barrier (AlO) and a thin metal (Cu) layer insertion between the ferromagnet and semiconductor for a device geometry similar to the one shown in Fig. 4.3a inset. Tunneling barriers like AlO [163] are an excellent solution to the conductivity mismatch problem, but one of the main practical problems with tunneling barriers is pinhole defects [164, 165], which are created during the deposition of tunneling barriers. Thus, due to these small pinholes the ferromagnetic bath is in direct contact with the semiconductor. Such defects are typically unavoidable in experiment due to the technological limitation of setting up a few layer thin uniform oxide barrier, but if we consider "ideal" tunneling barriers without any pinholes then Fig. 4.4 shows that they are robust to variations in contact area and SC height. But for small contact areas we can see that thin Cu films ($\sim$ 50 nm)[10] can be excellent substitutes for tunneling barriers. It should be noted here that although using thin Cu film will decrease the effective spin diffusion length of the device, atomistically thin metal films are easily producible using the current technology. Hence only for small contact areas and where the spin diffusion length is not very important for the device thin metal films can act as excellent injectors of spins.

Lastly we discuss pinholes in tunneling barriers and its effect on the

---

[10]The thickness of the Cu layer as 50 nm is chosen purely due to computational limitations and in an experimental situation the thickness of the Cu layer should be made as thin as possible. Also the spin-injection ratio P is measured at the Cu-SC interface, taking into account the spin relaxation within the Cu buffer layer.
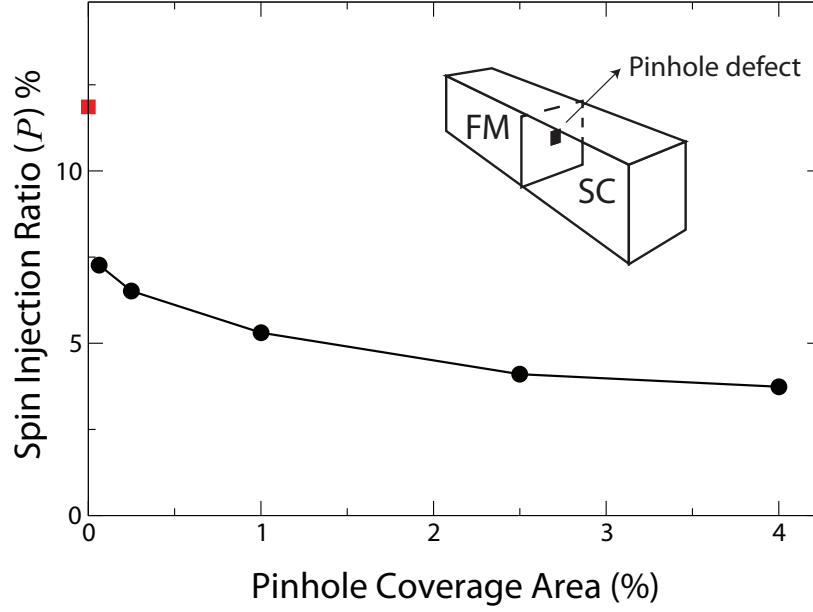
Figure 4.5: Graph of spin injection ratio (P) versus pinhole coverage area [= Area of pinhole/Total contact area] for a NiFe-GaAs device. The red square represents result for the "ideal" tunneling barrier. The NiFe ferromagnet parameters used in this calculation are: $\sigma_{\mathrm{NiFe}} = 8.62 \times 10^6/\Omega\mathrm{m}$, $\lambda_{\mathrm{NiFe}} = 10$ nm, and $\alpha_{\mathrm{NiFe}} = 0.4$. The GaAs parameters are: $\sigma_{\mathrm{GaAs}} = 10^3/\Omega\mathrm{m}$, $\lambda_{\mathrm{GaAs}} = 1$ μm, and $\alpha_{\mathrm{GaAs}} = 0$. The AlO tunneling barrier has parameters: $r_c = 10^{-7}$ $\Omega\mathrm{m}^2$ and $\Delta\Sigma/\Sigma = 0.3$.

spin injection ratio P. Although some discussions about pinholes [166] have been made in the tunneling magneto-resistance experiments based on a simple resistor model by Oliver *et al.* [167], there has been no work on this topic from the view point of the SDD model which is in general applicable to all spin-valve devices. In order to discuss pinholes we study a FM-SC (FeNi-GaAs) interface with a single pinhole in the tunneling barrier (AlO) as shown in Fig. 4.5 inset. Fig. 4.5 shows the effect of pinhole coverage area, i.e., the ratio of the pinhole area to the total contact area, on the spin

injection ratio for the device. There are two competing effects here that determine the spin injection ratio, one of the conduction electrons passing through the pinhole (reducing P) and second due to the tunneling electrons passing via the tunneling barrier (increasing P). In order to understand the results obtained via simulations and thus the effect of pinholes, let us consider two channels one for the conduction electrons (pinhole channel) and the second for the tunneling electrons (tunneling barrier channel). By assuming that these channels are independent it can be shown that the spin injection ratio of the device comprising of these two channels can be given by,

$$P = \frac{\mathbf{j_{1,\uparrow}} + \mathbf{j_{2,\uparrow}} - \mathbf{j_{1,\downarrow}} - \mathbf{j_{2,\downarrow}}}{\mathbf{j_{1,\uparrow}} + \mathbf{j_{2,\uparrow}} + \mathbf{j_{1,\downarrow}} + \mathbf{j_{2,\downarrow}}} = P_1 \frac{\mathbf{J_1}}{\mathbf{J_1} + \mathbf{J_2}} + P_2 \frac{\mathbf{J_2}}{\mathbf{J_1} + \mathbf{J_2}}, \qquad (4.18)$$

where $\mathbf{j_{1,2,\uparrow,\downarrow}}$, $\mathbf{J_{1,2}} = \mathbf{j_{1,2,\uparrow}} + \mathbf{j_{1,2,\downarrow}}$ are the up/down spin currents and total currents for the two channels and $P_{1,2} = (\mathbf{j_{1,2,\uparrow}} - \mathbf{j_{1,2,\downarrow}})/(\mathbf{j_{1,2,\uparrow}} + \mathbf{j_{1,2,\downarrow}})$ are the spin injection ratios of the two channels.

In case of the smallest pinhole, we simulate a direct contact system with the contact area equal to the size of the pinhole and obtain P_1 as 7.38%. Performing a similar calculation for the perfect tunneling barrier case we get $P_2 = 11.85\%$ and the fact that the pinhole acts like a short circuit causing most of the current to pass through the pinhole $(\mathbf{J_1}/(\mathbf{J_1} + \mathbf{J_2}) = 95\%$ from simulations) we get $P = 7.6\%$ (from Eq. (4.17)), which is quite close to

the value 7.26% obtained via simulations. The discrepancy of 0.34% seen is due to the fact that the tunneling barrier region now has a pinhole defect in it which was not considered while calculating P_2. This result cannot be understood using the 1D-SDD model, which gives $P = 0.6\%$, since the effect of area cannot be taken into account. Thus, overall effect of pinholes is not just the sum of two individual 1D channels. We also simulate more than one pinhole to see if there is any correlation between them and we observe no such correlations at distances of ~ 300 nm, ~ 500 nm and ~ 800 nm, which are typically the experimentally observable distances for such spin-valve devices. Hence we conclude that the spin injection ratio depends only on the effective coverage area of the pinholes and not the number of pinholes present in the tunneling barrier.

4.3   Summary

In summary, spin transport of fixed spins was studied in the first part using the example of magnetic insulators. The insulators were modeled as spin-1/2 anisotropic Heisenberg spin chains and based on the lattice continuity equation a local spin current operator was derived. Since current is a second order effect in the system-bath coupling the modified Redfield solution was used to evaluate the reduced density matrix in order to accurately capture all nonequilibrium effects. The baths were modeled as harmonic heat baths, which posses a microscopic Hamiltonian description, and due

to the spin Seebeck effect a spin current was induced in the presence of a temperature difference. As an example, we considered the technologically important phenomenon of spin rectification which was studied in the diffusive transport regime of $\mathcal{J} > 0$ and $\Lambda > 1$. At low temperatures the spin rectification oscillated with system size and the effect was attributed to the breaking of anti-ferromagnetic ordering due to spin frustration. In order to control rectification using an external field we studied the phenomenon by varying the magnetic field and found that at low temperatures the rectification ratio R can be easily tuned for $0 < h/\mathcal{J} < \Lambda$, whereas at high temperatures the magnetic field did not affect R. Thus, using the simple spin-1/2 anisotropic Heisenberg spin chain to model magnetic insulators spin rectification in finite systems was studied and interesting features were found and explained.

In the second part, in order to study spin transport in semiconductors on actual experimental scales we improved upon the semi-classical one-dimensional spin drift diffusion equations and applied them to realistic three-dimensional geometries. The effect of spin injection, which is a prerequisite to build efficient spintronic devices, in n-type GaAs semiconductor was studied and its dependence on the device geometry was investigated. The effects of semiconductor height and contact area on the spin injection ratio were discussed and we showed that direct contact spin injection is pos-

sible only for extremely small contact areas and height much greater than the spin diffusion length. Traditionally, tunneling barriers have been used to efficiently inject spin into semiconductors, but we proposed an alternative in the form of thin metal films to efficiently inject spin in the regime of small contact area. Lastly, the role of the technologically unavoidable problem of pinholes in tunneling barriers was discussed. We showed that the spin injection ratio depends only on the effective area of the pinholes and no correlation between the number of pinholes and the spin injection ratio was observed.

Chapter 5

Conclusions and Future Work

> If quantum mechanics hasn't
> profoundly shocked you, you
> haven't understood it yet.
>
> Niels Bohr

The main objective of this dissertation was to shed some light on the role of anharmonicity in transport and importantly to employ a wide array of techniques to achieve the goal. Our objectives were achieved by studying heat and spin transport and in this chapter we conclude and summarize the important results presented in this thesis and give directions for future work wherever possible.

We started with the introduction of the reduced density matrix (RDM) formulation, via the theory of open quantum systems, using perturbative quantum master equations (QMEs). A simple derivation showed that in the steady state the RDM obtained by the 2-nd order QME is correct only up to 0-th order in the system-bath coupling (the perturbative parame-

ter). In particular, the RDM obtained from a 2-nd order QME produced incorrect 2-nd order diagonal elements, whereas the 2-nd order off-diagonal elements were correct. This simple derivation was one of the key observations in order to obtain the modified Redfield solution (MRS), where we correctly obtained the 2-nd order diagonal elements using analytic continuation. One of the biggest advantage of our novel approach is the fact that it does not require any 4-th order relaxation tensors, which are extremely cumbersome and tedious to obtain. This not only simplifies the theoretical construction but also the numerical complexity of the problem reduces to N^3 from N^6, where N is the system Hilbert space dimension. We even attempted to correctly evaluate the 2-nd order diagonal elements using the Dyson expansion: In this context it must be noted that since the Dyson series is *asymptotically divergent* [168], and although the off-diagonals in fact agree, the second order diagonals are found *not* to match the *exact* result obtained via nonequilibrium Green's function (NEGF) by Dhar *et al.* [97] for the harmonic oscillator problem.

In order to validate our MRS, for the equilibrium limit, we compared it with canonical perturbation theory and demonstrated that the MRS agrees with the generalized Gibb's distribution up to 2-nd order in the system-bath coupling for a general system that is coupled to harmonic oscillator bath. This clearly indicates that even in the weak, but finite, coupling

limit, the system thermalizes to a generalized Gibb's distribution and *not* a canonical one as typically indicated by the Lindblad master equation. We also numerically tested our MRS by comparing against the *exact* NEGF results and found perfect agreement up to 2-nd order for a harmonic oscillator connected to both one and two baths. Comparisons of the RDM populations obtained via MRS with the Redfield quantum master equation (RQME) and Lindblad master equation showed that the MRS gives physically correct results for a wide range of system-bath coupling strengths and easily goes beyond the weak coupling limit established by the RQME for the single harmonic oscillator problem. On the other hand, the Lindblad formulation does not vary with system-bath coupling and always results in the incorrect canonical distribution (for finite coupling), whereas the RQME violates the positivity property of the RDM for weak but finite coupling strengths. Thus, the MRS turns out to be a novel and reliable approach which accurately captures weak but finite system-bath coupling effects.

Several unresolved challenges exist and a major one is the extension of our scheme to *time-dependent* relaxation of the RDM and to study the differing relaxation processes that stem from different initial preparation schemes. Another unresolved objective presents the perturbative, accurate study of multi-time correlations of open system observables, both time-homogeneous thermal and time-dependent nonequilibrium correlations be-

yond the weak coupling limit. These extensions would not only make the MRS advantageous but also place it on a rigorous theoretical ground.

We next considered the field of phononics and studied heat transport in anharmonic molecular junctions. Equipped with the theoretical tools of QMEs, we first introduced a fully quantum-mechanical *non-Markovian* theory based on perturbation in the system-bath coupling to evaluate heat current in general anharmonic systems. The approach was formulated using the basic definition of heat current, i.e., change in energy of the bath. In order to integrate the technique with the typical QME formulations, quantities like the bath correlators $C(\tau)$ and the transition rates $\tilde{W}_{ij}$ were used. The resulting quantum master equation *like* formulation can thus be used to study transient as well as steady-state heat transport and most importantly it requires only the 0-th order RDM. Since the RQME is accurate at the 0-th order in both transients and steady state it is employed to obtain the RDM and hence subsequently the heat current. Despite its ability to treat any system potential, the theory is limited by the weak coupling approximation. We overcome this limitation for a specific model of quartic anharmonicity with the help of NEGF technique and formulate the self-consistent mean-field (QSCMF) approach for heat transport. In the QSCMF approach we first show that the equations of motion for the Green's function on the Keldysh contour do not close on to themselves in

114

the presence of interactions, thus forming the BBGKY hierarchy. In order to provide a closure condition, we make an important approximation by replacing the 4-point correlation function with the Green's function and thus closing the 1-st BBGKY equation. The approximated closure condition leads to a modified force constant matrix $\tilde{K}$ which is then evaluated self consistently, thus giving rise to the QSCMF approach.

Several examples and corroborations were considered for both, quantum master equation *like* formulation and QSCMF approach. In case of the quantum master equation *like* formulation we first verified the approach for a harmonic system by comparing against the exact NEGF results given by the Landauer formula and found excellent agreement between both approaches for weak system-bath coupling, i.e. up to 10% of the spring constant of the harmonic oscillator. We then considered the systems with quartic anharmonicity namely the FPU-β and ϕ^4 model and found that anharmonicity can significantly affect not only the high-temperature behavior of thermal conductance, but also the low-temperature behavior. In specific for the quartic anharmonicity model we observed that whenever the translational invariance of the anharmonic potential is broken, i.e., in the presence of quartic on-site potential, the low-temperature thermal conductance differs significantly from the ballistic result. Next, we considered the Duffing oscillator model which acts like a double-well potential. In this

completely anharmonic model we found negative differential thermal conductance (NDTC) which can be easily tuned by varying the height of the barrier. The NDTC property is a purely quantum effect and is mainly because of the tunneling of the particles across the barrier. Importantly, our approach gave conservation of energy for all the systems considered. Energy conservation has been a major problem with master equation formulations and it is typically blamed on the perturbative nature of the theory. In our case since all equations were solved order-by-order we didn't have to resort to *ad-hoc* symmetrization of the current to obtain meaningful results.

After investigating these interesting anharmonic models using the quantum master equation *like* formulation we turned our attention to the QSCMF approach. Since the approximation involved in this approach is quite drastic, we compared the method with several existing techniques like: the quantum master equation *like* formulation, perturbative NEGF and quantum molecular dynamics. As QSCMF approach makes no approximation in the system-bath coupling strength, we numerically compared it with the master equation *like* formulation in the weak coupling limit and found excellent agreement for one and two particle systems, even for extremely strong anharmonicity. This surprising result prompted us to compare our approach with perturbative NEGF, where the anharmonicity is treated perturbatively at one level higher than the QSCMF approach

without a self-consistent procedure. Again, QSCMF showed excellent agreement for all values of system-bath coupling for small molecular junctions. Comparisons with quantum molecular dynamics showed similar agreement, however only for small system sizes. The concordance between the various theories, even for strong anharmonicity, is mainly accredited to the self-consistent procedure. The major limitation of the theory being that it is valid only for molecular junctions is because in our QSCMF approach the phonon mean free path is infinite. This is indicated by the fact that the modified spring constant $\tilde{K}$ is real and frequency independent, which is a valid assumption in case of molecular junctions, where the system-size is much smaller than the phonon mean-free path. Thus, both our proposed theories are excellent candidates to study strongly anharmonic molecular junctions, which seem to be an interesting prospect for future nano-devices.

Despite our advances several interesting problems are open for exploration. In case of the quantum master equation *like* formulation the extension of the theory to time-dependent Hamiltonians might be interesting from a technological point of view since it would allow us to control the thermal current and thus build tunable phononic devices. Also the selection of materials is an important factor to build devices and hence the merger of the approach with time-dependent density functional theory (TDDFT), similar to the QME+TDDFT formulations [169], would be an enriching experience

enabling us to study real systems. One of the most challenging theoretical extensions to the approach would be to go beyond the 2-nd order limitation and extend this theory to higher orders. Although this would be an interesting breakthrough, probably the QSCMF is the most reliable candidate to treat strong system-bath interactions and one of the most challenging issue with this approach is the incorporation of phonon life-times from a rigorous and quantum mechanical point of view.

Lastly, we considered the fascinating field of spintronics and studied spin transport in magnetic insulators and semiconductors. Keeping the QMEs as our central theme we first studied magnetic insulators modeled by a spin-1/2 anisotropic Heisenberg spin chain. Our model was unique since the baths were a set of harmonic oscillators containing *no spins* and the interface between the bath and the system generated a spin current due to the spin-Seebeck effect, thus allowing us to study spin transport. The absence of spins from the baths made it impossible to define spin current as $\mathrm{d}\sigma_{\mathrm{L}}^{z}/\mathrm{d}t$ and hence we used the local definition of spin current using the lattice continuity equation. Since the spin current at the lowest order of perturbation is second order in the system-bath coupling, the MRS became an essential ingredient to capture all the system-bath coupling effects in the spin current accurately.

Our unique model was then used to study the phenomenon of spin recti-

fication, which is an important factor to build spin diodes. We studied two important aspects of spin rectification in the spin-1/2 anisotropic Heisenberg spin chain namely, the effect of system size and the tunability of rectification with the external magnetic field. In case of system size dependence we found that the rectification ratio shows an oscillatory behavior with odd and even system size at low temperatures. This unusual oscillatory effect is mainly because of the fact that at low temperatures the system prefers to be in its ground state, which is anti-ferromagnetic, but due to the bath pinning the end spins the ground state is achieved only for odd number of spins. In case of even number of spins due to spin frustration the $\langle \sigma_i^z \rangle$ at each site reduces drastically which leads to the decrease of the rectification ratio. At high temperatures, as expected, the effect completely disappears due to the thermal influence of the heat bath. The low temperature quantum effects are even evident in case of tuning the rectification ratio with an external magnetic field. At low temperatures the rectification ratio can be tuned up to 50% by varying the external magnetic field and at low fields the ratio is the highest and it decreases to zero as the magnetic field increases. Thus, the large variation of the rectification ratio by an external field provides an extra accessible parameter for spin-diodes making magnetic insulators interesting candidates for spintronic devices.

From an application point of view semiconductors have been the most

popular material to build spintronic devices and hence we next investigated

the effects of device geometry on spin transport in semiconductors. Inspired

by the semi-classical one-dimensional spin drift diffusion (1D-SDD) equa-

tions, we developed the three-dimensional spin drift diffusion (3D-SDD)

model which takes into account the diffusion of spins in three spatial di-

mensions. The peculiarity in the 3D-SDD equations is mainly in the bound-

ary conditions which are adopted by studying actual experimental devices.

The important additional boundary condition of spin-current conservation

in the entire device, i.e., system + baths was essential in determining a

unique solution for the 3D-SDD model. The model was then applied to

study a basic, yet important, concept of spin-injection, which is essential to

build spintronic devices. We explored several device geometries and found

that a small contact area between the semiconductor and the ferromagnet is

essential to obtain a high spin-injection ratio and a minimum contact area

of 10^3 nm^2 is required to build a direct-contact device. The semiconductor

height also greatly affects the spin-injection ratio and a desirable spin injec-

tion is observed only if the height is greater than the spin diffusion length

of the semiconductor. Traditionally, in order to enhance the spin-injection

ratio a tunneling barrier is used, which is prone to pinhole defects. Hence

we also investigated the effects of pinholes in our 3D-SDD model and found

that the coverage area is the only factor affecting the spin-injection ratio

and the number of pinholes is not important. In order to completely avoid such pinhole defects we proposed an alternative to tunneling barriers in the form of thin metal films and found that these are excellent substitutes if the contact area between the ferromagnet and semiconductor is small. Even for large contact areas the metal films give much better results as compared to direct contact, but are poor against ideal tunneling barriers. Thus, our innovative semi-classical 3D-SDD model gives several insights into the problem of spin injection in semiconductors at macroscopic length scales, where fully quantum-mechanical theories fail.

Even though our efforts on spintronics were focused towards device applications, there are a few avenues where one could push the boundaries further. In case of magnetic insulators it would be quite interesting to add magnetic baths along with the thermal baths and study the Onsager relations leading towards thermomagnetic effects and thermomagneto power. The extensions to the 3D-SDD equations are quite challenging and one of the important extension would be to obtain all the parameters like spin-dependent conductivity $\sigma_{\uparrow,\downarrow}$, spin-diffusion length λ and spin-dependent boundary resistance r_c from first-principle calculations like density functional theory and then corroborate with experiments thus proving the validity of the SDD equations from a firm theoretical base.

Bibliography

[1] R. Kubo. *J. Phys. Soc. Jpn.*, **12**:570, 1957.

[2] R. Kubo, M. Yokota, and S. Nakajima. *J. Phys. Soc. Jpn.*, **12**:1203, 1957.

[3] R. Landauer. *IBM J. Res*, **1**:223, 1957.

[4] R. Landauer. *Philos. Mag.*, **21**:863, 1970.

[5] M. Buttiker, Y. Imry, R. Landauer, and S. Pinhas. *Phys. Rev. B*, **31**:6207, 1985.

[6] M. Buttiker. *Phys. Rev. Lett.*, **57**:1761, 1986.

[7] S. Datta. *Quantum Transport: Atom to Transistor*. Cambridge University Press, 2005.

[8] H. Haug and A.-P. Jauho. *Quantum Kinetics in Transport and Optics of Semiconductors 2nd Edition*. Springer, 2007.

[9] K. Saito. *Europhys. Lett.*, **61**:34, 2003.

[10] D. Segal and A. Nitzan. *Phys. Rev. Lett.*, **94**:034301, 2005.

[11] D. Segal. *Phys. Rev. B*, **73**:205415, 2006.

[12] L.-A. Wu, C. X. Yu, and D. Segal. *Phys. Rev. E*, **80**:041103, 2009.

[13] J. Wu and M. Berciu. *Phys. Rev. B*, **83**:214416, 2011.

[14] P. Carruthers. *Rev. Mod. Phys.*, **33**:92, 1961.

[15] H. Spohn. *J. Stat. Phys.*, **124**:1041, 2006.

[16] K. Aoki, J. Lukkarinen, and H. Spohn. *J. Stat. Phys.*, **124**:1105, 2006.

[17] J. Jin, X. Zheng, and Y. J. Yan. *J. Chem. Phys.*, **128**:234703, 2008.

[18] X. Zheng, J. Jin, and Y. J. Yan. *J. Chem. Phys.*, **129**:184112, 2008.

[19] A. Sakurai and Y. Tanimura. "numerical investigation of dissipative dynamics in a resonant tunneling diode using the caldeira-leggett model". *Private communication*, 2012.

[20] S. Lepri, R. Livi, and A. Politi. *Phys. Rep.*, **377**:1, 2003.

[21] A. J. H. McGaughey and M. Kaviany. *Adv. in Heat Transfer*, **39**:169, 2006.

[22] J. V. Alvarez and C. Gros. *Phys. Rev. B*, **66**:094403, 2002.

[23] L. Muhlbacher and E. Rabani. *Phys. Rev. Lett.*, **100**:176403, 2008.

[24] M. Schiro and M. Fabrizio. *Phys. Rev. B*, **79**:153302, 2009.

[25] S. Nakajima. *Prog. Theor. Phys.*, **20**:948, 1958.

[26] R. Zwanzig. *J. Chem. Phys.*, **33**:1338, 1960.

[27] A. Fulinski and W. J. Kramarczyk. *Physica*, **39**:575, 1968.

[28] M. Tokuyama and H. Mori. *Prog. Theor. Phys.*, **55**:411, 1976.

[29] P. Hängg and H. Thomas. *Z. Phys. B – Cond. Mat.*, **26**:85, 1977.

[30] H. Grabert, P. Talkner, and P. Hänggi. *Z. Phys. B – Cond. Mat.*, **26**:389, 1977.

[31] F. Shibata, Y. Takahashi, and N. Hashitsume. *J. Stat. Phys.*, **17**:171, 1977.

[32] G. Nan, Q. Shi, and Z. Shuai. *J. Chem. Phys.*, **130**:134106, 2009.

[33] R. Peierls. *Ann. Phys.*, **3**:1055, 1929.

[34] J. M. Ziman. *Electrons and Phonons*. Oxford University Press, Oxford, 1963.

[35] F. Bonetto, J. L. Lebowitz, and L. Rey-Bellet. In *Mathematical Physics*. Imperial College Press, London, 2000.

[36] J. Bricmont and A. Kupiainen. *Commun. Math. Phys.*, **274**:555, 2007.

[37] C. Liverani and S. Olla. *J. Am. Math. Soc.*, **25**:555, 2011.

[38] D. Segal, A. Nitzan, and P. Hänggi. *J. Chem. Phys.*, **119**:6840, 2003.

[39] G. Santhosh and D. Kumar. *Phys. Rev. E*, **76**:021105, 2007.

[40] A. Dhar. *Adv. Phys.*, **57**:457, 2008.

[41] K. Saito and A. Dhar. *Phys. Rev. Lett.*, **104**:040601, 2010.

[42] N. Mingo and L. Yang. *Phys. Rev. B*, **68**:245406, 2003.

[43] A. Dhar and D. Sen. *Phys. Rev. B*, **73**:085119, 2006.

[44] J.-S. Wang, J. Wang, and J. T. Lü. *Eur. Phys. J. B*, **62**:381, 2008.

[45] N. Mingo. *Phys. Rev. B*, **74**:125402, 2006.

[46] J.-S. Wang, J. Wang, and N. Zeng. *Phys. Rev. B*, **74**:033408, 2006.

[47] J.-S. Wang, N. Zeng, J. Wang, and C. K. Gan. *Phys. Rev. E*, **75**:061128, 2007.

[48] J.-S. Wang. *Phys. Rev. Lett.*, **99**:160601, 2007.

[49] S. Datta and B. Das. *Appl. Phys. Lett.*, **56**:665, 1990.

[50] I. Žutič, J. Fabian, and S. Das Sarma. *Rev. Mod. Phys.*, **74**:323, 2004.

[51] S. A. Wolf, D. D. Awschalom, R. A. Buhrman, J. M. Daughton, S. von Molnár, M. L. Roukes, A. Y. Chtchelkanova, and D. M. Treger. *Science*, **294**:1488, 2001.

[52] N. F. Mott. *Proc. R. Soc. London, Ser. A*, **153**:699, 1936.

[53] N. F. Mott. *Proc. R. Soc. London, Ser. A*, **156**:368, 1936.

[54] I. A. Campbell, A. Fert, and A. R. Pomeroy. *Philos. Mag.*, **15**:977, 1967.

[55] A. Fert and I. A. Campbell. *Phys. Rev. Lett.*, **21**:1190, 1968.

[56] T. Valet and A. Fert. *Phys. Rev. B*, **48**:7099, 1993.

[57] M. Ichimura, S. Takahashi, K. Ito, and S. Maekawa. *J. Appl. Phys.*, **95**:7255, 2004.

[58] J. Hamrle, T. Kimura, Y. Otani, K. Tsukagoshi, and Y. Aoyagi. *Phys. Rev. B*, **71**:094402, 2005.

[59] X. Zotos, F. Naef, and P. Prelovšek. *Phys. Rev. B*, **55**:11029, 1997.

[60] T. Prosen. *Phys. Rev. Lett.*, **106**:217206, 2011.

[61] X. Zotos. *Phys. Rev. Lett.*, **82**:1764, 1999.

[62] K. Louis and C. Gros. *Phys. Rev. B*, **67**:224410, 2003.

[63] J. Sirker, R. G. Pereira, and I. Affleck. *Phys. Rev. Lett.*, **103**:216602, 2009.

[64] K. A. van Hoogdalem and D. Loss. *Phys. Rev. B*, **84**:024402, 2011.

[65] T. Prosen and M. Žnidarič. *J. Stat. Mech.*, page P02035, 2009.

[66] M. Žnidarič. *New J. Phys.*, **12**:043001, 2010.

[67] M Žindarič. *Phys. Rev. Lett.*, **106**:220601, 2011.

[68] V. Popkov. *arXiv*, [cond-mat.stat-mech]:1210.4555, 2012.

[69] G. Schmidt, D. Ferrand, L. W. Molenkamp, A. T. Filip, and B. J. van Wees. *Phys. Rev. B*, **62**:4790 (R), 2000.

[70] E. I. Rashba. *Phys. Rev. B*, **62**:16267 (R), 2000.

[71] W. Pauli. In *Festschrift zum 60. Geburtstage A. Sommerfeld*. Hirzel, Leipzig, 1928.

[72] G. Lindblad. *Commun. Math. Phys.*, **48**:119, 1976.

[73] A. G. Redfield. *IBM J. Res. Dev.*, **1**:19, 1957.

[74] M. Esposito and P. Gaspard. *Phys. Rev. E*, **68**:066112, 2003.

[75] K. Blum. *Density Matrix Theory and Applications*. Plenum Press, New York, 1996.

[76] H. P. Breuer and F. Petruccione. *The Theory of Open Quantum Systems*. Oxford University Press, Oxford, 2002.

[77] U. Weiss. *Quantum Dissipative Systems*. World Scientific, Singapore, 2008.

[78] R. Zwanzig. *J. Stat. Phys.*, **9**:215, 1973.

[79] A. O. Caldeira and A. J. Leggett. *Phys. Rev. Lett.*, **46**:211, 1981.

[80] A. O. Caldeira and A. J. Leggett. *Ann. Phys.*, **149**:374, 1983.

[81] R. Kubo, M. Toda, and N. Hashitsume. *Statistical Physics II - Nonequilibrium Statistical Mechanics*. Springer-Verlag, Berlin, 1983.

[82] D. Zueco. *Quantum and Statistical Mechanics in Open Systems: Theory and Examples*. PhD thesis, Universidad de Zaragoza, 2007.

[83] T. Mori and S. Miyashita. *J. Phys. Soc. Jpn.*, **77**:124005, 2008.

[84] C. H. Fleming and N. I. Cummings. *Phys. Rev. E*, **83**:031117, 2011.

[85] B. B. Laird, J. Budimir, and J. L. Skinner. *J. Chem. Phys.*, **94**:4391, 1991.

[86] S. Jang, J. Cao, and R. J. Silbey. *J. Chem. Phys.*, **116**:2705, 2001.

[87] M. Schröder, M. Schreiber, and U. Kleinekathöfer. *J. Chem. Phys.*, **126**:114102, 2007.

[88] L. V. Ahlfors. *Complex Analysis: An Introduction to the Theory of Analytic Functions of One Complex Variable*. McGraw-Hill Inc., 1979.

[89] J. L. García-Palacios and D. Zueco. *J. Phys. A: Math. Gen.*, **39**:13243, 2006.

[90] H. B. Callen. *Thermodynamics and an Introduction to Thermostatistics*. John Wiley & Sons. Inc., 1985.

[91] P. C. Martin and J. Schwinger. *Phys. Rev.*, **115**:1342, 1959.

[92] H. Spohn and J. L. Lebowitz. *Adv. Chem. Phys.*, **38**:109, 1978.

[93] R. Kress. *Applied Mathematical Sciences: Linear Integral Equations*. Springer-Verlag, New York, 1999.

[94] V. Romero-Rochin and I. Oppenheim. *Physica (Utrecht)*, **155**:52, 1989.

[95] E. Geva, E. Rosenman, and D. J. Tannor. *J. Chem. Phys.*, **113**:1380, 2000.

[96] F. Hake. *Quantum Statistics in Optics and Solid State Physics*. Springer-Verlag, Berlin, 1973.

[97] A. Dhar, K. Saito, and P. Hänggi. *Phys. Rev. E*, **85**:011126, 2012.

[98] W. H. Press, S. A. Teukolsky, W. T. Vetterling, and B. P. Flannery. *Numerical Recipes: The Art of Scientific Computing (third edition)*. Cambridge Univ. Press, 2007.

[99] D. Honda, H. Nakazato, and M. Yoshida. *J. Math. Phys.*, **51**:072107, 2010.

[100] C. W. Gardiner. *Handbook of Stochastic Methods*. Springer, Berlin, 1990.

[101] W. J. Munro and C. W. Gardiner. *Phys. Rev. A*, **53**:2633, 1996.

[102] L. D. Blanga and M. A. Despòsito. *Physica A*, **227**:248, 1996.

[103] M. Terraneo, M. Peyrard, and G. Casati. *Phys. Rev. Lett.*, **88**:094302, 2002.

[104] B. Li, L. Wang, and G. Casati. *Phys. Rev. Lett.*, **93**:184301, 2004.

[105] B. Hu, L. Yang, and Y. Zhang. *Phys. Rev. Lett.*, **97**:124302, 2006.

[106] B. Li, L. Wang, and G. Casati. *Appl. Phys. Lett.*, **88**:143501, 2006.

[107] W. C. Lo, L. Wang, and B. Li. *J. Phys. Soc. Jpn.*, **77**:054402, 2008.

[108] N. Li, J. Ren, L. Wang, G. Zhang, P. Hänggi, and B. Li. *Rev. Mod. Phys.*, **84**:1045, 2012.

[109] F. M. Cucchietti, J. P. Paz, and W. H. Zurek. *Phys. Rev. A*, **72**:052113, 2005.

[110] K. A. Velizhanini, M. Thoss, and H. Wang. *J. Chem. Phys.*, **133**:084503, 2010.

[111] A. Kundu, A. Dhar, and O. Narayan. *J. Stat. Mech.*, page L03001, 2009.

[112] E. C. Cuansing and J.-S. Wang. *Phys. Rev. B*, **81**:052303, 2010.

[113] B. K. Agarwalla, B. Li, and J.-S. Wang. *Phys. Rev. E (refer Appendix B)*, **85**:051142, 2012.

[114] A. Dhar and D. Roy. *J. Stat. Phys.*, **125**:801, 2006.

[115] B. Ai, W. Zhong, and B. Hu. *Phys. Rev. E*, **83**:052102, 2011.

[116] N. Li, P. Tong, and B. Li. *Europhys. Lett.*, **75**:49, 2006.

[117] B. Hu, D. He, L. Yang, and Y. Zhang. *Phys. Rev. E*, **74**:060101 (R), 2006.

[118] N. Li and B. Li. *Phys. Rev. E*, **76**:011108, 2007.

[119] D. He, S. Buyukdagli, and B. Hu. *Phys. Rev. E*, **78**:061103, 2008.

[120] L. V. Keldysh. *Soviet Phys. JETP*, **20**:1018, 1965.

[121] M. L. Leek. *Theoretical Considerations in the application of Non-equilibrium Green's Functions (NEGF) and Quantum Kinetic Equations (QKE) to Thermal Transport*. PhD thesis, National University of Singapore, 2012.

[122] K. Saito and A. Dhar. *Phys. Rev. Lett.*, **99**:180601, 2007.

[123] J. Rammer. *Quantum Field Theory of Non-equilibrium States*. Cambridge University Press, 2007.

[124] G. D. Mahan. *Many Particle Physics 3rd Edition*. Kluwer Academic/ Plenum Publishers, New York, 2000.

[125] D. C. Langreth. In *Linear and Nonlinear Electron Transmission in Solids*. Plenum, 1976.

[126] Y. Meir and N. S. Wingreen. *Phys. Rev. Lett.*, **68**:2512, 1992.

[127] R. D. Mattuck. *A Guide to Feynman Diagrams in the Many-Body Problem*. McGraw-Hill Inc., 1967.

[128] A. L. Fetter and J. D. Walecka. *Quantum Theory of Many-Particle Systems*. McGraw-Hill Inc., 1971.

[129] J.-S. Wang, X. Ni, and J.-W. Jiang. *Phys. Rev. B*, **80**:224302, 2009.

[130] S. Furukawa, D. Ikeda, and K. Sakai. *J. Phys. Soc. Jpn.*, **74**:3241, 2005.

[131] T. Prosen and I. Pižorn. *Phys. Rev. Lett.*, **101**:105701, 2008.

[132] G. Benenti, G. Casati, T. Prosen, and D. Rossini. *Europhys. Lett.*, **85**:37001, 2009.

[133] T. Prosen and B. Žunkovič. *New J. Phys.*, **12**:025016, 2010.

[134] H. Adachi, J. Ohe, S. Takahashi, and S. Maekawa. *Phys. Rev. B*, **83**:094410, 2011.

[135] G. E. W. Bauer, E. Saitoh, and B. J. van Wees. *Nature materials*, **11**:391, 2012.

[136] K. Uchida, J. Xiao, H. Adachi, J. Ohe, S. Takahashi, J. Ieda, T. Ota, Y. Kajiwara, H. Umezawa, H. Kawai, G. E. W. Bauer, S. Maekawa, and E. Saitoh. *Nature materials*, **9**:894, 2010.

[137] H. Adachi, K. Uchida, E. Saitoh, J. Ohe, S. Takahashi, and S. Maekawa. *Appl. Phys. Lett.*, **97**:252506, 2010.

[138] F. Meier and D. Loss. *Phys. Rev. Lett.*, **90**:167204, 2003.

[139] T. Ami, M. K. Crawford, R. L. Harlow, Z. R. Wang, D. C. Johnston, Q. Huang, and R. W. Erwin. *Phys. Rev. B*, **51**:5994, 1995.

[140] N. Motoyama, H. Eisaki, and S. Uchida. *Phys. Rev. Lett.*, **76**:3212, 1996.

[141] M. Kenzelmann, R. Coldea, D. A. Tennant, D. Visser, M. Hofmann, P. Smeibidl, and Z. Tylczynski. *Phys. Rev. B*, **65**:144432, 2002.

[142] I. A. Zaliznyak, H. Woo, T. G. Perring, C. L. Broholm, C. D. Frost, and H. Takagi. *Phys. Rev. Lett.*, **93**:087202, 2004.

[143] E. Lieb and D. Mattis. *Mathematical Physics in One Dimension*. Academic Press, New York and London, 1966.

[144] M. Takahashi. *Thermodynamics of One-Dimensional Solvable models*. Cambridge University Press, 1999.

[145] N. W. Ashcroft and N. D. Mermin. *Solid State Physics*. Saunders College, 1976.

[146] H.-J. Mikeska and A. K. Kolezhuk. *Lect. Notes Phys.*, **645**:1, 2004.

[147] S. Langer, F. Heidrich-Meisner, J. Gemmer, I. P. McCulloch, and U. Sch-ollwöck. *Phys. Rev. B*, **79**:214409, 2009.

[148] R. Steinigeweg, H. Wichterich, and J. Gemmer. *Europhys. Lett.*, **88**:10004, 2009.

[149] B. S. Shastry and B. Sutherland. *Phys. Rev. Lett.*, **65**:243, 1990.

[150] P. C. van Son, H. van Kempen, and P. Wyder. *Phys. Rev. Lett.*, **58**:227, 1987.

[151] A. G. Aronov. *Pis'ma Zh. Eksp. Teor. Fiz. [Sov. Phys. - JETP Lett.]*, **24**:37, 1976.

[152] M. Johnson and R. H. Silsbee. *Phys. Rev. B*, **35**:4959, 1987.

[153] E. I. Rashba. *Eur. Phys. J. B*, **29**:513, 2002.

[154] S. B. Kumar, S. G. Tan, M. B. A. Jalil, and J. Guo. *Appl. Phys. Lett.*, **91**:142110, 2007.

[155] F. J. Jedema, A. T. Filip, and B. J. van Wees. *Nature*, **410**:345, 2001.

[156] F. J. Jedema, M. S. Nijiboer, A. T. Filip, and B. J. van Wees. *J. Superconductivity*, **15**:27, 2002.

[157] F. J. Jedema, M. S. Nijiboer, A. T. Filip, and B. J. van Wees. *Phys. Rev. B*, **67**:085319, 2003.

[158] T. Kimura, J. Hamrle, and Y. Otani. *Phys. Rev. B*, **72**:014461, 2005.

[159] T. Kimura and Y. Otani. *J. Phys: Condens. Matter*, **19**:165216, 2007.

[160] N. F. Mott. *Adv. Phys.*, **13**:325, 1964.

[161] Free fem 3d. http://www.freefem.org/ff3d/.

[162] S. S. Sastry. *Introductory Methods of Numerical Analysis (Fourth edition)*. Prentice-Hall of India Pvt. Ltd., New Delhi, 2006.

[163] A. Fert and H. Jaffrées. *Phys. Rev. B*, **64**:184420, 2001.

[164] N. Tombros, C. Jozsa, M. Popinciuc, H. T. Jonkman, and B. J. van Wees. *Nature*, **448**:571, 2007.

[165] B. Dlubak, P. Seneor, A. Anane, C. Barraud, C. Deranlot, D. Deneuve, B. Servet, R. Mattana, F. Petroff, and A. Fert. *Appl. Phys. Lett.*, **97**:092502, 2010.

[166] K. H. J. (Editor) Buschow. *Handbook of Magnetic Materials, Vol. **17***. Elsevier Science, 2007.

[167] B. Oliver, Q. He, X. Tang, and J. Nowak. *J. Appl. Phys.*, **91**:4348, 2002.

[168] F. J. Dyson. *Phys. Rev.*, **85**:631, 1952.

[169] D. G. Tempel, M. A. Watson, R. Olivares-Amaya, and A. Aspuru-Guzik. *J. Chem. Phys.*, **134**:074116, 2011.

[170] Y. Tanimura and R Kubo. *J. Phys. Soc. Jpn.*, **58**:101, 1989.

[171] C. Meier and D. J. Tannor. *J. Chem. Phys.*, **111**:3365, 1999.

[172] R. J. Rubin. *Phys. Rev.*, **131**:964, 1963.

[173] A. P. Prudnikov, Yu. A. Brychkov, and O. I. Marichev. *Integrals and Series, Vol. I: Elementary Functions.* Gordon and Breach Science Publishers, 1986.

[174] C. M. Bender and S. A. Orszag. *Advanced Mathematical Methods For Scientists and Engineers.* McGraw-Hill Inc., 1978.

[175] R. Peierls. *Z. Physik,* **8**:763, 1933.

[176] L. D. Landau and E. M. Lifshitz. *Statistical Physics.* Pergamon, Oxford, 1980.

[177] M. Campisi, P. Talkner, and P. Hänggi. *Phys. Rev. Lett.,* **102**:210401, 2009.

THIS PAGE IS INTENTIONALLY LEFT BLANK

Bath correlators and transition rates

One of the most important aspects while solving the master equation

is the evaluation of the bath correlators Eq. (2.10). In this appendix we

evaluate the bath correlators and the transition rates for different types of

harmonic heat baths and also discuss ways to numerically simplify their

evaluation.

A.1   Bath correlator

But first we try to obtain Eq. (2.10) from the basic definition of harmonic

heat baths, i.e., Eq. (2.2). The bath correlators as defined after Eq. (2.9)

are given by,

$$
\begin{aligned}
\mathrm{C}(\tau) &= \left\langle B(\tau)B(0)\right\rangle, \\
B &= -\sum_{n=1}^{\infty} c_n x_n.
\end{aligned}
\tag{A.1}
$$

where the bath operator in terms of the second quantized creation and annihilation operators is given by,

$$
\begin{aligned}
B(0) &= -\sum_{n=1}^{\infty} c_n \sqrt{\frac{1}{2m_n\omega_n}} (b_n^+ + b_n^-), \\
B(\tau) &= -\sum_{n=1}^{\infty} c_n \sqrt{\frac{1}{2m_n\omega_n}} (b_n^+ \, e^{i\,\omega_n\tau} + b_n^- \, e^{-i\,\omega_n\tau}).
\end{aligned}
\tag{A.2}
$$

Substituting Eq. (A.2) in Eq. (A.1) and noting that the number operator $N_n = \langle b_n^+ b_n^- \rangle_{\text{Thermal}} = [\exp[\beta\omega_n] - 1]^{-1}$ we obtain,

$$
\mathrm{C}(\tau) = \int_0^{\infty} \frac{\mathrm{d}\omega}{\pi} \mathrm{J}(\omega) \left(\coth\left(\frac{\beta\omega}{2}\right) \cos(\omega\tau) - i\sin(\omega\tau) \right), \quad \text{(A.3)}
$$

Above we have used the definition of the spectral density,

$$
\mathrm{J}(\omega) = \pi \sum_{n=1}^{\infty} \frac{c_n^2}{2m_n\omega_n} \delta(\omega - \omega_n). \tag{A.4}
$$

Using the spectral density we define the damping kernel at zero time as,

$$
\gamma_0 = \sum_{n=1}^{\infty} \frac{c_n^2}{m_n\omega_n^2} = 2\int_0^{\infty} \frac{\mathrm{d}\omega}{\pi} \frac{\mathrm{J}(\omega)}{\omega}, \tag{A.5}
$$

so that the renormalization term in the Hamiltonian Eq. (2.3) can be written

as,

$$H_{\mathrm{RN}} \;=\; S^2 \left(\frac{1}{2} \sum_{n=1}^{\infty} \frac{c_n^2}{m_n \omega_n^2} \right) = S^2 \frac{\gamma_0}{2} \,, \tag{A.6}$$

In order to ease the computational complexity of solving the time transient Redfield master equation it is favorable to obtain the bath correlator analytically, which is sometimes done using a special decomposition of the spectral density [170, 171].

A.2 Transition rates via Plemelj

In this thesis we will mainly be interested in the steady state and in this limit it is sometimes easier to obtain the transition rates rather than the bath correlator. According to Eq. (2.17) the transition rates in the long time limit are given by,

$$\tilde{W}_{ij} \;=\; \int_0^{\infty} \mathrm{d}\tau \, e^{-i\,\Delta_{ij}\tau} \int_0^{\infty} \frac{\mathrm{d}\omega}{\pi} \mathrm{J}(\omega) \left(\coth\left(\frac{\beta\omega}{2} \right) \cos(\omega\tau) - i\sin(\omega\tau) \right) . \tag{A.7}$$

Exchanging the ω and τ integrals[1] and performing the τ integral using the

---
[1]The exchange is only true iff the ω integral is convergent.

Sokhotskyi - Plemelj formula we obtain,

$$
\tilde{W}'_{ij} = \begin{cases} \mathrm{J}(\Delta_{ij})\, n(\Delta_{ij}) & \Delta_{ij} > 0\,, \\[1.5em] -\mathrm{J}(-\Delta_{ij})\, n(\Delta_{ij}) & \Delta_{ij} < 0\,, \\[1.5em] \frac{\mathrm{J}(\Delta_{ij})}{\beta \Delta_{ij}} & \Delta_{ij} = 0\,, \end{cases} \tag{A.8}
$$

$$
\tilde{W}''_{ij} + \frac{\gamma_0}{2} = \frac{\Delta_{ij}}{\pi} \left[\left(\frac{2}{\beta} - \Delta_{ij}\right) \mathrm{P}\left(\int_0^\infty d\omega \frac{\mathrm{J}(\omega)}{\omega\,(\omega^2 - \Delta_{ij}^2)}\right) \right.
$$
$$
\left. + \frac{4}{\beta}\sum_{l=1}^\infty \mathrm{P}\left(\int_0^\infty d\omega \frac{\mathrm{J}(\omega)\omega}{(\omega^2 - \Delta_{ij}^2)(\omega^2 + \nu_l^2)}\right)\right]\,. \tag{A.9}
$$

where $n(\Delta_{ij})$ is the Bose-Einstein distribution function. In order to obtain the above formula we have decomposed the hyperbolic cotangent[2] into Matsubara frequencies $\nu_l = 2\pi l T$. Although this trick does not solve our problem completely it helps us to obtain the real part of the transition rates analytically. Now if the Lamb-shifts are neglected as described in Sec. 2.1.2 then the transition rates are known analytically by Eq. (A.8), since in this approximation the imaginary parts are set to zero.

A.3   Thermal bath models

While obtaining the bath correlator we defined a spectral density $\mathrm{J}(\omega)$ which would be used for phenomenological modeling of the bath. In this section we discuss some of the most commonly used bath models and ob-

---

[2]The exact decomposition of the hyperbolic cotangent is given by $\mathrm{Coth}(ax) = 1/ax + (2x/a)\sum_{l=1}^\infty 1/\left(x^2 + \nu_l^2\right)$, where $\nu_l = \pi l/a$.

tain an explicit expression for their bath correlators (where possible) and transition rates.

A.3.1 Rubin Bath

One of the most commonly used bath models is the Rubin bath [172] in which the bath is modeled as a infinite set of particles connected by a harmonic nearest neighbor spring. This model exactly represents the bath Hamiltonian described in Eq. (2.2). As shown in ref. [77] the spectral density for the Rubin model is given by,

$$
J(\omega) = \frac{m\omega_R}{2}\omega\left(1 - \left(\frac{\omega}{\omega_R}\right)^2\right)^{1/2}\Theta(\omega_R - \omega), \tag{A.10}
$$

where $\omega_R = 2\sqrt{(k/m)}$, k is the harmonic spring constant of the bath and m is the mass of each bath particle. Using the technique outlined in Sec. A.2 the transition rates are given by,

$$
\tilde{W}'_{ij} = \begin{cases} \frac{m\omega_R}{2}\Delta_{ij}\left(1 - \left(\frac{\Delta_{ij}}{\omega_R}\right)^2\right)^{1/2} n(\Delta_{ij})\Theta(\omega_R - \Delta_{ij}) & \Delta_{ij} \neq 0 \\ \frac{m\omega_R}{2\beta}\left(1 - \left(\frac{\Delta_{ij}}{\omega_R}\right)^2\right)^{1/2} & \Delta_{ij} = 0 \end{cases} \tag{A.11}
$$

$$
\tilde{W}''_{ij} = \frac{m\Delta_{ij}}{4}\left(\frac{2}{\beta} - \Delta_{ij}\right)
$$
$$
+ \frac{m\Delta_{ij}}{\beta}\sum_{l=1}^{\infty}\left[\frac{\nu_l^2\left((\Delta_{ij}/\omega_R)^2 - \frac{1}{2}\right) + \frac{1}{4}{}_2F_1\{1, 3/2; 3; -1/\nu_l^2\}}{\nu_l^2(\nu_l^2 + \Delta_{ij}^2/\omega_R^2)}\right],
$$
$$
\frac{\gamma_0}{2} = \frac{m\omega_R^2}{4}. \tag{A.12}
$$

where $_2F_1$ is the Gauss hyper-geometric function. Unfortunately for this model an analytical expression for the correlator cannot be obtained, but fortunately the imaginary part of the steady state transition rates can be obtained analytically as given above. Hence the Rubin model is best applied to study the steady state properties of a system.

A.3.2   Ohmic bath with exponential cut-off

In most phenomenological heat bath models the spectral density is chosen of the ohmic type, i.e., $J(\omega) \propto \omega$. Such a phenomenological modeling is based on the notion that the lowest frequencies of the heat bath are most important and significantly contribute to the physical processes. Thus the ohmic heat bath with exponential cut-off has a spectral density of the form:

$$J(\omega) \;\; = \;\; \eta\omega\,e^{-\frac{\omega}{\omega_c}} \, , \tag{A.13}$$

where η decides the strength of the collective coupling to the bath and the cut-off is chosen of the exponential form and determined by ω_c. Realistic spectral densities should decay in the frequency domain which leads to the decay of bath correlators in real time. Interested readers should refer ref. [77] Sec. 7.3 for a detailed discussion on the cut-off in the spectral density.

In this case an analytic expression for the bath-correlator can be ob-

tained [173] and is given by,

$$
\begin{aligned}
\mathrm{C}(\tau) \;=\; & \frac{\eta}{2\pi}\left[\frac{2}{\beta^2}\sum_{l=0}^{\infty}\left\{\frac{1}{\left(\frac{1}{\beta\omega_c}-\frac{i\tau}{\beta}+l\right)^2}+\frac{1}{\left(\frac{1}{\beta\omega_c}+\frac{i\tau}{\beta}+l\right)^2}\right\}\right. \\
& \left.-\frac{1}{\left(\frac{1}{\omega_c}-i\,\tau\right)^2}-\frac{1}{\left(\frac{1}{\omega_c}+i\,\tau\right)^2}-\frac{i\,4\tau}{\omega_c}\frac{1}{\left(\frac{1}{\omega_c^2}+\tau^2\right)^2}\right]. \quad \text{(A.14)}
\end{aligned}
$$

Unfortunately an analytic expression for the steady state transition rates is quite difficult to obtain for this case implying that the exponential cut-off model is better suited for transient studies.

A.3.3 Lorentz-Drude Bath

Lastly, we look at one of the most commonly used phenomenological models known as the Lorentz-Drude model. As compared to the exponential cut-off case this model has a much slower cut-off in the spectral density, whose form is given by

$$
\mathrm{J}(\omega) \;=\; \frac{M\gamma\omega}{1+(\omega/\omega_D)^2}\,, \quad\quad\quad \text{(A.15)}
$$

where ω_D is the cut-off frequency, $\gamma \propto \sum_n c_n^2$ is the phenomenological Stokesian damping coefficient which characterizes the system-bath coupling strength. One peculiar feature about this model is that it shows a logarithmic divergence as $\omega \to 0$, but this divergence is quite harmless and the

correlator obtained is a smooth function of τ given by

$$
\begin{aligned}
C(\tau) &= \frac{M\gamma}{2}\omega_D^2\left(\cot\left(\frac{\beta\omega_D}{2}\right) - i\,\mathrm{sgn}(\tau)\right)e^{-\omega_D\tau} \\
&\quad -\frac{2M\gamma}{\beta}\sum_{l=1}^{\infty}\frac{\nu_l\,e^{-\nu_l\tau}}{1 - (\nu_l/\omega_D)^2}\,. \qquad \tau > 0
\end{aligned}
\tag{A.16}
$$

Fortunately for this model we can not only obtain $C(\tau)$ but also the steady state transition rates W_{ij} analytically which are given by,

$$
\begin{aligned}
\tilde{W}_{ij}' &= \begin{cases} \frac{M\gamma\Delta_{ij}}{1+(\Delta_{ij}/\omega_D)^2}\,n(\Delta_{ij}) & \Delta_{ij} \neq 0 \\[2ex] \frac{M\gamma}{\beta(1+(\omega/\omega_D)^2)} & \Delta_{ij} = 0 \end{cases} \\[3ex]
\tilde{W}_{ij}'' &= \frac{2M\gamma\Delta_{ij}}{\beta}\sum_{l=1}^{\infty}\frac{\nu_l}{(1-(\nu_l/\omega_D)^2)(\nu_l^2 + \Delta_{ij}^2)} \\
&\quad -\frac{M\gamma\omega_D^2\Delta_{ij}}{2(\omega_D^2 + \Delta_{ij}^2)}\left[\cot\left(\frac{\beta\omega_D}{2}\right) + \frac{\omega_D}{\Delta_{ij}}\right], \\[2ex]
\frac{\gamma_0}{2} &= \frac{M\gamma\omega_D}{2}\,.
\end{aligned}
\tag{A.17}
$$

$$
\tag{A.18}
$$

Thus since both the bath correlator and the steady state transition rates can be obtained analytically this model is preferred for both transient and steady state calculations. Another nice feature of this model is that in the limit $\omega_D \to \infty$ the model represents a pure ohmic model with $J(\omega) = M\gamma\omega$, which is frequently used in Langevin and classical simulations.

A.4 Richardson extrapolation

In the previous section we evaluated the transition rates for different types of heat baths using a Matsubara expansion for the hyperbolic cotangent. The simplest idea to evaluate the Matsubara sum is a brute force calculation, but this typically leads to summing up millions of terms (especially at low temperatures) to reach a decent $\approx 10^{-6}$ convergence. This is undesirable when the system Hilbert space is large and alternative methods to calculate this sum are much needed. In this section we will discuss a simple approach known as the Richardson extrapolation [174], which will help us drastically reduce the computational complexity. We begin with a n-th partial sum A_n of a slowly converging series which has the form

$$A_n \quad \approx \quad A + \frac{a_1}{n} + \frac{a_2}{n^2} + \frac{a_3}{n^3} + \cdots , \tag{A.19}$$

where A is the infinite series we would like to obtain. In the Richardson expansion it is not important to know the exact form of the coefficients $a_1, a_2, \cdots$ but the fact that such a series exists is crucial.

In order to obtain the first Richardson expansion we keep only the first correction term and assume $a_2 = a_3 = a_4 = \cdots = 0$. Now using the n and

$n + 1$ partial sums we eliminate the coefficient a_1 to obtain

$$A_n^{[1]} = (n + 1)A_{n+1} - nA_n \,, \qquad (A.20)$$

where the left-hand side represents the first order (indicated by the super-script) Richardson extrapolation to the exact series sum. Similar to the first order, a general N-th order Richardson extrapolation can be obtained by solving a set of $N + 1$ simultaneous equations given by

$$
\begin{aligned}
A_n &= A + \frac{a_1}{n} + \frac{a_2}{n^2} + \frac{a_3}{n^3} + \cdots + \frac{a_N}{n^N} \,, \\
A_{n+1} &= A + \frac{a_1}{n+1} + \frac{a_2}{(n+1)^2} + \frac{a_3}{(n+1)^3} + \cdots + \frac{a_N}{(n+1)^N} \,, \\
&\;\;\vdots \\
A_{n+N} &= A + \frac{a_1}{n+N} + \frac{a_2}{(n+N)^2} + \frac{a_3}{(n+N)^3} + \cdots + \frac{a_N}{(n+N)^N} \,.
\end{aligned}
$$

The above set has a closed-form solution for A which is known as the N-th order Richardson extrapolation given by

$$A_n^{[N]} = \sum_{k=0}^{N} \frac{A_{n+k} (n + k)^N (-1)^{k+N}}{k! (N - k)!} \,. \qquad (A.21)$$

In case of the Lorentz-Drude model described in Sec. A.3.3 the imaginary part of the transition rates $\tilde{W}_{ij}''$ satisfies Eq. (A.19) and hence we can apply the Richardson expansion for the Lorentz-Drude model to reduce the

computational costs especially at low temperatures.

THIS PAGE IS INTENTIONALLY LEFT BLANK

Canonical Perturbation Theory

With this Appendix we outline the basic reasoning underlying canonical perturbation theory [83, 94, 95] (CPT). This will assist us in determining the correct equilibrium reduced density matrix in the weak coupling regime up to second order. The basic idea dates back to the works of Peierls [175] and Landau [176] who calculated the free energy of the full system using a similar expansion. Here we employ similar techniques for the reduced density matrix, which in the case of the equilibrium problem is well defined by the generalized Gibbs distribution [177]:

$$\rho^{\mathrm{eq}} = \frac{\mathrm{Tr_B}\, \mathrm{e}^{-\beta H_{\mathrm{tot}}}}{\mathrm{Tr}\, \mathrm{e}^{-\beta H_{\mathrm{tot}}}}\, , \tag{B.1}$$

where H_{tot} is defined in Eq. (2.1) with only one bath. We now use the Kubo identity to expand $\mathrm{e}^{-\beta H_{\mathrm{tot}}}$ up to second order in the coupling strength.

Tracing over the bath degrees of freedom we obtain,

$$
\begin{aligned}
\mathrm{Tr_B}(e^{-\beta H_{\mathrm{tot}}}) \;=\; & e^{-\beta H_S}\left[\mathbb{I} - \frac{\gamma_0}{2}\int_0^\beta d\beta_1 \tilde{S}(-i\,\beta_1)\tilde{S}(-i\,\beta_1)\right.\\
& \left. + \int_0^\beta d\beta_1 \int_0^{\beta_1} d\beta_2 \tilde{S}(-i\,\beta_1)\tilde{S}(-i\,\beta_2)\mathrm{C}(-i\,(\beta_1-\beta_2))\right],
\end{aligned}
$$
(B.2)

where $\tilde{S}(-i\,\beta_1) = e^{\beta_1 H_S}\,S\,e^{-\beta_1 H_S}$ is the free evolving system operator in imaginary time and $\mathrm{C}(-i\,(\beta_1-\beta_2))$ is the imaginary-time bath correlator as defined in Append. A. Using Eq. (B.2) in Eq. (B.1) the CPT reduced density matrix thus reads

$$
\rho^{\mathrm{CPT}} \;=\; \frac{e^{-\beta H_S}}{Z_S} + \frac{D}{Z_S} - \frac{e^{-\beta H_S}\,\mathrm{Tr_S}(D)}{(Z_S)^2},
$$
(B.3)

where $Z_S = \mathrm{Tr_S}(\exp[-\beta H_S])$ and the matrix D is given by,

$$
\begin{aligned}
D \;=\; & \int_0^\beta d\beta_1 \int_0^{\beta_1} d\beta_2 \tilde{S}(-i\,\beta_1)\tilde{S}(-i\,\beta_2)\mathrm{C}(-i\,(\beta_1-\beta_2))\\
& - \frac{\gamma_0}{2}\int_0^\beta d\beta_1 \tilde{S}(-i\,\beta_1)\tilde{S}(-i\,\beta_1).
\end{aligned}
$$
(B.4)

Next writing Eq. (B.3) in the basis of the system Hamiltonian we obtain,

$$
\rho_{nm}^{\mathrm{CPT}} \;=\; \frac{e^{-\beta E_n}}{Z_S}\delta_{n,m} + \frac{D_{nm}}{Z_S} - \frac{e^{-\beta E_n}\sum_i D_{ii}}{(Z_S)^2}\delta_{n,m},
$$
(B.5)

wherein

$$
\begin{aligned}
D_{nm} &= \sum_l S_{nl} S_{lm} \, \mathrm{e}^{-\beta \mathrm{E}_n} \left[\int_0^\beta \mathrm{d}\beta_1 \, \mathrm{e}^{\beta_1 \Delta_{nl}} \int_0^{\beta_1} \mathrm{d}\beta_2 \, \mathrm{e}^{\beta_2 \Delta_{lm}} \, \mathrm{C}(-i \, (\beta_1 - \beta_2)) \right. \\
&\quad \left. - \frac{\gamma_0}{2} \int_0^\beta \mathrm{d}\beta_1 \, \mathrm{e}^{\beta_1 \Delta_{nm}} \right] .
\end{aligned}
\tag{B.6}
$$

In Eq. (B.6) $\Delta_{nm} = E_n - E_m$ has the same definition as in Sec. 2.1.1.

The main task in CPT is to evaluate the elements of the matrix D, Eq. (B.6). In order to do this we split the matrix D into its diagonal and off-diagonal elements and deal with each part separately, as detailed below.

B.1   Off-diagonal elements of the matrix D

In order to obtain the off-diagonal elements of the matrix D we make the following change of variables: $x = \beta_1 - \beta_2, y = \beta_1 + \beta_2$ and then perform the y integral analytically to find,

$$
D_{nm} = \frac{1}{\Delta_{mn}} \sum_l \left(\tilde{D}_{nl} S_{lm} - \tilde{D}_{ml} S_{ln} \right) ,
\tag{B.7}
$$

where,

$$
\tilde{D}_{nl} = S_{nl} \, \mathrm{e}^{-\beta E_n} \left(\int_0^\beta \mathrm{d}x \, \mathrm{C}(-i \, x) \, \mathrm{e}^{-x \Delta_{ln}} - \frac{\gamma_0}{2} \right) .
\tag{B.8}
$$

B.2 Diagonal elements of the matrix D

For the diagonal elements of D, by using the same set of transformations as before, the integrals simplify and the diagonal elements of matrix D emerge as

$$D_{nn} = \sum_l \bar{D}_{nl} S_{ln} \,, \tag{B.9}$$

where,

$$\bar{D}_{nl} = S_{nl}\, e^{-\beta E_n} \left[\beta \left(\int_0^\beta \mathrm{d}x C(-i\,x)\, e^{-x\Delta_{ln}} - \frac{\gamma_0}{2} \right) \right.$$
$$\left. - \int_0^\beta \mathrm{d}x C(-i\,x) x\, e^{-x\Delta_{ln}} \right]. \tag{B.10}$$

In summary, the thermal equilibrium reduced density matrix obtain via CPT is given, up to second order, by the generalized Gibbs state, reading:

$$\rho_{nm}^{\mathrm{CPT}} = \rho_{nm}^{(0),\mathrm{CPT}} + \rho_{nm}^{(2),\mathrm{CPT}} \,, \tag{B.11}$$

where,

$$\rho_{nm}^{(0),\mathrm{CPT}} = \frac{e^{-\beta E_n}}{Z_{\mathrm{S}}} \delta_{n,m} \,, \tag{B.12}$$

$$\rho_{nm}^{(2),\mathrm{CPT}} = \frac{D_{nm}}{Z_{\mathrm{S}}} - \frac{e^{-\beta E_n} \sum_i D_{ii}}{(Z_{\mathrm{S}})^2} \delta_{n,m} \,. \tag{B.13}$$

Here, the off-diagonal elements of D_{nm} are given by Eq. (B.7) and the diagonal elements are given by Eqs. (B.9) and (B.10). Eq. (B.11) exhibits that the equilibrium reduced density matrix obtained via CPT is Hermitian and is normalized properly with trace over the system degrees of freedom equal to 1.